**BAŞKENT UNIVERSITY**
**INSTITUTE OF SCIENCE AND ENGINEERING**
**DEPARTMENT OF BIOMEDICAL ENGINEERING**
**MASTER OF SCIENCE IN BIOMEDICAL ENGINEERING**

# NOVEL ELECTROSPUN NANOFIBERS LOADED DIFFERENT MEDICAMENT APPROACHES AS DRUG DELIVERY SYSTEMS FOR REGENERATIVE ENDODONTICS

**By**

**NURA BRIMO**

**MASTER OF SCIENCE THESIS**

**ANKARA-2020**

**BAŞKENT UNIVERSITY**
**INSTITUTE OF SCIENCE AND ENGINEERING**
**DEPARTMENT OF BIOMEDICAL ENGINEERING**
**MASTER OF SCIENCE IN BIOMEDICAL ENGINEERING**

# NOVEL ELECTROSPUN NANOFIBERS LOADED DIFFERENT MEDICAMENT APPROACHES AS DRUG DELIVERY SYSTEMS FOR REGENERATIVE ENDODONTICS

**By**

**NURA BRIMO**

**MASTER OF SCINCE THESIS**

**ADVISOR**

**PROF. DR. DILEK ÇÖKELILER SERDAROĞLU**

**ANKARA-2020**

**BAŞKENT UNIVERSITY**
**INSTITUTE OF SCIENCE AND ENGINEERING**

This study, which was prepared by Nura Brimo, for the program of Master of Science in Biomedical Engineering, has been approved in partial fulfillment of the requirements for the degree of MASTER OF SCINCE in Biomedical Engineering Department by the following committee.

Date of Thesis Defense: 26/ 08/ 2020

**Thesis Title**: Novel Electrospun Nanofibers Loaded Different Medicament Approaches as Drug Delivery Systems for Regenerative Endodontics

| **Examining Committee Members (Title, Name-Surname, Institution)** | **Signature** |
|---|---|
| Prof. Dr. Dilek Çökeliler Serdaroğlu (advisor)<br>Başkent University | ……. |
| Prof. Dr. Necdet Sağlam<br>Hacettepe University | ……. |
| Prof. Dr. Selim Erkut<br>Başkent University | ……. |

**APPROVAL**

Prof. Dr. Faruk ELALDI

Director, Institute of Science and Engineering

Date: … / … / …

**BAŞKENT ÜNİVERSİTESİ**
**FEN BİLİMLERİ ENSTİTÜSÜ**
**YÜKSEK LİSANS ÇALIŞMASI ORİJİNALLİK RAPORU**

Tarih: / /

Öğrencinin Adı, Soyadı: Nura Brimo

Öğrencinin Numarası: 21810517

Anabilim Dalı: Biyomedikal Mühendisliği Ana Bilim Dalı

Programı: Biyomedikal Mühendisliği Yüksek Lisans

Danışman Adı, Soyadı: Prof. Dr. Dilek Çökeliler Serdaroğlu

Tez Başlığı: Novel Electrospun Nanofibers Loaded Different Medicament Approaches as Drug Delivery Systems for Regenerative Endodontics

Yukarıda başlığı belirtilen Yüksek Lisans çalışmamın; Giriş, Ana bölümler ve Sonuç Bölümünden oluşan, toplam 81 Sayfalık kısmına ilişkin, 08/09/2020 tarihinde şahsım tarafından Turnitin adlı intihal tespit programından aşağıda belirtilen filtrelemeler uygulanarak alınmış olan orijinallik raporuna göre, tezimin benzerlik oranı %11'dır.
Uygulanan filtrelemeler:

1. Kaynakça hariç
2. Alıntılar hariç
3. Beş (5) kelimeden daha az örtüşme içeren metin kısımları hariç

''Başkent Üniversitesi Enstitüleri Tez Çalışması Orijinallik Raporu Alınması ve Kullanılması Usul ve Esaslarını'' inceledim ve bu uygulama esaslarında belirtilen azami benzerlik oranlarına tez çalışmamın herhangi bir intihal içermediğini; aksinin tespit edileceği muhtemel durumda doğabilecek her türlü hukuki sorumluluğu Kabul ettiğimi ve yukarıda vermiş olduğum bilgilerin doğru olduğunu beyan ederim.

Öğrenci İmzası

**ONAY**

/ /2020

Öğrenci Danışmanı Unvan, Ad, Soyad

**Prof. Dr. Dilek Çökeliler Serdaroğlu**

# ACKNOWLEDGEMENT

First of all, I would like to express my special gratitude to my supervisor Prof. Dr. Dilek Çökeliler Serdaroğlu, for her best supporting, attention, and motivation in this journey. I would also like to show special thanks to Associate Prof. Dr. Tansel Uyar and Dr. Busra Uysal, for giving many valuable advices and for their supporting. Additionally, I would like to express special thanks to Examining Committee members; Prof. Dr. Necdet Sağlam and Prof. Dr. Selim Erkut for their valuable advices.

I would like to thank and express my deepest gratitude to my hero my dad, my supportive mom, my sisters, my lovely brother for everything, this step of my live would not have been possible without them.

NURA BRIMO

ANKARA-2020

# ABSTARCT

**Nura BRIMO**

**NOVEL ELECTROSPUN NANOFIBERS LOADED DIFFERENT MEDICAMENT APPROACHES AS DRUG DELIVERY SYSTEMS FOR REGENERATIVE ENDODONTICS**

**Başkent University, Institute of Science and Engineering**

**Department of Biomedical Engineering**

**2020**

Generally, traumatic tooth injuries with incomplete apical development in addition to dental caries are common causes of pulpal necrosis or infections. Recently, regenerative endodontic therapy has changed the therapeutics of infected teeth to be a viable therapy option. Disinfection of the root canal is an essential step of the most clinically regenerative procedures. Mainly, it is accomplished with calcium hydroxide or antibiotic mixtures either double antibiotics paste (Metronidazole and Ciprofloxacin) or triple antibiotics paste (Metronidazole, Ciprofloxacin, and Minocycline), which have gained increased interest to obtain maximum disinfection.

Regrettably, even though the antimicrobial capabilities of these medicaments are renowned, recent findings showed negative effects of these forms such as cell toxicity, difficulties in completely removing of the antibiotics from the root canal system, and tooth discoloration associated with the use of high levels of antibiotics, which may lead to limit regenerative outcomes. Drug release systems have been proven to control infections by the controlled release of a wide variety of antibiotics.

In light of this, the ability of nano/microfibers to deliver intracanal, uniform, and controlled amounts of drugs can lead to positive therapy impacts through achieving lower toxicity effects associated with their paste forms and a bacteria-free environment conducive to tissue regeneration.

In addition, these systems have a demonstrated significant clinical potential in order to translate fibrous mats coated gutta-percha cones into clinics for regenerative endodontics via their hand-ability, geometry, chemical, and physical prosperities.

Here in this study, besides Ca(OH)2, Metronidazole, Ciprofloxacin, and Minocycline were added to Poly(vinylpyrrolidone) polymer solution and spun into fibrous mats with separated, double, and triple forms.

Fibers' morphology, Fibers' chemical characterization, physical and chemical characterization of the dentin surface were evaluated by Scanning Electron Microscope and Energy Dispersive X-Ray Spectroscopy, Nano-SEM, and Fourier Transform Infrared Spectroscopy, respectively. Characterization of the gutta-percha cones after the air irradiation via plasma and after coating them with fiber mats was achieved by X-Ray Photoelectron Spectroscopy and light microscope, respectively.

Scanning Electron Microscope and Energy Dispersive X-Ray Spectroscopy results confirmed that electrospinning was able to produce antibiotic-containing fibers with diameters ranged between nano- and microscales. Nano-SEM and Fourier Transform Infrared Spectroscopy results presented that fibers mats achieved better affects on the chemical and morphological structures of the dentin tubules. X-Ray Photoelectron Spectroscopy results showed a better hydrophilic form of the gutta-percha surface in order to obtain a better coating process.

**KEYWORDS:** Drug delivery, Electrospinning, Nano/microfibers, Regenerative Endodontic, Gutta-percha.

# ÖZET

**Nura BRİMO**

**REJENERATİF ENDODONTİK TEDAVİSİNDE FARKLI BİR MEDİKAL YAKLAŞIM OLARAK İLAÇ SALINIM SİSTEMLİ ELEKTROSPİN NANOFİBER UYGULAMASI**

**Başkent Üniversitesi Fen Bilimleri Enstitüsü**

**Biyomedikal Mühendisliği Anabilim Dalı**

**2020**

Apikal gelişimi tamamlanmamış travmatik diş yaralanmaları; genellikle diş çürüklerine ek olarak pulpa nekrozu veya enfeksiyonlara neden olur. Son zamanlarda geliştirilen rejeneratif endodontik tedaviler, enfekte dişlerin tedavisinde terapötik ajanların uygulanmasını mümkün kıldı. Kök kanalının dezenfeksiyonu ise klinik olarak geliştirilen rejeneratif prosedürlerde karşılaşılan kritik noktalardan biridir. Performansı en yüksek dezenfeksiyonu elde etmek için kullanılan yöntemler kalsiyum hidroksit kullanılması, antibiyotik karışımları kullanılması ya da çift antibiyotikle hazırlanan macunların (Metronidazol ve Siprofloksasin) veya üçlü antibiyotik macunu (Metronidazol, Siprofloksasin ve Minosiklin) kullanılması şeklinde belirtilebilir. Her ne kadar bu ilaçların antimikrobiyal yetenekleri biliniyor olsa da son bulgular göstermiştir ki hücre toksisitesi üzerinde, antibiyotiklerin kök kanal sisteminden tamamen çıkarılmasında ve yüksek seviyede antibiyotik kullanılmasına bağlı olarak dişte renk değişikliği gibi olumsuz etkilere sebep olmaktadır. Bu olumsuz etkilere antibiyotiklerin rejeneratif yeteneklerini sınırlandırabilmektedir. İlaç salınım sistemlerinin ise çeşitli antibiyotiklerin kontrollü salınımını sağlayabildiği için enfeksiyon tedavisinde başarılı oldukları kanıtlanmıştır. Bu veriler ışığında nano/mikrofiberlerin ise kanal içi, tek tip ve kontrollü miktarlarda ilaç verme yetenekleri ve macunsu formları sayesinde bakteri içermeyen bir ortamda doku rejenerasyonuna yardımcı olabileceği çıkarımı yapılabilir. Buna ek olarak bu sistemler el becerisi, geometrisi, kimyasal ve fiziksel zenginlikleri aracılığıyla, gutta-perka konileri ile kaplanmış lifli matlar sayesinde rejeneratif endodonti kliniklerinde kullanılmak üzere önemli bir klinik potansiyele sahiptir.

Bu çalışmada; Poli(vinilpirolidon) polimer çözeltisine $Ca(OH)_2$'nin yanı sıra Metronidazol, Siprofloksasin ve Minosiklin ilave edilerek ayrılmış, ikili ve üçlü formlarda lifli matlar hazırlanmıştır. Fiberlerin morfolojisi, Fiberler'in kimyasal karakterizasyonu, dentin yüzeyinin fiziksel ve kimyasal karakterizasyonu, sırasıyla Taramalı Elektron Mikroskobu ve Enerji Dağılımlı X-Işını Spektroskopisi, Nano-SEM ve Fourier Dönüşümü Kızılötesi Spektroskopi ile değerlendirilmiştir. Gutta-perka konilerinin karakterizasyonu ise, plazma yoluyla hava ışınlamasından sonra ve fiber matlarla kaplandıktan sonra sırasıyla X-Ray Fotoelektron Spektroskopisi ve ışık mikroskobu ile gerçekleştirilmiştir. Gerçekleştirilen testlerde, Taramalı Elektron Mikroskobu ve Enerji Dağılımlı X-Işını Spektroskopisi sonuçları, elektroeğirme'nin, nano- ve mikro-ölçekler arasında değişen çaplarda antibiyotik içeren lifler üretebildiğini doğrulamıştır. Nano-SEM ve Fourier Dönüşümü Kızılötesi Spektroskopi sonuçları, fiber matların dentin tübüllerinin kimyasal ve morfolojik yapıları üzerinde daha iyi etkiler sağladığını göstermiştir. X-Işını Fotoelektron Spektroskopisi sonuçları ise Gutta-perka yüzeyinin daha iyi kaplama elde etmek için iyi bir hidrofilik forma sahip olduğunu göstermiştir.

**ANAHTAR KELİMELER:** İlaç salınımı, Elektroeğirme, Nano/mikrofiberler, Rejeneratif Endodontik, Gutta-perka.

# TABLE OF CONTENTS

Page

**ACKNOWLEDGEMENT** ..... i

**ABSTARCT** ..... ii

**ÖZET** ..... iv

**TABLE OF CONTENTS** ..... vi

**LIST OF TABLES** ..... x

**LIST OF FIGURES** ..... xi

**LIST of SYMBOLS AND ABBREVIATIONS** ..... xv

**1. INTRODUCTION** ..... 1

**2.BACKGROUND** ..... 3

**2.1. Endodontics Over-out History** ..... 3

**2.2. The Concept of Endodontics** ..... 4

**2.3. Endodontic Techniques** ..... 7

**2.4. Dental Stem Cells** ..... 8

**2.5. Dental Biofilms** ..... 9

**2.6. The Past and Present Contributions as Preface for Modern Dental Therapy** ..... 10

**2.7. Regenerative Endodontic Therapy** ..... 11

**2.8. The Emerge of Nanotechnology** ..... 14

**2.8.1 Definition of nanofibers** ..... 15

**2.8.2 Unique properties of nanofibers** ..... 15

**2.8.2.1 Fiber's size effect on surface area** ..... 16

**2.8.2.2 Fiber's size effect on electro activity** ..... 16

**2.8.2.3 Fiber's size effect on bioactivity** ..... 17

**2.8.2.4 Fiber's size effect on strength** ..... 18

**2.8.3 Nanofibers design and fabrication methods** ..... 18

**2.8.3.1 ElectrospinningtTechnique** ..... 18

**2.8.3.1.1 Prosperities of polymer solutions** ..... 20

**2.8.3.1.2 Process parameters** ..... 21

**2.8.3.2 Non-electrospinning techniques** ..... 22

**2.8.3.3 Poly(vinylpyrrolidone) PVP** ..... 23

**2.9. Electrospun Nanofibers as Drug Delivery Systems for Regenerative Endodontic** ..... 24

**2.10. Electrospun Nanofibers Characterization Techniques** ..... 27

**2.10.1Structural characterization** ..... 28

**2.10.2Mechanical characterization** ..... 29

**2.10.3Chemical characterization** ..... 29

**3. Materials and Methods** ..... 29

**3.1. Materials** ..... 29

**3.2. Pre-experiments** ..... 31

**3.3. Preparation of Electrospinning Solutions** ..... 33

**3.3.1 Preparation of poly(vinylpyrrolidone) solution** ..... 33

**3.3.2 Preparation of single antibiotic-poly(vinylpyrrolidone) containing solutions** ..... 33

**3.3.3 Preparation of double antibiotic-poly(vinylpyrrolidone) containing solutions** ..... 34

**3.3.4 Preparation of triple antibiotic-poly(vinylpyrrolidone) containing solutions** ..... 35

**3.3.5 Preparation of calcium hydroxide-poly(vinylpyrrolidone) containing solutions** ..... 35

**3.4. Electrospinning Process** ..... 36

**3.5. Characterization of Electrospun Polymeric Nanofibers** ..... 36

**3.5.1 Scanning electronmicroscope (SEM) morphological analysis, fiber diameter and distribution determination** ..... 36

**3.5.2 Energy dispersive x-ray spectroscopy (EDX)** ..... 37

**3.6. Study of Modifying Gutta-Percha Surface via Plasma Irradiation** ..... 38

**3.7. Characterization of Gutta-Percha** ..... 40

**3.7.1 X-ray photoelectron spectroscopy (XPS) analysis** ..... 40

**3.8. Coating Gutta-Percha with Nanofiber mats via Electrospinning Strategy** . 41

**3.9. Chemical Characterization of Dentin Surface** ..... 43

**3.10. Physical Characterization of Dentin Surface** ..... 46

**4.Results** ..... 47

**4.1. Pre-experiments Characterizations** ..... 47

**4.2. Fabrication and Characterization of Poly(vinylpyrrolidone) Nanofiber Samples** ..... 50

**4.2.1 Scanning electron microscope (SEM) morphological analysis, fiber diameter and distribution determination** ..... 51

**4.2.2 Energy dispersive x-ray spectroscopy (EDX)** ..... 51

**4.3. Fabrication and Characterization of Metronidazole-Poly(vinylpyrrolidone) Containing Nanofiber Samples** ..... 52

**4.3.1.1 Scanning electron microscope (SEM) morphological analysis, fiber diameter and distribution determination** ..... 53

**4.3.1.2 Energy dispersive x-ray spectroscopy (EDX)** ..... 56

**4.3.2 Fabrication and characterization of ciprofloxacin-poly(vinylpyrrolidone) containing nanofiber samples** ..... 58

**4.3.2.1 Scanning electron microscope (SEM) morphological analysis, fiber diameter and distribution determination** ..... 59

**4.3.2.2 Energy dispersive x-ray spectroscopy (EDX)** ..... 62

**4.4. Fabrication and Characterization of Double Antibiotics Loaded-Poly(vinylpyrrolidone) Nanofibers Samples** ..... 64

**4.4.1 Scanning electron microscope (SEM) morphological analysis, fiber diameter and distribution determination** ..... 65

**4.4.2 Energy dispersive x-ray spectroscopy (EDX)** ..... 68

**4.5. Fabrication and Characterization of Triple Antibiotics Loaded-Poly(vinylptrrolidone) Nanofiber Samples** ..... 69

**4.5.1 Scanning electron microscope (SEM) morphological analysis, fiber diameter and distribution determination** ..... 70

**4.5.2 Energy dispersive x-ray spectroscopy (EDX)** ..... 72

**4.6. Fabrication and Characterization of Calcium Hydroxide-Poly(vinylpyrrolidone) Containing Nanofiber Samples** ..... 74

**4.6.1 Scanning electron microscope (SEM) morphological analysis, fiber diameter and distribution determination** ..... 75

**4.6.2 Energy dispersive x-ray spectroscopy (EDX)** ..... 77

**4.7. Characterization of Bare Modified Gutta-Percha** ..... 79

**4.7.1 X-ray photoelectron spectroscopy (XPS) analysis** ..... 79

**4.8. Characterization of Gutta-Percha Coated with Nanofiber Mats** ..... 81

**4.9. Chemical Characterization of Dentin Surface** ..... 82

**4.10. Physical Characterization of Dentin Surface** ..... 84

**5.Discussion** ..... 86

**6.Conclusion** ..... 87

**References** ..... 88

# LIST OF TABLES

Page

Tablo 2.1. Affecting parameters on morphology of electrospun polymeric nanofibers..... 22

Table 4.1. Percent atoms by XPS analysis ..... 81

Table 4.2. Light microscope images of gutta-percha cones with different forms a) Bare gutta-percha b) coated with PVP-nanofiber mats c) double-antibiotics loaded PVP-nanofiber mats d) triple-antibiotics loaded PVP-nanofiber mats e) $Ca(OH)_2$ loaded PVP-nanofiber mats ..... 82

Table 4.3. Representative attenuated total reflectance (ATR) spectra of dentin from control group (untreated) a). Representative attenuated total reflectance (ATR) spectra of dentin after treated with DAP b), DA-NFs c), TAP d), TA-NFs e), $Ca(OH)_2$-paste f), and $Ca(OH)_2$-NFs g)..... 84

Tablo 4.4. SEM micrographs showed the morphology of the dentin, light microscope figures showed the gutta-percha coated with nanofiber mats, and dentin discoloration results ..... 85

# LIST OF FIGURES

Page

Figure 2.1. The Structure of the Tooth [29] ..... 5

Figure 2.2. Schematic of the Root Canal System Components [32] ..... 7

Figure 2.3. The Chemical structure of metronidazole, minocycline, ciprofloxacin, and calcium hydroxide ..... 14

Figure 2.4. Surface area to fiber diameter elation [105] ..... 16

Figure 2.5. The relationship and effect of nanofibers size on cell growth [105] ..... 17

Figure 2.6. Effect of fiber diameter on the electrical conductivity of the fibers [105] ..... 17

Figure 2.7. Effect of nanotube diameters on (a) the glass fiber strength, and (b) strain energy [105] ..... 18

Figure 2.8. Electrospinning Setup ..... 19

Figure 2.9. Formation of Taylor Core ..... 20

Figure 2.10. Effect of polymeric solution viscosity on the nanofiber morphology ..... 21

Figure 2.11. The Chemical Structure of Poly(vinylpyrrolidone) ..... 23

Figure 2.12. Drug loading electrospun polymeric nanofibers with four different techniques ..... 25

Figure 2.13. Schematic of the general parts of SEM device [122] ..... 28

Figure 3.1. The applied Ethyl Alcohol solvent and Poly(vinylpyrrolidone) Polymer ..... 30

Figure 3.2. 2-D structures, 2-D conformers and 3-D conformer of the chemical structures of a) MET [123], b) CIP [124], c) MINO [125], and d) $Ca(OH)_2$ [126] ..... 30

Figure 3.3. Preparing the antibiotic powders ..... 31

Figure 3.4. Electrospinning Device ..... 32

Figure 3.5. Bare-PVP solution preparing process ..... 33

Figure 3.6. Polymer solutions on the magnetic stirrer ..... 34

Figure 3.7. a). Scanning electron microscope (ESEM), b). Preparing nanofiber samples for SEM analysis ..... 37

Figure 3.8. Energy Dispersive X-Ray Spectroscopy (EDX) device ..... 38

Figure 3.9. Preparing and cutting gutta-percha cones before placing them inside plasma device ..... 39

Figure 3.10. Gutta-percha surface modification was applied via plasma air irradiation ..... 40

Figure 3.11. a). Vacuum device, b). Samples analyzing on XPS ..... 41

Figure 3.12. Coating process of Gutta-Percha with Nanofiber mats via Electrospinning device ..... 42

Figure 3.13. Light microscope device used to analysis the morphology of the gutta-perchas after coating with nanofibrous mats ..... 42

Figure 3.14. The shape and number of used teeth specimens at the different steps of this study ..... 43

Figure 3.15. Electrospinning process upon human dentin specimens for injecting themedicament-NF samples in the root canals ..... 44

Figure 3.16. Teeth samples injected with different medicaments for four weeks before washing process for mineral content analysis ..... 45

Figure 3.17. Teeth samples injected with different antibiotics for four weeks after washing process for mineral content analysis ..... 45

Figure 3.18. a), b), and c) Fourier-transform infrared spectroscopy (FT-IR) device, d). and e). placing teeth samples in the FT-IR device ..... 46

Figure 4.1. SEM images of electrospun one fibers in different concentrations of MET with PVP and different focus points of each concentration; a1). 20% MET-PVP (x1500), a2). 20% MET-PVP (x5000), a3). Fiber diameter distribution of 20% MET-PVP; b1). 25% MET-PVP (x1500), b2). 25% MET-PVP (x5000), b3). Fiber diameter distribution of 25% MET-PVP ..... 48

Figure 4.2. SEM images of electrospun nanofibers in different concentrations of CIP with PVP and different focus points of each concentration; a1). 20% CIP-PVP (x1500), a2). 20% CIP-PVP (x5000), b1). 25% CIP-PVP (x1500), b2). 25% CIP-PVP (x5000) ..... 49

Figure 4.3. Chemical compositions of a) % 20 of MET-PVP and b) % 20 of CIP-PVP .... 50

Figure 4.4.The optical photos of the 8%(w/w) of PVP nanofiber mat produced via electrospinning strategy ..... 50

Figure 4.5. SEM images of %8 (w/w) Electrospun PVP fibers with a). x1500 and b). x10000 focused points c). fiber diameter distribution analysis of PVP electrospun fibers ..... 51

Figure 4.6.SEM-Energy Dispersive X-Ray Spectroscopy of pure PVP nanofiber mat ..... 52

Figure 4.7.The optical photos of the MET-loaded nanofibers mats with different concentrations produced via electrospinning strategy ..... 53

Figure 4.8.SEM images of electrospun nanofibers in different concentrations of MET with PVP and different focus points of each concentration; a1). 2.5% MET-PVP (x1500), a2). 2.5% MET-PVP (x10000), a3). Fiber diameter distribution of 2.5% MET-PVP; b1). 5% MET-PVP (x1500), b2). 5% MET-PVP (x10000), b3). Fiber diameter distribution of 5% MET-PVP; c1). 7.5% MET-PVP (x1500), c2). 7.5% MET-PVP (x10000), c3). Fiber diameter distribution of 7.5% MET-PVP; d1). 10% MET-PVP (x1500), d2). 10% MET-PVP (x10000), d3). Fiber diameter distribution of 10% MET-PVP ..... 55

Figure 4.9.SEM-Energy Dispersive X-Ray Spectroscopy of a)2.5, b).5, c).7.5, and d).10% (w/w) MET-PVP electrospun nanofiber mats..... 58

Figure 4.10.The optical photos of the CIP-loaded nanofibers mats with different concentrations produced via electrospinning strategy ..... 59

Figure 4.11. SEM images of electrospun nanofibers in different concentrations of MN with PVP and different focus points of each concentration; a1). 1% CIP-PVP (x1500), a2). 1% CIP-PVP (x10000), a3). Fiber diameter distribution of 1% CIP-PVP; b1). 2.5% CIP-PVP (x1500), b2). 2.5% CIP-PVP (x10000), b3). Fiber diameter distribution of 2.5% CIP-PVP; c1). 5% CIP-PVP (x1500), c2). 5% CIP-PVP (x10000), c3). Fiber diameter distribution of 5% CIP-PVP; d1). 7.5% CIP-PVP (x1500), d2). 7.5% CIP-PVP (x10000), d3). Fiber diameter distribution of 7.5% CIP-PVP ..... 61

Figure 4.12.SEM-Energy Dispersive X-Ray Spectroscopy of a)1, b).2.5, c).5, and d).7.5% (w/w) CIP-PVP electrospun nanofiber mats..... 64

Figure 4.13.The optical photos of the 9%(w/w) of double antibiotics loaded nanofibers mat produced via electrospinning strategy ..... 65

Figure 4.14.SEM images of electrospun nanofibers in different concentrations of CIP-MET. with PVP and different focus points of each concentration; a1). 5% CIP-MET-PVP (x1500), a2). 5% CIP-MET-PVP (x10000), a3). Fiber diameter distribution of 5% CIP-MET-PVP; b1). 7% CIP-MET-PVP (x1500), b2). 7% CIP-MET. -PVP (x10000), b3). Fiber diameter distribution of 7% CIP-MET-PVP; c1). 9% CIP-MET-PVP (x1500), c2). 9% CIP-MET-PVP (x10000), c3). Fiber diameter distribution of 9% CIP-MET-PVP; d1). 11% CIP-MET-PVP (x1500), d2). 11% CIP-MET-PVP (x10000), d3). Fiber diameter distribution of 11% CIP-MET-PVP ..... 67

Figure 4.15.SEM-Energy Dispersive X-Ray Spectroscopy of a)5, b).7, c).9, and d).11% (w/w) CIP-MN-PVP electrospun nanofiber mats..... 69

Figure 4.16.The optical photos of the 9%(w/w) of triple antibiotics loaded nanofibers mat produced via electrospinning strategy ..... 70

Figure 4.17.SEM images of electrospun nanofibers in different concentrations of CIP-MET-MINO. with PVP and different focus points of each concentration; a1). 5% CIP-MET-MINO-PVP (x1500), a2). 5% CIP-MET-MINO-PVP (x10000), a3). Fiber diameter distribution of 5% CIP-MET-MINO-PVP; b1). 7% CIP-MET-MINO-PVP (x1500), b2). 7% CIP-MET-MINO-PVP (x10000), b3). Fiber diameter distribution of 7% CIP-MET-MINO-PVP; c1). 9% CIP-MET-MINO -PVP (x1500), c2). 9% CIP-MET-MINO-PVP (x10000), c3). Fiber diameter distribution of 9% CIP-MET-MINO-PVP; d1). 11% CIP-MET-MINO-PVP (x1500), d2). 11% CIP-MET-MINO-PVP (x10000), d3). Fiber diameter distribution of 11% CIP-MET-MINO-PVP..... 72

Figure 4.18.SEM-Energy Dispersive X-Ray Spectroscopy of a)5, b).7, c).9, and d).11% (w/w) CIP-MN-MINO-PVP electrospun nanofiber mats..... 74

Figure 4.19.The optical photos of the 3%(w/w) of calcium hydroxide loaded nanofibers mat produced via electrospinning strategy ..... 75

Figure 4.20.SEM images of electrospun nanofibers in different concentrations of MN with PVP and different focus points of each concentration; a1). 2% $Ca(OH)_2$-PVP (x1500), a2). 2% $Ca(OH)_2$-PVP (x10000), a3). Fiber diameter distribution of 2% $Ca(OH)_2$-PVP; b1). 3% $Ca(OH)_2$-PVP (x1500), b2). 3% $Ca(OH)_2$-PVP (x10000), b3). Fiber diameter distribution of 3% $Ca(OH)_2$-PVP; c1). 4% $Ca(OH)_2$-PVP (x1500), c2). 4% $Ca(OH)_2$-PVP (x10000), c3). Fiber diameter distribution of 4% $Ca(OH)_2$-PVP; d1). 5% $Ca(OH)_2$-PVP (x1500), d2). 5% $Ca(OH)_2$-PVP(x10000)..... 77

Figure 4.21.SEM-Energy Dispersive X-Ray Spectroscopy of a)2, b).3, c).4, and d).5% (w/w) $Ca(OH)_2$-PVP electrospun nanofiber mats ..... 79

Figure 4.22.XPS analyzing data for a) Gutta-percha$_{control}$ surface, b). C1s, c) O1s ..... 80

Figure 4.23.XPS analyzing data for a) Gutta-percha$_{modified}$ surface, b). C1s, c) O1s ..... 81

# LIST of SYMBOLS AND ABBREVIATIONS

| Abbreviation | Explanation |
|---|---|
| RET | Regenerative endodontics treatment |
| SAP | Single antibiotic paste |
| DAP | Double antibiotic paste |
| TAP | Triple antibiotic paste |
| MET | Metronidazole |
| CIP | Ciprofloxacin |
| MINO | Minocycline |
| $Ca(OH)_2$ | Calcium hydroxide |
| PDS | Polydioxanone |
| PVP | Poly(vinylpyrrolidone) |
| Et-OH | Ethyl Alcohol |
| TA-NFs | Triple antibiotics loaded nanofibers |
| DA-NFs | Double antibiotics loaded nanofibers |
| $Ca(OH)_2$-NFs | Calcium hydroxide loaded nanofibers |
| DPSCs | Dental pulp stem cells |
| NaOCl | Sodium hypochlorite |
| EDTA | Ethylene Diamine Tetra-Acetic |
| $H_2O_2$ | Hydrogen Peroxide |
| CHX | Chlorhexidine Gluoconat |
| D | Dimension |
| nm | Nanometre |
| µm | Micrometer |
| PLA | Polylactic acid |
| PEG | Polyethylene glycol |
| SEM | Scanning electron microscopy |
| TEM | Transmission electron microscopy |
| OM | Optical microscopy |
| AFM | Atomic force microscopy |
| STM | Scanning tunneling microscopy |
| FTIR | Fourier transform infrared |
| ATR | Attenuated total reflectance |
| EDX | Energy dispersive X-Ray device |
| XPS | X-Ray Photoelectron Spectroscopy |
| ESCA | Electron Spectroscopy for Chemical Analysis |
| SD | Standard deviation |

# 1. INTRODUCTION

Dental-pulp tissue subjected to mechanical trauma or necrosis shows many periapical infects and effects in the system of root canal [1]. One of the most known treatment strategies in dentistry especially in endodontic is regenerative endodontics treatment (RET), where this strategy is applied to achieve effective root system disinfection and regeneration the tissue of the pulp dentin [2]. RET is a biologically dependent treatment method designed for necrotic pulps in order to change and replace infected canals and dentin structures. This method of treatment has become one of the novel modalities in the endodontic therapy field, besides it is contemplated as an alternative option to the traditional method apexification. Despite this treatment strategy showed many successes via its low financial costs and simplification of performance, various limitations are reported. That is because of the tooth has a highly organized structure of vital soft pulp enclosed by the mineralized hard tissue, and the of pulp-dentin tissue regeneration has been challenging to attain. According to the unique dental anatomy, it is necessary to release the repair processes of dentine tissue through inflammatory-proliferative-remodeling stage alterations [3]. In order to achieve an effective regenerative strategy, it is necessary obtaining suitable disinfection processes also using suitable biocompatible molecules to control the differentiation of dental stem cells and releasing of growth factors. As a summary, pulp-dentin complex regeneration aids in extending the normal function of the natural dentition, especially in cases of traumatized permanent immature teeth, which hinders completion of root development and maturation.
The application of antibiotics mixtures in RET was introduced in 2001 [4]. Since their going out, these antibiotic pastes, i.e., either single antibiotic paste (SAP), double antibiotic paste (DAP) (metronidazole (MET) and ciprofloxacin (CIP)) or triple antibiotic paste (TAP) (metronidazole, ciprofloxacin, and minocycline (MINO)), has been the most widely applied intracanal medicaments. Besides that, using root canal irrigants (i.e, NaOCl) besides these antibiotic pastes during the treatment process has led to better bacterial elimination for the root canals, but in situations, during the use, either the irrigants or antibiotic pastes with high doses have led to a negative effect on the function of dental stem cells. It was presented that the commonly applied creamy paste with (1 g/mL) dose of the TAP mixture has a toxic effect on dental stem cells [5]. However, other reports showed radiographic root enhancing of infected teeth treated with DAP and TAP [3], [6], but it is caused to difficulties in completely

removing the injurious remnants from the intracanal system [7]. Althumairy et al. showed that the TAP concentrations ranging from 0.01-0.1 $mg.mL^{-1}$ didn't show a cytotoxic effect but doses of 1 mg/mL showed harmful effects onto apical papilla stem cells. Where they appreciated the impact on dentin condition with TAP on the ability of stem cells located in connection with pre-treated dentin [8].

Hence, there are requirements to apply those antibiotics with lower concentrations in the regenerative treatment of endodontics. Those needs led to the introduction of scaffolds that can preserve the antimicrobial effects with lower antibiotic concentrations and enhance the proliferation and viability of the stem cells. Many researchers have been searching in order to develop biologically predictable scaffolds by applying nanotechnology. Nanotechnology has been growing fact in various approaches due to its ability to develop many systems. In drug delivery systems, coating drugs with electrospun fiber is considered to be effective in controlling the release kinetics of the drugs [9]. So, according to get over the natural toxicity of the medicaments mentioned above, the meaning of cell friendly disinfection method was introduced through developing effective antibiotic-loaded polymeric nanofibers [10]–[12]. These systems for drug delivery and releasing developed for regeneration concept are based on the principle that controlling the release rate and doses of the antibiotics can enhance the viability of the stem cells in the same time providing anti-microbial behavior [13], [14].

Importantly, in this strategy, the anti-microbial agents are delivered directly onto the dentinal walls, where microbial biofilms are present. So, using these medicaments-loaded polymeric nanofibers as a drug delivery system leads to eliminating the infections and forms a bacterial-free environment [14]–[16].

Bottino et al. incorporated MET and CIP with polydioxanone (PDS) electrospun scaffolds, where they noticed that these forms of scaffolds were more effective than paste forms at the delivery of the antibiotics [11]. By the electrospinning method, the polymer solution can incorporate with one or more of antibiotics in order to obtain fibers with a wider antibacterial effect to inhibit the growth of endodontic pathogens [17], [18]. In a study, ciprofloxacin-loaded polymeric nanofibers were applied against E. faecalis biofilm and found maximum elimination of the bacterial biofilms [19], and provide great stem cells viability [18]. Where tissue engineering methods have been considered clinical methods to regenerate the teeth pulp-dentin complex with infected pulps [10]. It is important to bear in

mind that successful RET requires effective root canal disinfection with no or minimal harm to stem cells present in the dental matrix [3]. To that end, the idea of antibiotic-loaded nanofiber materials was recognized and broadly explored with many research groups as more cell friendly disinfection, non-toxic, non-crown discoloration approach [20]. As mentioned above, using high levels of antibiotics lead to many limitations associated with currently advocated regenerative endodontic procedures, i,e., tooth discoloration caused by high doses of MINO [21], limited regenerative outcomes, difficulty with antibiotic completely removal from dental canals, and cell toxicity.

In this thesis, different antibiotic concentrations were injected within Poly(vinylpyrrolidone) (PVP) for the first time in order to achieve more cell-friendly disinfection drug release systems by nanofiber mats coated gutta-percha via modifying its surface by plasma irradiation compared to the currently used paste forms. Besides that, they are designed to investigate the antimicrobial efficacy of our three main experiment groups (triple antibiotics loaded nanofibers (TA-NFs), double antibiotics loaded nanofibers (DA-NFs), and calcium hydroxide loaded nanofibers ($Ca(OH)_2$-NFs)) against different bacteria, measurement the cytocompatibility of the nanofiber mats, evaluate the ability of dental pulp stem cells (DPSCs) to adhere and proliferation, and measurement the effect of the used medicaments on the dentin chemical structure.

# 2. BACKGROUND

## 2.1. Endodontics Over-out History

The beginning of endodontics trace back to the 17th century when Charles Allen wrote the first book on dentistry, ‘’Describing the techniques of dental transplants,’’ in English-language in 1687[22]. In 1725, Lazare Riviere described the use of oil cloves for its sedative properties [22]. In 1746, Pierie Fouchard described in his own book accessing the pulp chamber to aid in removing the pulp providing for abscess drainage [22]. During the mid-1880s many advancements were achieved in this field. Many years later, the first root canal instrument has been introduced by Edwin Maynard. In 1847, gutta-percha has been introduced as a filling material. After a few years, gutta-percha cones have been used as the

sole materials for obturating the root canal by G.A. Bowman [22]. At the same time, Maginot also recommended the use of an electric current to examine pulp vitality.

In 1891, the use of camphorated chlorophenol as a medication in order to disinfect the root canal has been introduced by a German dentist. Four years later, scientist Roentgen founded a form of energy used to penetrate solid materials. But because of their unfamiliar phenomena, Roentgen decided to call these rays ‘’X’’ [23]. At the beginning of the 1900s, periapical radiolucency has been described as ‘’blind abscess’’ by Pricfe where he recommended using the radiography for establishing the diagnosis of pulp-less teeth. During 1908, the length of the canal and the size of the apical foramen have been determined by G.V. Black [22]. Then Grossman has been introduced imprisonment of instruments to the root canal; averting sturdy entry of instrumentation and using biomechanical instrumentation principles [24]. Besides these principles, bathing the root system with an antiseptic solution was discussed and many disinfectants were used such as metallic sodium, sodium dioxide, and sulfuric acid [22]. In the early 1990s, endodontics therapy started to acquire a huge consenting in the dental community by occurring many new techniques, materials, and technologies. After that, William Hunter, an English physician, and pathologist gave a lecture on focal infection at the University of Montreal which titled ‘’The Role of Sepsis and Antisepsis in Medicine’’, where the endodontic field took a roundabout route due to him. Although Hunter’s concern was directed more toward the septic conditions found around poorly constructed prosthetic restorations. In 1940, the detour of endodontic stopped when scientific research showed devitalized teeth did not play a role in the causation of system discuses. During the late 1940 and early 1950s, a group of 20 dentists met in Chicago to organize an organization for endodontic. After that meeting, the American Association of Endodontists was created and continued its growth. In 1956, the association created the American Board of Endodontics. By supporting the ADA to AAE their membership has increased gradually to 7800 AAE members over the world [25].

## 2.2. The Concept of Endodontics

Endodontics is a branch of dentistry interested in morphology, pathology, and physiology of the human dental pulp and also periapical tissues. The research and practice of endodontics encompass the clinical sciences of the dental pulp such as diagnosis, protection, and medication of the injured pulps. The major aim of endodontics is to save the

natural tooth for as long as possible by eliminating the microbial insult in primary or secondary infections [26]. When bacteria enter the root canal space, which contains the tooth's nerves, arterioles, lymphatic tissue, ranulas, and fibrous tissue can lead to periapical injures or damages. If this elimination process is not achieved at the right time, bacterial byproducts can move into the periductular tissue through the root canal system and lead to inflammation [27], [28].

The human tooth has two main parts, as mentioned in **Figure 2.1** the first one is the crown part and the second one is the root part. The crown part is the part of the tooth that protrudes over the line of the gum and the root part is firmed into the jaw of the tooth, also these two parts are united by a soft tissue called neck area. The anatomic of the upper part of the tooth is known as the part of the tooth that is warped by enamel; otherwise the anatomic of the root is known as the part of the tooth that is warped by cementum. The internal structure of the tooth mainly is formed from three harsh tissues and one smooth tissue contains enamel, dentin, cementum, and soft tissue is the pulp.

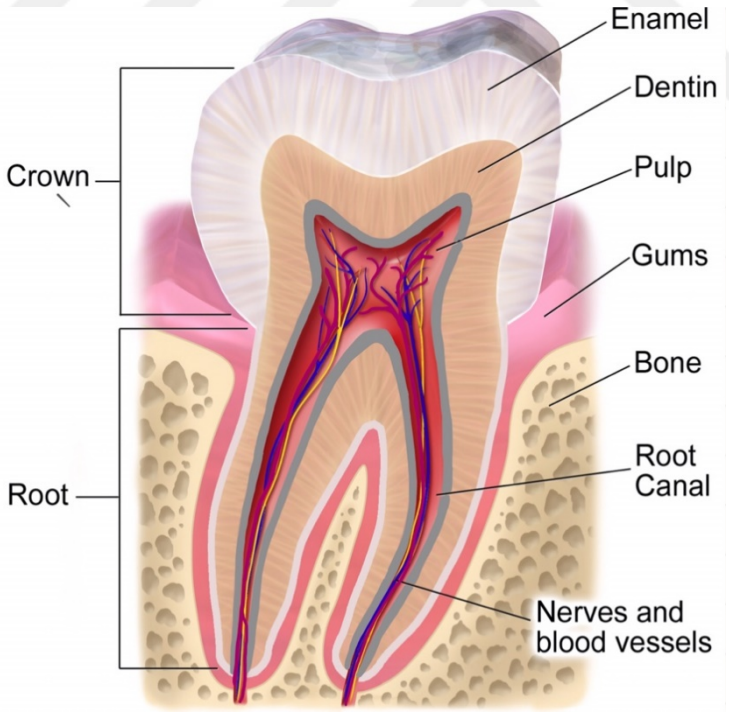


**Figure 2.1.** The Structure of the Tooth [29]

Firstly, enamel is the part of the tooth that helps to protect it and gives teeth its own white color. Enamel is the hardest material in the body; where develops from the enamel organ. The layer under the enamel is dentin, which contains the main bulk of the teeth. This

layer is a hard, thick, and elastic layer but not so hard as the enamel. The dentine layer also attends in both crown and root parts. The dentin layer contains 70% inorganic material in hydroxyapatite crystals form and about 15-20% of the organic matrix consists of collagen whereas, the remaining part is 10-12% of water. The dentin of the mainly formed teeth is called primary dentin. Primary dentin is generally characterized by existence of dentinal tubules where it forms the bulk of the teeth. These tubules commonly radiated from the area of the dentin cementum and dentin enamel junctions to the pulp. They are surrounded by highly mineralized tissue is peritubular dentin. Mineralized pre-dentin lines the pulpal aspect of the dentin. Physiologic secondary dentin forms during the growth of the dentinogenesis, which differs from the primary dentin. As a rule, the secondary dentin creates in response to external irritants is more irregular than the physiologic secondary dentin [30].

The dental pulp shapes the main enteral (focal) chamber of the tooth. The dental pulp is the central soft tissue located in the tooth center. This tissue forms and encourages the dentin layer where it consists of blood vessels, nerves, and other soft tissues, the nerves. As well, there are small lymph vessels and these vessels load white blood cells to the tooth. Incidentally, it's in communication with the periodontium and the rest of the body through the apical foramen of the tooth. There are two main functions of the pulp, the first one is formative where shapes the dentin and provides interact with the dental epithelium to initiate the formation of enamel by allowing rise to odontoblasts. The second function of the pulp is considered by conferring the sensitivity, hydration, and protection to the tooth. So, the dental pulp considers as an important element to regenerate or disinfection operations [31].

The root canal system starts as a funneled slot and ends as the apical foramen. The shape of the canal differs over root form and size, the age and situation of the tooth, and also the degree of bowing. **Figure 2.2** presents the components of the root canal system. When two canals take place in a root, they head for getting oval shape. As well, the number of root canals matches with the number of roots, but an oval-shaped root may have more than one canal. The lateral and accessory canals sustain from the pulp to the periodontium [32]. The lateral and accessory canals improve due to a break-in 'Hertwig's epithelial root sheath' or during enhancing the sheath grows around existing blood vessels [33].

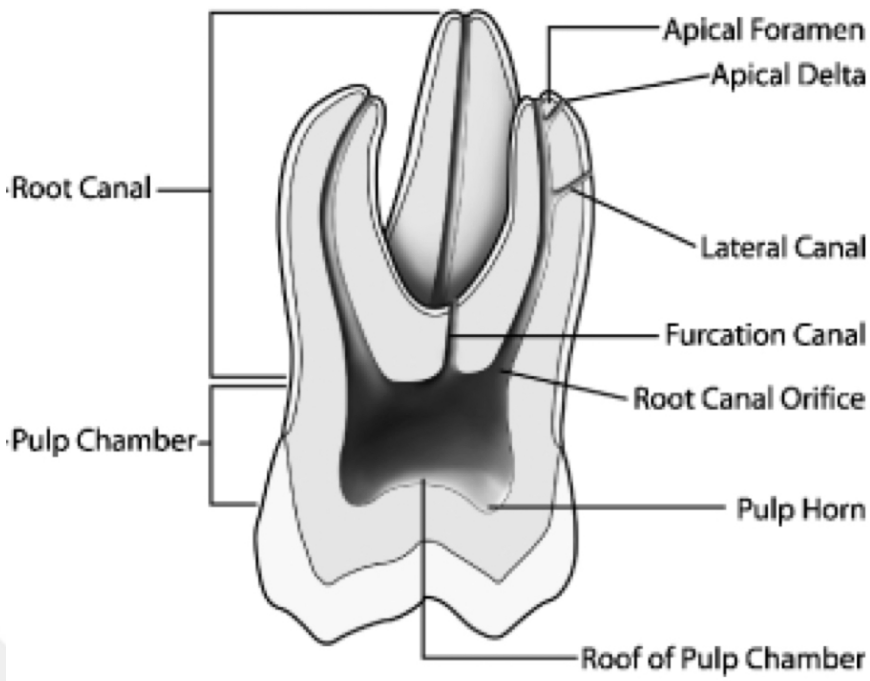


**Figure 2.2.** Schematic of the Root Canal System Components [32]

## 2.3. Endodontic Techniques

Generally, endodontic therapy of tooth contains from three main stages, that can be identical significant for the therapy results, these three stages are preparation for treatment, instrumentation, and obturation of the root canal. The first stage provides the aseptic operation field to tooth treatment. This stage contains the provision of a sufficient access cavity, the safe disinfection of a rubber dam, and the pulp chamber. The aim of the inlet cavity is in order to service as unimpeded access to the root canals of the teeth. The rubber dam step consists of placing a rubber dam on teeth to provide treatment endodontically mainly to protect the patient from incidentally aspirating an instrument, to save the patient from any effect of drugs or irrigating solutions during the treatment process, and to provide a field of operation that can be disinfected. The second stage is root canal instrumentation which is applied to prepare the access cavity, then removing the rubber dam. Regardless of the technique applied, the length of the root canal is determined, extirpation of the pulp and chemo-mechanical instrumentation is achieved. The principle and goals of the chemo-mechanical instrumentation stage during endodontic treatment is the same regardless of instruments or technique used. After these phases, using gutta-percha points is obturated. Here, gutta-percha points are applied for filling the root canal space with various methods.

The most common ones are the thermoplasticized gutta-percha mechanisms, the dipping techniques, the lateral condensation, and the standardized techniques [30], [34]. Gutta-percha has a 60% crystalline structure at room temperature, where it is as the common polymers viscoelastic thus, it has in the same time elasticity and viscous structure. As a result, to present heat on gutta-percha, it softens and deforms then transforms into a liquid structure. Also, it can dissolve in various organic solvents such as chloroform and eucalyptol. Gutta-percha has been used as a filler material for root canals since the 1860s and continued the most commonly applied material for this aim. Nowadays, this material is provided in two types, standardized and accessory points. Standardized ones are synthesized to match standardized root canal instruments with the sizes and shapes and the accessory ones generally have varied shapes according to the using aim. The most important features of gutta-percha are its biological prosperities, it doesn't have a discolor effect on the teeth, doesn't have antibacterial behavior and it is easily interested into the root canal [35], [36].

## 2.4. Dental Stem Cells

Generally, stem cells are undifferentiated cells that have a potential to renew to any cell type and they can give rise to specific types of cells. Stem cells can be classified according to the basis of origin, the basis of source, and the basis of potency. Based on the origin, stem cells dived to embryonic and adult stem cells, based on the source they contain autologous, allogenic, xenogenic, and syngenic stem cells, and based on the basis of potency, they dived to totipotent, pluripotent, and multipotent stem cells. The autologous stem cells are attained from the same individual, allogenic stem cells from the donor of the same species, xenogenic cells from the donor of another species, and the syngenic stem cells from genetically identical organisms [37], [38]. Totipotent stem cells have an ability to differentiate to whole embryonic and extraembryonic cell types, pluripotent stem cells can differentiate to all types of cells except cells of the embryonic membrane, where the multipotent cells can differentiate into more than mature cell [39], [40]. DPSCs can differentiate to multiple stromal cell lines and to their clonogenic capacities. Various in vitro studies demonstrate that these cells show a high rate of colony formation and produce specified nodules. Besides, DPSCs seeded on mechanically and chemically treated dentin surfaces differentiated to odontoblast-like cells. In vivo studies including the transplantation of dental stem cells into immunocompromised mice demonstrated their ability to create

tooth-like tissues consistent with odontoblastic differentiation. DPSC was able to produce a pulp-like texture when the tooth slices were seeded on scaffolds that were poured into the pulp chamber [41]–[43]. On the side, stem cells have many therapeutic applications included many fields of research areas besides the dental field. Stem cells have also been found to be effective in treating other systemic disorders such as thalassemia [44] and breast cancer treatment [45] with a good prognosis rate.

### 2.5. Dental Biofilms

Dental biofilm is any group of oral microorganisms (typically bacteria) that stick together inside the oral cavity. The endodontic disease generally happens due to occurring of infection in the inner side of the root canal system. The microorganisms play a highly important role in infecting and persistence of this type of diseases. The endodontic infections form nearly 40-50% of the general oral diseases. Where pulpal and periapical pathology are the unexceptional configurations of oral diseases. During the whole time that the enamel and cementum layers of the tooth are undamaged, the pulp and root canal are saved from infection. Dental caries is the majority ordinary creator of pulp and periapical harms, according to losing the enamel and cementum layers by caries, trauma, dental intervention, cracks allow to be puncturing the dentinal tubules by bacteria [46].

As well, microorganisms have various ways to enter into pulp space contain dentinal tubules, lateral/accessory/furcation canals, anchoress, and direct exposure such as trauma, and dental procedures [47], [48]. The bacteria start in the root canal system to stick to the dentinal walls, they don't have separated colony forms or planktonic cells but forms with crowded bacterial accumulation recognized as biofilm [49]. The cells of the biofilm create a large amount of extracellular polysaccharide, these polysaccharides enhance the attachment of the cells to the dental walls. Where the biofilm considers as the most ordinary cause of the infections in endodontic, after a period from creating the amount of extracellular polysaccharide, the members of the biofilm detach to the walls becoming planktonic bacteria [50].

The endodontic microorganisms can categorize as primary and secondary infectious bacterizes. In both the primary and secondary infections, the bacteria exist biofilm. 90% of the endodontic infections are caused by *E. faecalis*, and other types isolated in similar

cases *D. invisus, P. propionicum, D. pneumosintes, F. aloci*, and *D. P. alactolyticus* [46]. The primary type of infections is collected of mixed flora, predominately gram-negative anaerobic rods. For example, *A. naeslundii* is an anaerobic, gram-positive, shaped microbe facultative rod that is presented in primary infections [26]. It considers as the main virulence factor which plays an important role in operating an inflammatory reply [51]. Another primary endodontic bacterium established in patients with periodontal disease is *F. nuclestum* [52]. This bacterium is a gram-negative, non-spore-forming spindle-shaped, and acts an important role in the formation of the biofilm and has been related as a middle colonizer according to its own capability to attach to various gram-positive and gram-negative ones [23]. *P. gingivalis* has been presented in around half of the primary endodontic infections, where it is an anaerobic gram-negative and non-motile [53]. Besides, secondary endodontic infections generally happened due to collect mixed flora and this type of bacteria doesn't exist among the initial therapy [54].

### 2.6. The Past and Present Contributions as Preface for Modern Dental Therapy

According to the ideological activities and the mental contributions which were occurred during the eighteenth, nineteenth, and twentieth centuries a lot of principles and standards have been provisioned nowadays for science and technology. Whereas, the quantity and the rate of scientific discoveries increase quickly day by day. Depending on these biological and digital revolutions, the concourse of them with medicine and clinical dentistry is variating and converting many diagnostics and therapeutic methods [55]–[60]. Besides that, many discoveries had appeared related to emerging fields such as microbiology, pathology, physiology, immunology, biology, and the technologies of computer science over the last century. Furthermore, especially the education in both dental and medical fields were truly transformed to another side that includes all of these discoveries and develops, and nowadays we are expecting with enthusiasm the next of major transformation in the health education [61]–[63]. Among the transforming advances which occurred during the last decade, founding identifying informative biomarkers and oral buccal epithelial cells in saliva. Saliva provides direct detection for many antigens like streptococcus group A, several breast cancer biomarkers, influenzas A and B, and zinc-binding cystic fibrosis antigen. On the side, by saliva different types of hormones, organisms, and drugs such as cortisol, insulin, aldosterone, carbamazepine, lithium, caffeine, cocaine,

ethanol, and methadone can be identified and also measured. Currently, due to the convergence of the health fields with the technologic foundations, highly advantageous mini devices like microcapillary electrophoresis, and micro-fluidics are developed in order to diagnosis the saliva. Along with this, the main foundations and discoveries of science and technology are translated to medicine too. Tissue engineering is a synchronous biomedical therapist field focused on enhancing procedures and improving biomaterials for creating and design tissues to exchange harmed tissues and organs. For instance, dentin, enamel, cementum, bone furthermore, periodontal ligament, oral muscle, nerves, and mucosa. Tissue engineering is a field that included stem cell biology, genomics, molecular biology, biotechnology, information, and biomaterials technologies to present more advanced approaches. These approaches provide a bridge between scientific developments and human diseases [57]–[59], [64]–[71]. In comparison with the dental field, the expectance for tooth regeneration is hugely promising. During previous years and depending on various developments to understand the biology, histogenesis, and differentiation of the oral organs, also according to the knowledge of biological essentials, it is becoming more possible to regeneration the oral and tooth organs and tooth replacement [65].

## 2.7. Regenerative Endodontic Therapy

The endodontic therapy of immature permanent teeth presented to trauma or any caries generally is a complex process according to the incomplete root development. This type of teeth is disinfected according to the endodontic treatment [72], then the disinfected canals traditionally are treated with apexification techniques then filled with gutta-percha. But this technique may result in incomplete root development. Consequently, many recent studies were toward to present new therapy technique, this technique named REP. Regenerative endodontic is generally based on the application of stem cells acquired from a dental pulp tissue in order to replace injured root structures, dentin, and pulp dentin complex. The essential contents of REP are using dental stem cells in tissue engineering concepts. These cells are possessing the ability of self-renewal then multilineage differentiation, whereas bioengineering, biology, biotechnology, and clinical basics are carried together in order to regenerate the proposed tissues, continued root development, and apical closure. Besides, regenerative endodontics as scaffold materials in order to support the cells organization, vascularization, differentiation, and proliferation [60].

The main clinical RET steps include chemical disinfection of the canal system without any instruments, followed with an implement of intracanal medicaments during a specific period, intracanal evoked bleeding induction, providing the differentiation of stem cells. The used medicament and irrigant in REPs should have a balance between the antimicrobial activity and can form an intra-canal environment that holds up the differentiation and proliferation of stem cells [73]. Sodium hypochlorite (NaOCl) is one of the most commonly used irrigating solutions. Sodium hypochlorite usually uses with concentrations between 0.5-75. It is a very sturdy antimicrobial agent and effectively dissolves pulpal remnants. Between pH 4-7, chlorine provides predominates as HClO, the active moiety, and up 9 of pH [74]. In 1993, one study reported the procedure of smear layer elimination, during this study 40 rooted teeth were separated into four groups with ten teeth inside every group. The second group considered an irrigation result with 17% of ethylenediamine tetra-acetic acid succeeds by 5.25% of NaOCl in order to eliminate the smear layer. The results showed that calcium hydroxide was removed from the root system toward the outer surface [75]. By an in vitro scanning electron microscopic study, the debridement ability of NaOCl was assessed with various temperatures. After using the NaOCl with two different temperatures 50ºC and 21ºC, they evaluated that the smear layer which was used at 50ºC was thinner and has fewer orderly particles than where it had used at other temperatures [76]. After a few years, another study was reported in order to measurement the effect of various irrigation solutions NaOCl with concentrations of 2.5% and 24 minutes and Ethylene Diamine Tetra-Acetic (EDTA) with 17% and 3 minutes. As a summary, the long period time of the NaOCl is recommended did affect the dentin parameters [77]. Another type of irrigant is EDTA, which is used commonly in the endodontic field. 17%, pH=7 of EDTA has an antibacterial activity, where divorces bacteria's surface proteins through joining with metal ions from the cell warp. This could cause the death of the bacteria [78]. EDTA had a very effective role in eliminating the smear layer too when used with other irrigation solutions such as NaOCl for removal of the inorganic components of the dentin. Besides the effective role of the EDTA on the smear layer, it has also function to eliminate bacteria in the root canal [79], [80]. In 2002, Semra Çalt and Ahmet Serper reported a study to examine the elimination ability of EDTA on the structure of dentin and on the smear layer at the same time. Using 17% of EDTA solution, all the samples were irrigated for two different period times. After that, all the samples were irrigated again with 5% NaOCl. The results of SEM exhibited that the irrigation term with EDTA in order to remove the smear layer should not be more than 1 min [81]. In 2005, was conducted a study aimed to quantify the volume of 17 % EDTA for eliminating the smear

layer after rotary instruments, another aim of this study was to define assuming additional irrigation has any effect on removing the debris. The results of these studies showed that the effective smear layer removal was achieved with a wash by 17% EDTA for 1 min, pursued by 5.25% of NaOCl [82].

Hydrogen Peroxide ($H_2O_2$) is one of the most popular biocides that has uses in many areas for sterilization and disinfection. In endodontics using of $H_2O_2$ is based on antimicrobial aim. For instance, it has used earlier in order to clean the pulp chamber from blood and tissue remnants, and in canal irrigation too. Where it has antimicrobial activity against many types of microorganisms [83].

Chlorhexidine Gluoconate (CHX) has commonly used in disinfection due to its good antimicrobial activity. Especially, in the endodontic area has popularity as an irrigation solution [84], [85]. Otherwise, it is the most commonly used antimicrobial agent in antiseptic products. It shows its own effect on the bacteria penetrating the wall of the cell then attacks the cytoplasm of the bacteria [86], [87].

Intra-canal medicaments are commonly applied in REPs according to their perfect ability to disinfecting the root canals [88]. There are many studies advised that the doses of these medicaments should have the antibacterial effect but at the same time have low harm effects on proliferation and differentiation of the host's dental cells [87]. Many types of intra-canal medicaments were tested and used in clinics, where the commonly applied ones are antibiotics in the paste form like TAP, DAP, and ($Ca(OH)_2$) **Figure 2.3** shows the chemical structures of the antibodies contained these paste forms [89]. Despite many studies recommended using TAP, many studies advised the exchange of TAP by DAP in order to inhibit and minimalist the dentin discoloration effected by MINO [90]. Also, $Ca(OH)_2$ is a strong base (pH 12.5– 12.8), which eliminates the bacteria from the infected root canal by direct contact with it [91]. TAP group was provided ideal antimicrobial behavior with forming a suitable environment for attachment to the stem cells [92]. In addition, other researchers reported that using these mixed medicaments with low doses leads to maximal antibacterial effect too, but minimal effect on dental stem cell viability and proliferation [93], [94], [90].

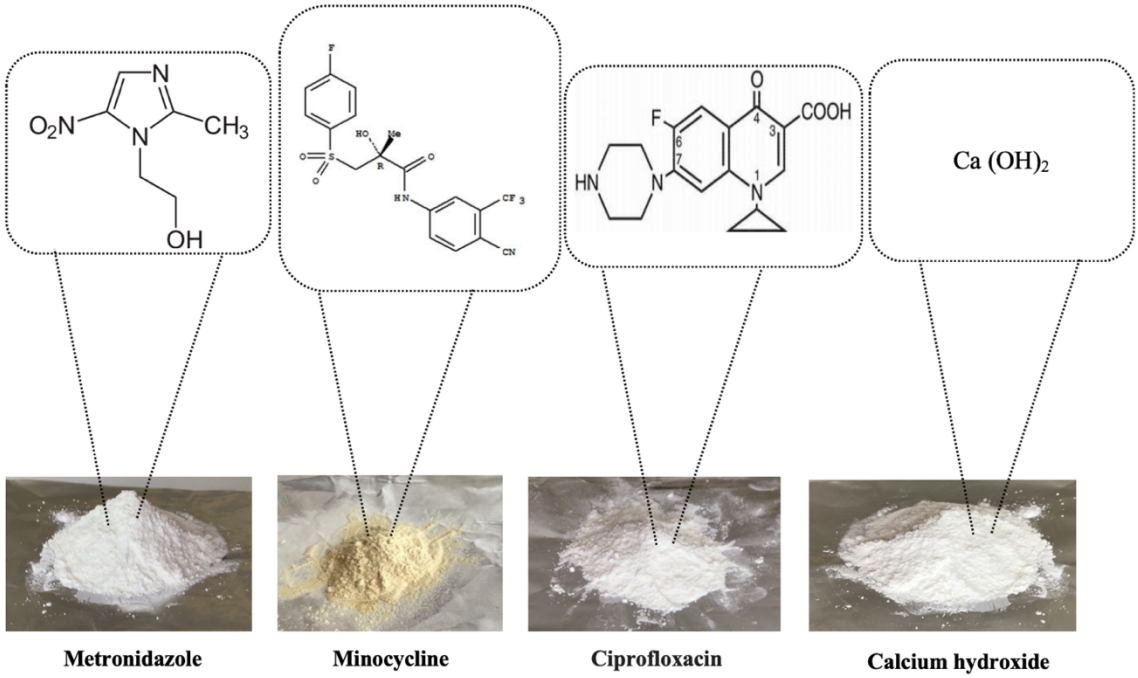


**Figure 2.3.** The Chemical structure of metronidazole, minocycline, ciprofloxacin, and calcium hydroxide

## 2.8. The Emerge of Nanotechnology

Nanotechnology has a magical role in contemporary technological advances in many areas such as diagnosis, drug design, and drug delivery. It joins the activity of biological materials and the principles of basic sciences such as chemical, physics, etc. and also biology, genetics in order to produce nano-sized materials. Nanotechnology can reference as a technology able to develop nanomaterials. Generally, it includes material characterization, design, synthesis, and production of the material and its utilization in industry and technology. Where it depends on producing a single molecule into synthesis materials that exhibit the desired characterization. These materials have critical importance that they have a relatively larger surface area to the volume ratio compared to the bulk materials. In addition, their mechanical, morphology, physical, and chemical features present their unparalleled characteristics. There are many techniques for producing these types of materials such as ‘’bottom-up’’ and ‘’top-down’’. In the top-down technique, smaller devices are formed by applying larger devices to direct their assembly. In the bottom-up technique, smaller ones are coordinated into a more complex structure. The classification of nanomaterials commonly doing based on their dimension (D) (0-D, 1-D, 2-D, and 3-D), chemical composition, materials properties, their application areas, and their morphology

(fiber, particle, tube, and flower). According to the chemical composition of the nanomaterials, they are classified as nano-polymers, nano-ceramics, nano-metals, nano-glasses, and nanocrystals [95]. Nanotechnology has been growing fact in various approaches due to its ability to develop the execution of many systems [96]. It provides the ability to decrease the size [97] and at the same time increase the strength of materials [98], which makes them more suitable for employment in the medical area and other fields [99].

### 2.8.1 Definition of nanofibers

Nanofiber technology is a procedure including the synthesis, manufacturing, processing, and application of the nanofibers. According to this technique of fabrication 1-D nanomaterials, nanofibers have a hopeful method in order to achieve 2-D and 3-D nanomaterials. Generally, nanofibers are materials defined as fibers that have diameters equal to or below 100 nm. These nanomaterials have an essential practical and fundamental importance related to the combination of high surface area, flexibility, and superior directional strength [100], [101]. The reduction in dimension and increase in the surface area strongly effect on the chemical, biological reactivity, mechanical features, and also electro-activity of polymeric nanofibers. According to these protentional features achieved by nanofibers, there is increasing attention in the manufacturing technology of the nanofibers [102]–[104].

### 2.8.2 Unique properties of nanofibers

Reducing the diameters of the electrospun polymeric nanofibers down to the nanoscale range allows us to have many advantages related to increasing the surface area to 1000 $m^2/g$ level. Reduction of the fibers' dimension and increasing the surface area of the same fibers mainly plays an important role in the effecting of the chemical, biological reactivity, and also on the electro activity of the fibers. Thus, according to reduce the diameters to 10 nm, the flexibility of the fibers increases million times. There are magic growth and improvements in this field around the world to integrate this high impact technology in different applications.

#### 2.8.2.1 Fiber's size effect on surface area

One of the most important characteristics of the nanofibers is the huge availability of the surface area per one mass unit **Figure 2.4.** The fibers having 5-500 nm, their surface area in one mass unit is about 10 000- 1 000 000 $m^2$/Kg. As a result, the high surface area of the nanofibers presents an exceptional ability to release functional molecules had loaded them [105].

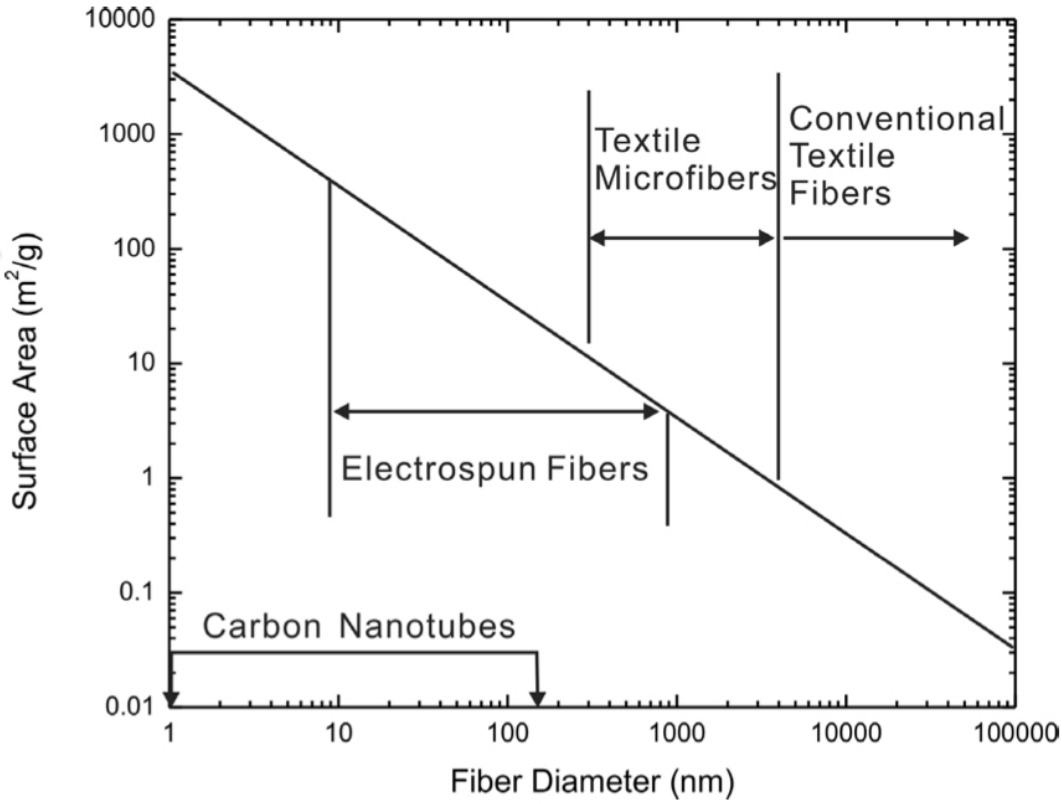


**Figure 2.4.** Surface area to fiber diameter elation [105]

#### 2.8.2.2 Fiber's size effect on electro activity

The surface plays an important role in adhesion and migration the cells carried them **Figure 2.5.** The small fiber diameters provide great viability by present a surface for the cell's attachments, thus growth differentiation and proliferation [105].

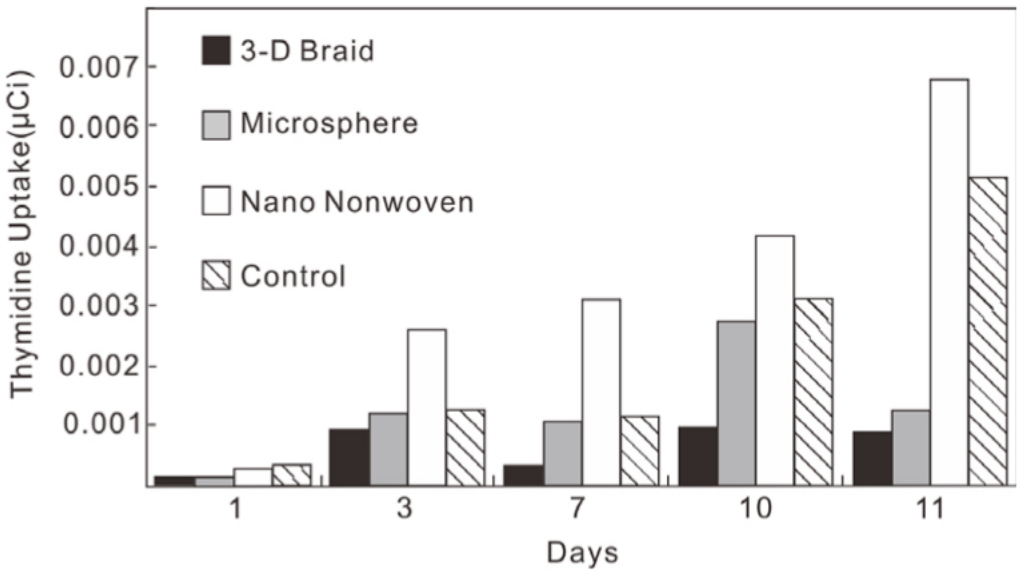


**Figure 2.5**. The relationship and effect of nanofibers size on cell growth [105]

#### 2.8.2.3 Fiber's size effect on bioactivity

The conductivity of the fibers directly affects the packing density and the geometric surface **Figure 2.6.** So, the size of the fiber conductive has enormous importance and effect on the time of the systematic response [105].

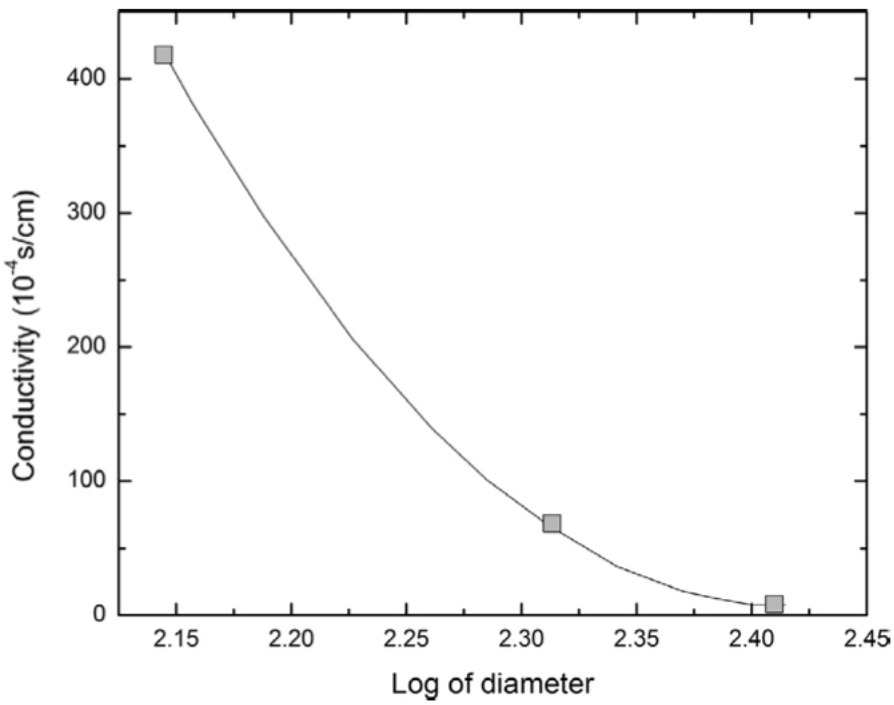


**Figure 2.6.** Effect of fiber diameter on the electrical conductivity of the fibers [105]

#### 2.8.2.4 Fiber's size effect on strength

The nanofibers generally are stronger than the bulk materials due to their unique structures. According to a decrease in the diameter of the fibers, the strength of the fibers increases via the reduction of the probability of having any flaws in **Figure 2.7** [105].

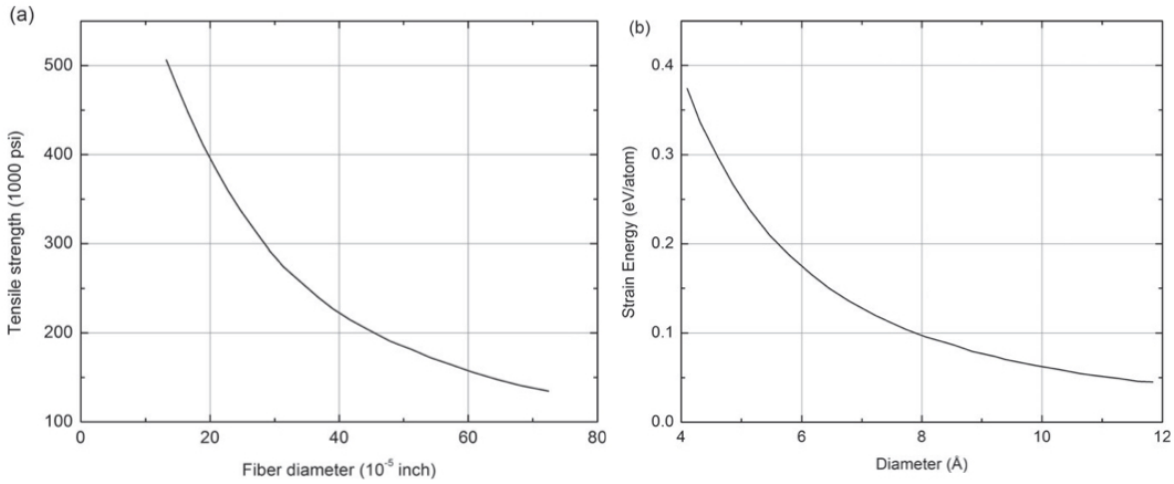


**Figure 2.7.** Effect of nanotube diameters on (a) the glass fiber strength, and (b) strain energy [105]

### 2.8.3 Nanofibers design and fabrication methods

#### 2.8.3.1 ElectrospinningtTechnique

Electrospinning is a fiber synthesis technique in the range from micro to nanometer by applying a high voltage electric field. The applied electrospun nanofibers have unparalleled features such as the high value of surface-volume ratio and easy to spin into various shapes. The electrospinning basic setup mainly involves three essential contents: a high voltage power supply, an electrically conducting spinneret, and a collector separated at a defined distance **Figure 2.8** [105]. During the electrospinning process, an electric field is applied among a grounded collector and another capillary. In order to form the intensity of the electric field larger than one of polymer solution surface tension, the polymeric solution starts to inject toward the grounded collector and forming the fibers.

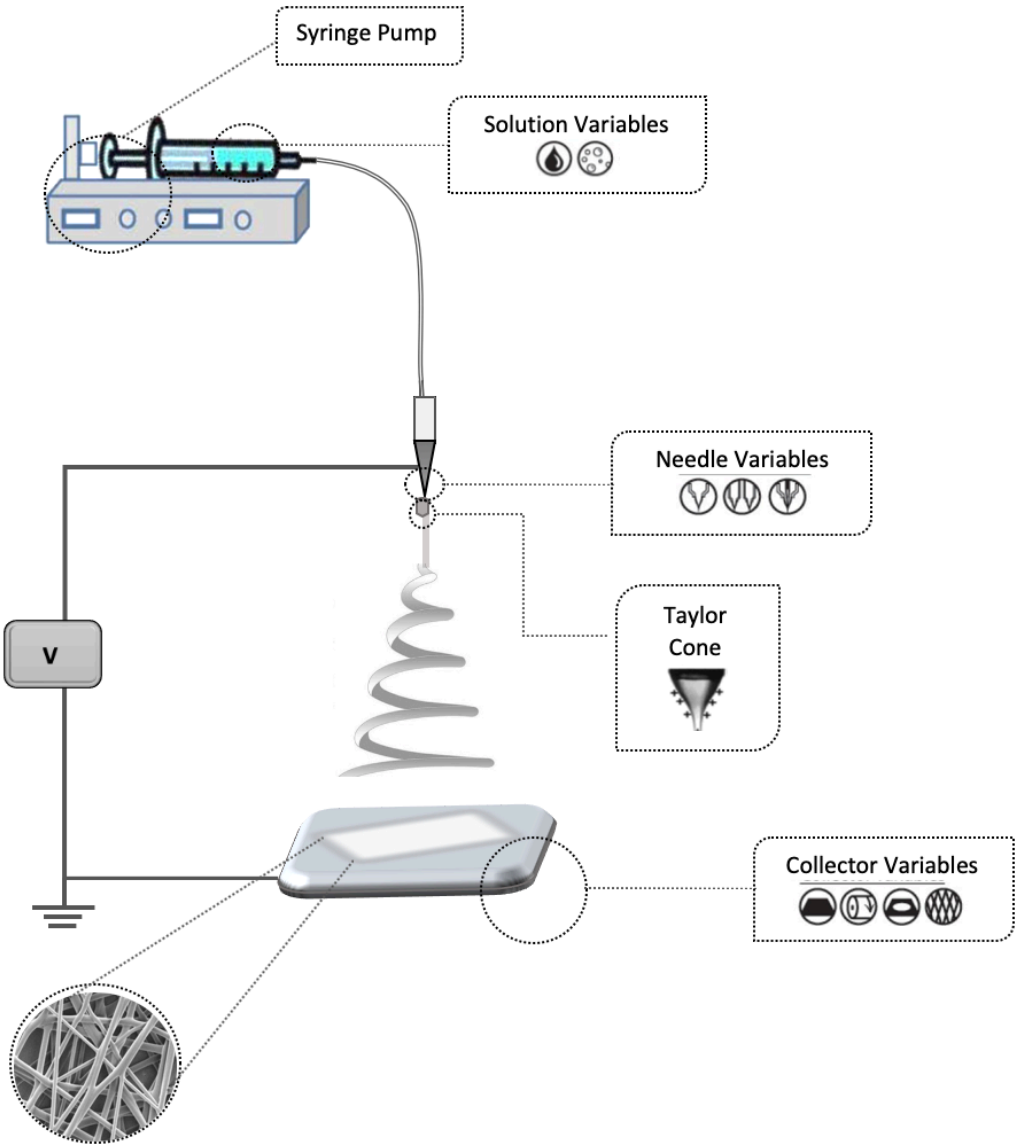


**Figure 2.8**. Electrospinning Setup

When a high voltage (typically in the 0-30 kV range) is used to a nozzle which is electrostatically charged, the liquid surface droplet held with its tension. Then, the drop falls down the influence of two electrostatic forces. By these electrostatic interactions, the liquid drop extends into conical object called a Taylor cone. When the density of the electric field reaches a certain critical value, the electrostatic forces overcome the surface tension of the polymer solution and force the jet of liquid to eject from the tip of the Taylor cone. The liquid jet continues to be ejected in a steady manner. Before arriving the screen of the collector, the solvent evaporates, leading to the formation of polymeric fibers on the collector **Figure 2.9** [106].

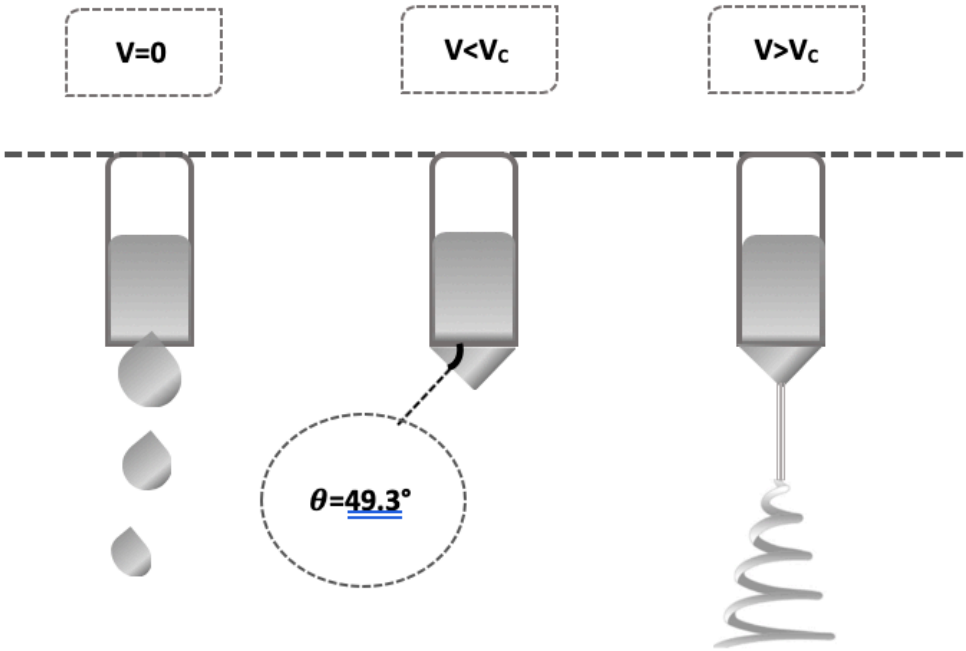


**Figure 2.9.** Formation of Taylor Core

#### 2.8.3.1.1 Prosperities of polymer solutions

One important parameter of the polymer is the relative molecular mass. Where it is affecting the electrospinning process due to its direct effects on rheological and electrical electrospinning prosperities. Generally, when the polymers have low molecular mass, during electrospinning fibers beads forms and increase the polymer molecular mass, fibers form with a uniform diameter. The second property is the viscosity, which is considered one of the most important and necessary features for the solution in order to synthesize fibers the electrospinning method. The viscosity **Figure 2.10** of the solution increases according to an increase in the concentration of the polymer. So, during the electrospinning process should control the viscosity of the polymer that is should be in a specific range. The surface tension of the polymer solution is an important property which has a major role in forming the fibers with electrospinning. So, the electrostatic power on the charged polymer solution surface should be larger than its surface tension. An essential factor during the electrospinning process is the conductivity of the polymer solution which is related to the polymer electrocution ability. Where, this feature may directly affect the morphology of the fibers, and it increases according to the increase the electric quantity solution carried it. However, the solvents used in the solution should have some of the features such as; volubility,

conductivity, solubility ability to the polymers. In addition, the electrospun fibers' diameters decrease related to increasing the solvent conductivity ability [105], [107].

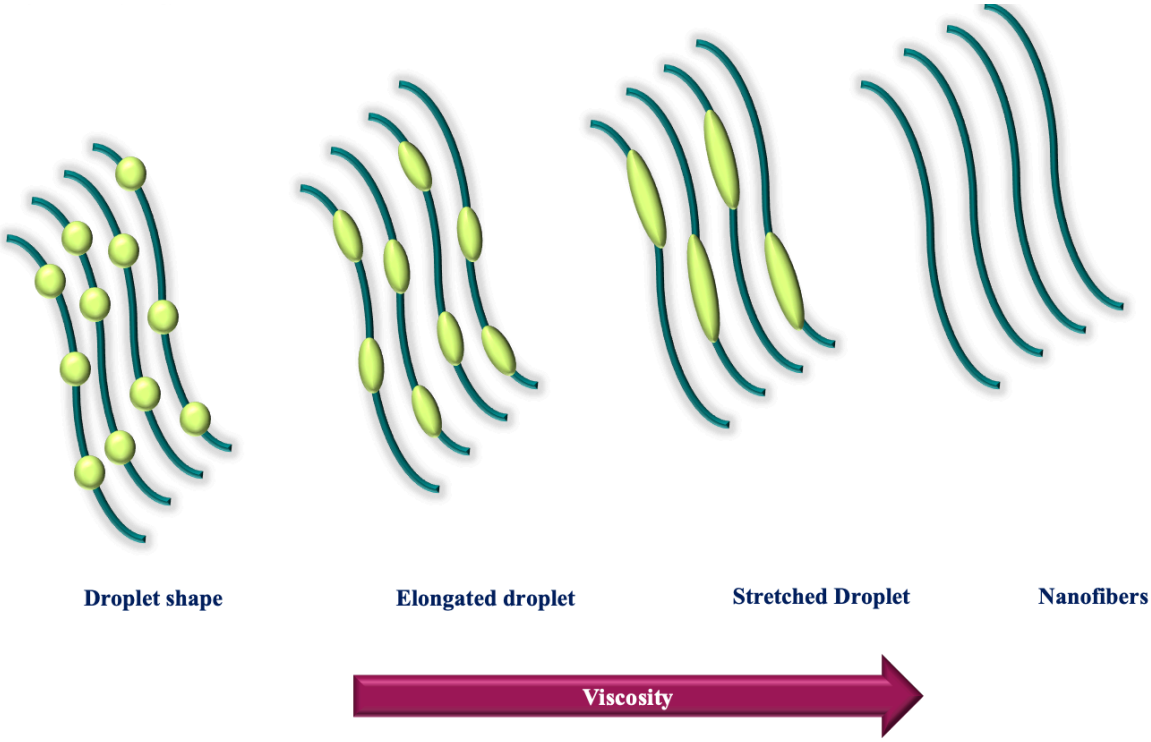


**Figure 2.10.** Effect of polymeric solution viscosity on the nanofiber morphology

#### 2.8.3.1.2 Process parameters

The electrospinning process mainly has some essential parameters which are played an essential role in achieving the nanofiber materials. The first one is the applied voltage on the polymer solution that is passed a specific value to form a micro-jet that creates the fibers. During apply higher voltage, the diameters of the achieved fibers will be smaller, but the number of the beads in the mats' surface is higher. The flow rate of the solution is another important process parameter that is affected directly on the last shape of the electrospun fibers and determines the spinnable solution amount in the process. The diameters of the jet are increase related to increase the flow rate of the solution and to stabilize the voltage and when the flow rate be lower, the solvent evaporates and leads to accelerate the material transfer rate. Another essential parameter is the distance between the syringe nozzle and the grounded collector which directly affects the degree of solvent volatilization and controls the morphology and sizes of the will achieve fibers [107]. So, according to increase the distance between those two components the fibers' diameters will be smaller because the

solvent can be evaporating more. At the same time, the strength of the electric field will be decreased according to increase distance and lead to decrease jet velocity leading to larger diameters of the fibers **Table 2.1** [105].

**Tablo 2.1**. Affecting parameters on morphology of electrospun polymeric nanofibers

| Parameters | Effect on fiber morphology |
|---|---|
| Processing parameters | |
| Voltage | Fiber formation, sometimes with beads formation |
| Spinning distance | Fiber formation with optimal distance<br>Bead formation with too short or too far distance |
| Flow rate | Fiber formation with optimal flow<br>Bead formation with very high feed rate |
| Solution parameters | |
| Molecular weight | Beads and droplet formations |
| Polymer viscosity | Bead formation<br>Fiber formation with optimal diameter |
| Solution conductivity | Uniform bead-free fibers |
| Environment parameters | |
| Temperature | Fiber diameter and viscosity |
| Humidity | Generation of circular pores on the fibers |

#### 2.8.3.2 Non-electrospinning techniques

Besides electrospinning, that is based on the use of electrostatic force and is the most frequently used one, other non-electrospinning methods are developed, such as phase separation, drawing, self-assembly, and template synthesis production method among others. The phase separation method has a few advantages, such as the ability to control scaffolds mechanical, and morphological properties. Just by changing the freezing temperature, polymer type, and concentration, nanofiber matrix properties can be controlled. The negative side would be its incapability to produce long continuous nanofibers and restriction to a few polymers (PEG, PLLA) that can be converted into nanofibers with this

method, the reason being that not all polymers have the capability to undergo complete phase separation [108]. The drawing nanofibers method was first introduced in 1998 and are a process of drawing nanofibers from a single polymer solution droplet by micropipette pulling at a certain rate determined by the polymer type [108]. The biggest advantage of this process is that it allows studying the properties of a single nanofiber with the minimal need for other devices. On the other hand, the biggest withdraw is that only those polymers that have high enough viscoelastic properties to resist deformation and disruption developed during pulling and individual nanofiber formation can withstand the developed stress. The self-assembly method is a nanofiber fabrication process with a bottom-up approach which is designed to assemble smaller units into more complex systems. The idea of this method is to put molecules together by noncovalent bonding, hydrogen bonding for an instance, and form a stable hydrogel structure. The process is suitable for the production of nanofibers small in diameter (up to 100nm), though it is complex, laborious, and arduous [108]. The template synthesis method is based on the chemical or electrochemical oxidative polymerization where a template or mold is used in order to form solid or hollow-shaped nanofibers.

#### 2.8.3.3 Poly(vinylpyrrolidone) PVP

Poly(vinylpyrrolidone) (PVP) is a very commonly used synthetic hydrophilic polymer excipient in pharmaceutical applications. Poly(vinylpyrrolidone) is the first polymerized product of N-vinylpyrrolidone produced by a free radical mechanism **Figure 2.11.**

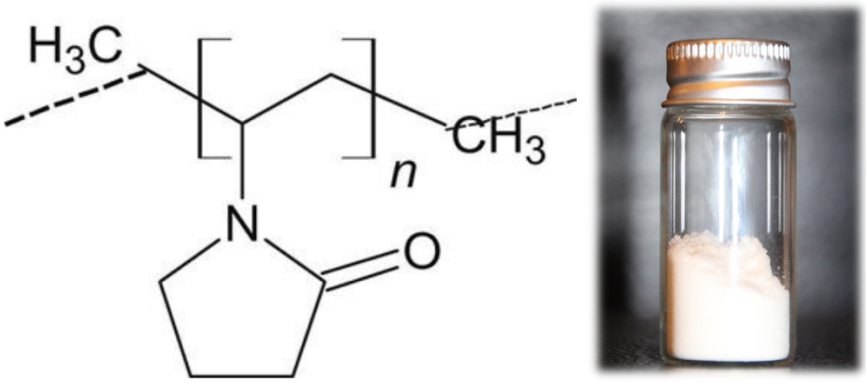


**Figure 2.11.** The Chemical Structure of Poly(vinylpyrrolidone)

PVP has many prosperities that make it very common applied polymer such as; chemically inert, non-toxic, water-soluble, temperature-resistant, biocompatible, nonionic, pH-stable, and colorless. In dry form, it is a light flaky white to yellowish-white hygroscopic powder with different particle sizes, which absorbs up to 40% of water by its weight.

PVP is a cross-linked homo-polymer of pure vinylpyrrolidone where it has a soluble feature in the polar solvents like methanol, ethanol, and also in water. PVP has molecular weight ranged between 2500 to 2,900,000 Daltons related to the technology applied in order to synthesis it. As the most polymers, the density of PVP changes related to increasing the concentration of the polymer. PVP is thoroughly applied in different fields such as pharmaceutics, medicine, electrical applications, membranes, and food industries. This polymer has various prosperities make it one of the most used synthetic polymer such as; chemical stability, good solubility in water and many organic solvents, nontoxic, affinity to complex both hydrophobic and hydrophilic substances [109].

## 2.9. Electrospun Nanofibers as Drug Delivery Systems for Regenerative Endodontic

There are two widespread techniques for drug delivery, oral and vascular ways, but they are not the most effective methods for some special therapies. These traditional drug delivery techniques have various side effects and disadvantages like toxic side effects on the healthy tissues, dissolution of the applied drugs before arriving at the target point, and the low biological effectiveness of the drugs at the target point too. Besides that, the drug delivery systems are intended to provide the dispersion of the drug by a style able to interact its main fraction only with the target tissue and to provide the wanted kinetics for a special time. Therefore, by this method, problems incorporated with the traditional techniques can be overcome. The release rate of drug delivery systems can handle by controlling the features of the carrier, the type of drug carrier system, and the prosperities of the used drug. Another using stimulants to control the release rate of the drug, temperature, the type of release vehicle, ionic strength, pH, magnetism, and ultrasound. By enhancing the design of the drug delivery system, the used drugs can selectively deliver to the aim site with the necessary doses without any side effects on the healthy organs and tissues. The electrospinning technique is applied under controlled factors and parameters and can produce different materials with different shapes and sizes. This technique has several mechanisms to integrate therapeutic antibiotic release systems; coaxial, emulsion, blending, and surface uploading

by electrospinning **Figure 2.12.** There has been major attention of polymer-based nanosized carriers in biomedical applications, such as dendrimers, liposomes, nanoparticles, nano-gels, and NFs for therapeutic drug delivery [110]. In the pharmaceutical area, these nanocarriers have been helped to enhance the therapeutic efficacy and minimizing the troubles of the drugs due to their properties such as smart, targeted, and controlled release. Besides, they have also played an important role to enhance the potency of various suboptimal but pharmacologically active moieties that were previously excluded from the drug development pipelines [111].

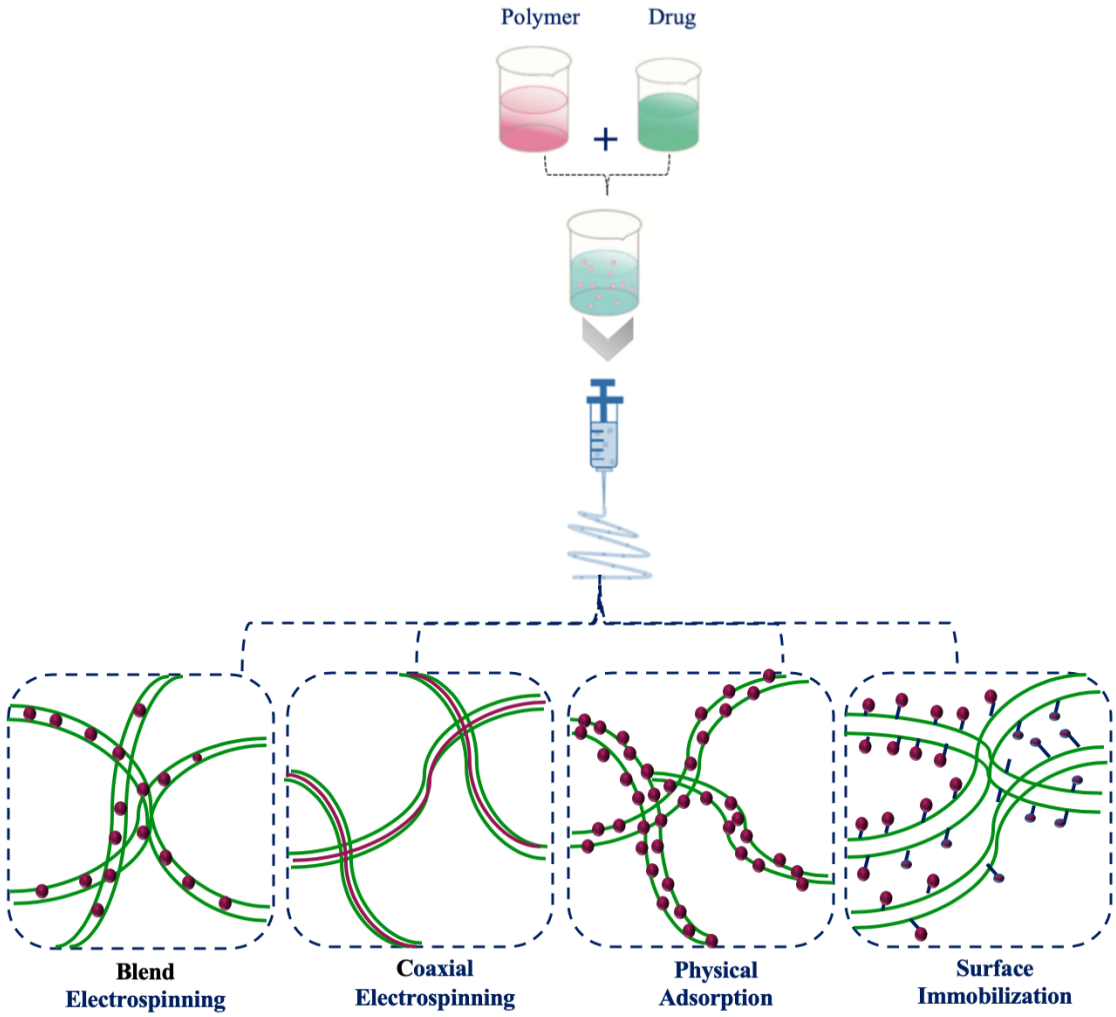


**Figure 2.12**. Drug loading electrospun polymeric nanofibers with four different techniques

Antimicrobials can act negatively on dental stem cells through the interaction of residual drugs that migrate to the apical papilla during entry into the root canal system and/or stem cells migrating to the pre-created blood clot. Of the DAP's two combinations, no alteration in either viability or proliferation of MET-only including scaffolds was observed.

Although studies have shown that MET is responsible in vitro and in vivo for dose-dependent cytotoxic effects [112], it has been shown to support the viability of eukaryotic cells. MET has been provided increasing the proliferation of lymphocyte. One reasonable statement is that through the release of inflammatory cytokines MET could modulate proliferation as monitored in human periodontal ligament cells [113]. Thus, despite its certain antimicrobial features, may also be counted to be a potential inducer to stem cell proliferation when released locally to remove the infections of root canals. An inhibitory impact of all polymeric scaffolds loaded CIP was observed on the viability and proliferation of human dentin pulp stem cells. Recently, a necessary reduction in the viability of human dentin pulp stem cells for all samples exposed to CIP with a dose-dependent trend, where the lowest toxicity was shown in cells exposed to scaffolds with (3:1 MET/CIP).

As a choice, DAP including CIP and MET is used to evaluate both the drug delivery profile and the impacts on human dentin pulp stem cell viability and proliferation of double antibiotic-including scaffolds. A CIP/MET release was recorded during the first 24 hours, followed by continuous maintenance of the antibiotic's concentrations for 14 days. As a result, the purpose of antibiotics loaded scaffolds had a significantly lower effect on human dentin pulp stem cells proliferation compared to CIP/MET solution DAP [114]. Palasuk et al. synthesized a double antibiotics-containing scaffold in order to eliminate bacterial growth inside the root canal system. Synthesized scaffolds showed sufficient mechanical properties that could be handled and ultimately placed in the root canals. Morphologically, the average fiber diameter was in the nanoscale range and was even smaller than pure PDS. This provides a potential benefit because the smaller diameter creates more surface area and theoretically more drug release over a longer period [115].

The triple antibiotic paste is an incorporation of three different antibiotics such as CIP, MINO, and MET. Triple antibiotic pastes were introduced by Hoshino et al. who recommended that the use of three different antibiotics in the single antibiotic paste can provide effective elimination of the microorganisms developed in the root canal system [116].

The idealistic carriage for antibiotics delivery in the root canal system should have the ability to provide better release of the antibiotics through dentinal tubules and anatomical aberrations like lateral canals or isthmuses. Based on the mentioned information, successful pulp-dentin regeneration is highly dependent on the effective elimination of the

microorganisms from the root canal system [117]. Recently, using antibiotic mixtures such as TAP has gained a high interest due to their disinfection role within intra-canal [118]. The most common used triple-antibiotics mixture for regeneration and disinfection of intra-canal is a blend of CIP, MET, and MINO paste. Different studies have shown the antimicrobial efficacy of TAP on the root canal system. Nonetheless, they are founded that the previously recommended clinical doses of TAP (1 g/mL) had a highly toxic effect on dental stem cells [87]. Also, studies have shown other obstacles related to not effectively remove TAP from root canal systems [119]. The interfere of TAP with growth factors release which could inhibit the regeneration of the dentin matrix and the discoloration of the crown [120]. According to the critical need for a strategy able to disinfect the canals without any harm to differentiation and proliferation of dental stem cells and growth factor release, Pankajakshan et al. [94] have developed triple antibiotic-containing nanofibers (TA-NFs) to discuss its antimicrobial effects on a dual-species biofilm and its ability to proliferate and adhere dental pulp stem cells. CLSM test showed significant bacterial elimination on a triple antibiotic (30wt%) containing polymer NFs compared with antibiotic-free NFs. About the cell proliferation, SEM images showed higher rates on dentin treated with TA-NFs on day 7 and the spreading of the stem cells showed enhancing with it too compared with TAP solution (50 mg/mL). Some studies were compared the clinical use of clindamycin as an intra-canal medicament with $Ca(OH)_2$ and TAP, which presented no significant difference between data at 200 and 400 μm in all groups except the $Ca(OH)_2$ group. It is mentioned that the antibiofilm effect of clindamycin was comparable with TAP, so it may be used instead of TAP. Besides, $Ca(OH)_2$ didn't show any cytotoxic effect on dentin stem cells, but during a few weeks, it can affect negatively on the physical and mechanical prosperities of the dentin surface [121].

## 2.10. Electrospun Nanofibers Characterization Techniques

Understanding the prosperities of synthesized fibers such as chemical structure, mechanical features, and their morphology is an important stage after the synthesizing process because they help to figure out the nanofiber's materials and how much the design and synthesis processes are effective. To measurement and evaluate the synthesis processes, the composition, structure, and physical properties should characterize in order to determine if the developed fibers are suitable for their special applications. There are various

mechanisms applied in order to characterize different materials to provide wide figuration about the quality of the materials and how we can provide and enhance them if have been any drawbacks [105].

### 2.10.1 Structural characterization

There are many morphological characterization methods like scanning electron microscopy (SEM) **Figure 2.13**, transmission electron microscopy (TEM), optical microscopy (OM), atomic force microscopy (AFM), and scanning tunneling microscopy (STM). This type of technique is mainly used in order to measure and determine the fiber's diameters, figure out the fiber's morphology, pore size, etc [105].

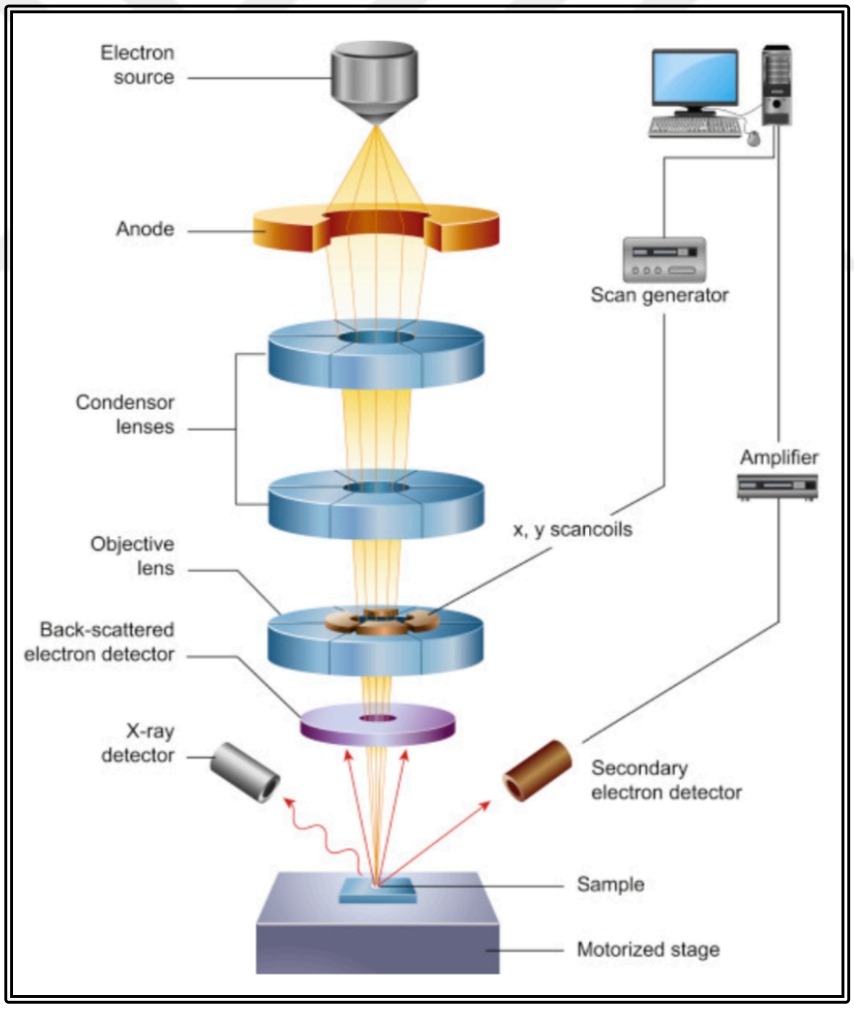


**Figure 2.13.** Schematic of the general parts of SEM device [122]

### 2.10.2 Mechanical characterization

Mechanical properties of materials show us their characteristic responses to applied loads in order to test their tensile, strength, and breaking prosperities. These tests tend to whole appearances of the science-technology materials. Related to how the loads are applied to the materials, they have different responses of deformation models such as tensile, compression, bending, shear, and torsion [105].

### 2.10.3 Chemical characterization

Fourier transform infrared (FTIR) spectroscopy transfers the detector output to an interpretable spectrum and forms spectra with patterns that provide structural insights. A Fourier transform infrared spectrometer is a Michelson interferometer with a movable mirror. By scanning the movable mirror over some distance, an interference pattern is produced that encodes the spectrum of the source, which turns out to be its Fourier transform [105].

# 3. Materials and Methods

## 3.1. Materials

Poly(vinylpyrrolidone) (437190-500G) (Mw=1,300,000), $(C_6H_9NO)_n$ was obtained from Sigma-Aldrich (PVP, Sigma-Aldrich, St. Louis, MO, USA). Ethyl Alcohol solvent **Figure 3.1** was purchased from Sigma-Aldrich (Et-OH, Sigma-Aldrich, St. Louis, MO, USA) too. The antibiotics MET ($C_6H_9N_3O_3$), CIP ($C_{17}H_{18}FN_3O_3$), MINO ($C_{23}H_{27}N_3O_7$), and $Ca(OH)_2$ **Figure 3.2** were obtained from Spot Dis Store (MET, CIP, MINO, $Ca(OH)_2$ , Spot Dis Store, St. Izmir, Turkey). Gutta-percha cones (size: 50/.02) were obtained from Pearl Dent Company (Pearl Dent Co., Ltd. Gyeonggi-Do, Korea). About the Electrospinning device was fabricated by BIMAG, Prof. Dr. Dilek Cokeliler Seradroğlu research group (Nanotechnology& Nanomaterials Laboratory, Baskent University, Ankara, Turkey).

**Figure 3.1.** The applied Ethyl Alcohol solvent and Poly(vinylpyrrolidone) Polymer

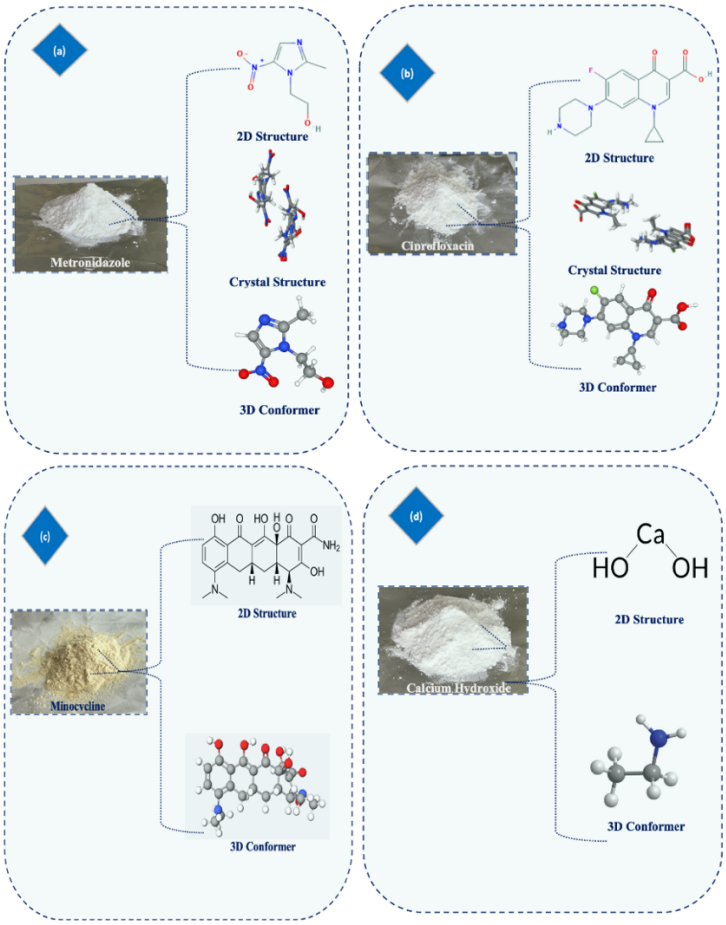


**Figure 3.2.** 2-D structures, 2-D conformers and 3-D conformer of the chemical structures of a) MET [123], b) CIP [124], c) MINO [125], and d) $Ca(OH)_2$ [126]

### 3.2. Pre-experiments

For optimizing of PVP nanofibers loaded different medicaments with defect-less, bead-less, and uniform structures many pre-experiments had achieved. First of all, different medicaments used in this thesis were approached in the solid tablet form and they were grinded into powder form **Figure 3.3.**

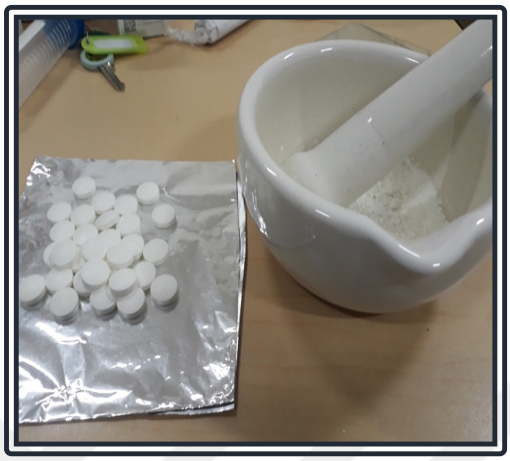

**Figure 3.3.** Preparing the antibiotic powders

Et-OH was used to dissolve of 8%(w/w) concentration of PVP powder with 20% and 25%(w/w) separately of MET medicament. The PVP-MET solutions were stirred for two overnight at the room temperature. The second pre-experiment group, 8%(w/w) of PVP powder was dissolved in Et-OH with two different concentrations of CIP separately. The PVP solutions with 20% and 25%(w/w) of CIP concentrations were stirred for two overnight too. The last pre-experiment group had two different concentrations of $Ca(OH)_2$ dissolved in Et-OH with 8%(w/w) of PVP powder separately. PVP-20% and 25%(w/w) of $Ca(OH)_2$ were stirred at the room temperature for two overnight too. In order to synthesis monolayer nanofibers, the single nozzle was used through electrospinning system, which can be seen in **Figure 3.4.**

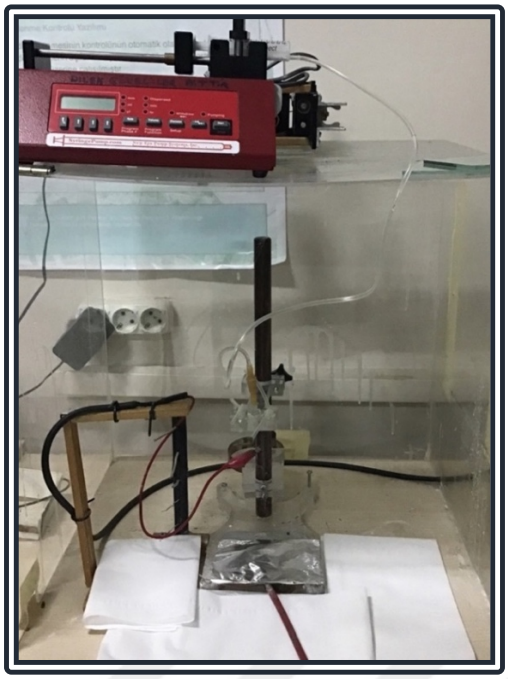

**Figure 3.4**. Electrospinning Device

Previously prepared polymeric solutions were filled in a plastic syringe (2 ml) (Set medical, Turkey) then connected to a metallic nozzle. Solutions were infused to the nozzle end with syringe pumps in a controllable manner of flow rate. A high voltage (0-40 kV) was applied for spinning the polymer solutions which infused the syringe pumps between the nozzle and the grounded collector with (15 cm) distance at the electrospinning device. The grounded electrode of the system was connected to the conductive collector and the positive electrode was connected too to the metallic needle. Electrospinning process was achieved for all pre-experiment sample groups by applying the parameters 0.9 $ml.h^{-1}$ of flow rate and for 15 second at the room temperature. The produced electrospun nanofiber webs were collected on an aluminum foil for each sample, separately.

Consequently, the morphology of all prepared nanofiber mats was achieved by scanning electron microscope (SEM, FEI-Quanta 200 FEG) after coated with gold-palladium (Au/Pd) for 60 seconds. The diameters and distributions of the nanofibers were measured via imageJ software (SmartSEM, Zeiss) by choosing 80 fibers from each SEM image randomly. The collected data were transferred to OriginPro software for further analysis of electrospun nanofibers distributions. The chemical characterization of the prepared samples was obtained by energy dispersive X-Ray device (EDX) detector (SEM-EDX, SU1510, Hitachi, Japan, Ordu University, Turkey), then the collected data transformed to EDX TEAM™ software.

## 3.3. Preparation of Electrospinning Solutions

### 3.3.1 Preparation of poly(vinylpyrrolidone) solution

Bare-PVP nanofibers group was used as a control group to compare the differences after adding specific medicaments to the other samples. Et-OH solvent was used to dissolve 8% (w/w) concentration of PVP powder. Then, the solution left to stir on a magnetic stirrer **Figure 3.5** and it was kept safe from air contact for two days at the room temperature.

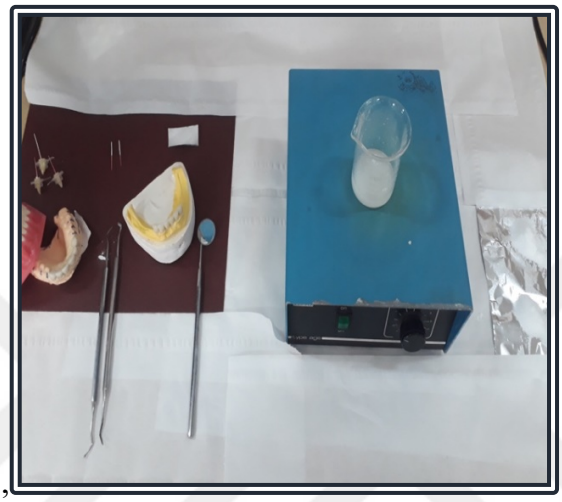

**Figure 3.5**. Bare-PVP solution preparing process

### 3.3.2 Preparation of single antibiotic-poly(vinylpyrrolidone) containing solutions

According to the pre-experiments in this study, different MET concentrations were used to obtain the purpose MET-PVP nanofiber samples. One of them was dissolved with 8%(w/w) of PVP powder in (17.9g) Et-OH as 2.5%(w/w) concentration. The 2.5% MET-PVP solution was stirred two nights on the magnetic stirrer at the room temperature. During the mixture process the solution was saved from the air connect. After two days, the polymer solution was filling in 2 mL plastic syringe and connected to the electrospinning system with tubing. The second concentration of the MET was 5%(w/w), the MET and 8% (w/w) PVP powders were dissolved in (17,4g) Et-OH at the room temperature. The polymer solution was lift to magnetic mixture with saving from the air contact for two nights, too.

The third sample of MET-PVP combination had 7.5%(w/w) of MET powder and 8% of PVP powder. These powders were dissolved in (16.9g) Et-OH and were stirred for two days on the magnetic stirrer **Figure 3.6** at the room temperature. For the last sample, Et-OH was used again to dissolve of 8%(w/w) PVP with 10%(w/w) of MET at the room

temperature. After two days from stirring the solution samples on the magnetic stirrer, each of the polymeric solutions were connected to the electrospinning system by plastic syringes.

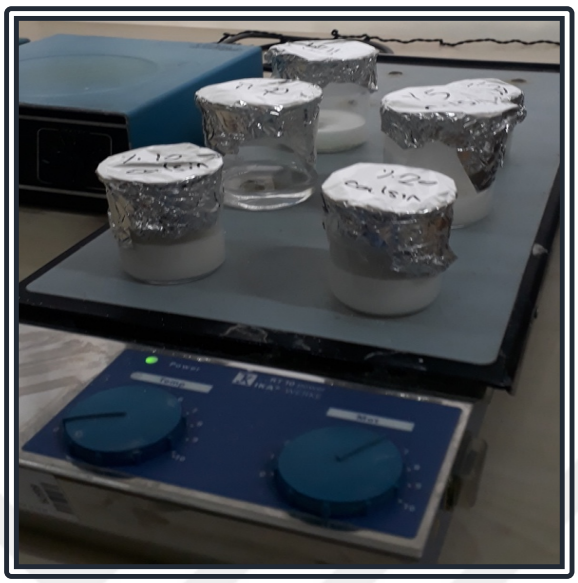

**Figure 3.6.** Polymer solutions on the magnetic stirrer

In order to prepare CIP-PVP containing solutions firstly, (18.2g) Et-OH was used to dissolve 1%(w/w) of CIP powder with 8%(w/w) of PVP powder at the room temperature. 2.5% and 5%(w/w) concentrations of CIP powder were mixed separately with two different 8%(w/w) PVP samples and dissolved in (17.9g) and (17,4g) of Et-OH, respectively. All the prepared solutions were stirred at the room temperature for two nights without any contact with the air. The last example had 7.5%(w/w) of CIP and 8%(w/w) of PVP powders, these powders were dissolved in Et-OH too as a solvent. The polymer solution was lift on the magnetic stirrer at the room temperature for two nights. After 2 days, all the polymer solutions were filling in 2 mL plastic syringe and connected to the electrospinning system.

### 3.3.3 Preparation of double antibiotic-poly(vinylpyrrolidone) containing solutions

The 5% (w/w) double antibiotics-PVP solution was prepared by dissolving 5%(w/w) of antibiotic powder with 8%(w/w) of PVP powder in (16.4g) Et-OH. After totally mixing of the powders, the polymer solution lifts to stir on the magnetic stirrer at the room temperature for two overnights. During mixing process, the polymer solution was saved from the air contact at the room temperature. The second sample of double antibiotics-PVP had 7%(w/w) of each MET and CIP powders and 8%(w/w) of PVP polymer powder. Et-OH

was used to dissolve the powders in 16g. This solution lift to stir for the same period and in the same conditions. The next polymer solution of double antibiotics-PVP was prepared by dissolve 9%(w/w) of each antibiotic powder with 8%(w/w) of PVP powder in 14,8g of solvent. The last sample was prepared by dissolve 11%(w/w) MET and 11%(w/w) CIP in Et-OH with 8%(w/w) of PVP and they were stirred at the room temperature for 2 overnights. After two days, all solutions were filling in 2 mL plastic syringe to connect them the electrospinning system.

### 3.3.4 Preparation of triple antibiotic-poly(vinylpyrrolidone) containing solutions

5%(w/w) concentration group of triple antibiotics-PVP solution was prepared by dissolving 5%(w/w) of MET, 5%(w/w) of CIP, and 5%(w/w) of MINO powders with 8%(w/w) PVP in 15.4g of Et-OH as a solvent. After totally mixing of these powders, the polymer solution lifts to stir on the magnetic stirrer at the room temperature for the same period applied for the previous groups. The second sample of triple antibiotics-PVP had 7% (w/w) of each MET, CIP, and MINO powders with 8%(w/w) of PVP powder. Et-OH was used to dissolve the powders in 14,6g. This solution lifts to stir for two days too. The next polymer solution of triple antibiotics-PVP was prepared by dissolve 9%(w/w) from each antibiotic with 8% (w/w) of PVP powder in 13g of Et-OH. The last sample was prepared by dissolve 11%(w/w) of MET, CIP, and MINO with 8%(w/w) of PVP. During the mixture process, all the polymer solutions were saved from the air contact and stirred at the room temperature for 2 days. After two days, all solutions were filling in 2 mL plastic syringe to connect them the electrospinning system.

### 3.3.5 Preparation of calcium hydroxide-poly(vinylpyrrolidone) containing solutions

The concentrations that used for Calcium Hydroxide-Poly(vinylpyrrolidone) samples were 2%,3%, 4%, and %5(w/w) of Calcium Hydroxide powder mixed separately with 8%(w/w) of PVP powder for each sample separately. Et-OH was used to dissolve each powder complex in 18g, 17.8g, 17,6, and 17,4g, respectively. The polymer solutions were lifted to stir on the magnetic stirrer at the room temperature for 2 days with saving them from the air contact. After 2 days, all the polymer solutions were filling in 2 mL plastic syringe again and connected to the electrospinning system.

## 3.4. Electrospinning Process

To fabricate monolayer nanofibrous mats for each prepared polymer solution, a single nozzle was used in the electrospinning system. Blending electrospinning process was achieved by applying the parameters 0.9 $ml.h^{-1}$ of flow rate and for 15 second. The syringe pump was infused the polymer solution into the spinneret thorough an electric field (0-40 kV) was applied by using a high voltage power supply with 15-cm distance between the nozzle and grounded collector at the electrospinning device. A rectangular metal plate covered with aluminum foil was used as a grounded collector. The prepared polymeric solutions were filled before in 2 mL plastic syringes and connected to a metallic nozzle (inner diameter=0.4 mm) by plastic tubing. In this device, the positive electrode of the system was connected to the metallic needle, while the grounded one was connected to the conductive collector. All of the electrospinning experiments were implemented at room temperature.

## 3.5. Characterization of Electrospun Polymeric Nanofibers

### 3.5.1 Scanning electronmicroscope (SEM) morphological analysis, fiber diameter and distribution determination

The morphology of the fibrous mats was investigated by scanning electron microscopy (SEM, FEI-Quanta 200 FEG ESEM) at (Bilkent University, UNAM, Ankara) **Figure 3.7a.** Before measurement process, the prepared samples **Figure 3.7b** were covered with an Au/Pd layer (~5 nm) by a Gatan 682 Precision Etching and Coating System (PECS) to minimize problems of charging. For SEM imaging, it was implemented at the excitation voltage of ~12 kV and images of each nanofiber sample were taken with different focused points (x1500 and x10000). The average diameter of the fibers was calculated by analyzing (n=80) from different locations in fibers images using ImageJ software (SmartSEM, Zeiss) and the fiber diameters were reported as (AD, mean ± standard deviation SD). The collected data were transferred to OriginPro software for further analysis of electrospun nanofibers distributions.

a). b).

**Figure 3.7.** a). Scanning electron microscope (ESEM), b). Preparing nanofiber samples for SEM analysis

### 3.5.2 Energy dispersive x-ray spectroscopy (EDX)

Energy dispersive X-Ray device (EDX) detector **Figure 3.8** (SEM-EDX, SU1510, Hitachi, Japan, Ordu University, Turkey) with a maximal magnification and equipped with a burker analytical X-ray system was used for analyzing the chemical structure of the synthesized whole samples. All samples were taken in focused points (2000x) during the measurement process, then the collected data transformed to EDX TEAM$^{TM}$ software.

**Figure 3.8.** Energy Dispersive X-Ray Spectroscopy (EDX) device

### 3.6. Study of Modifying Gutta-Percha Surface via Plasma Irradiation

Study of gutta-percha cones' surface modification was applied via plasma instrument (E=30Watt, Pa=7.4X10$^{-3}$mbar) by air irradiation for the first time, in order to change the surface property from hydrophobic to hydrophilic structure. About the plasma device was fabricated by BIMAG research group (Prof. Dr. Dilek Cokeliler Seradroğlu) at (Nanotechnology& Nanomaterials Laboratory, Baskent University, Ankara, Turkey). First of all, gutta-percha cones were cut handily 12mm (n=10) for each experiment group according to the easily usage inside the root canal system during treatment process **Figure 3.9.**

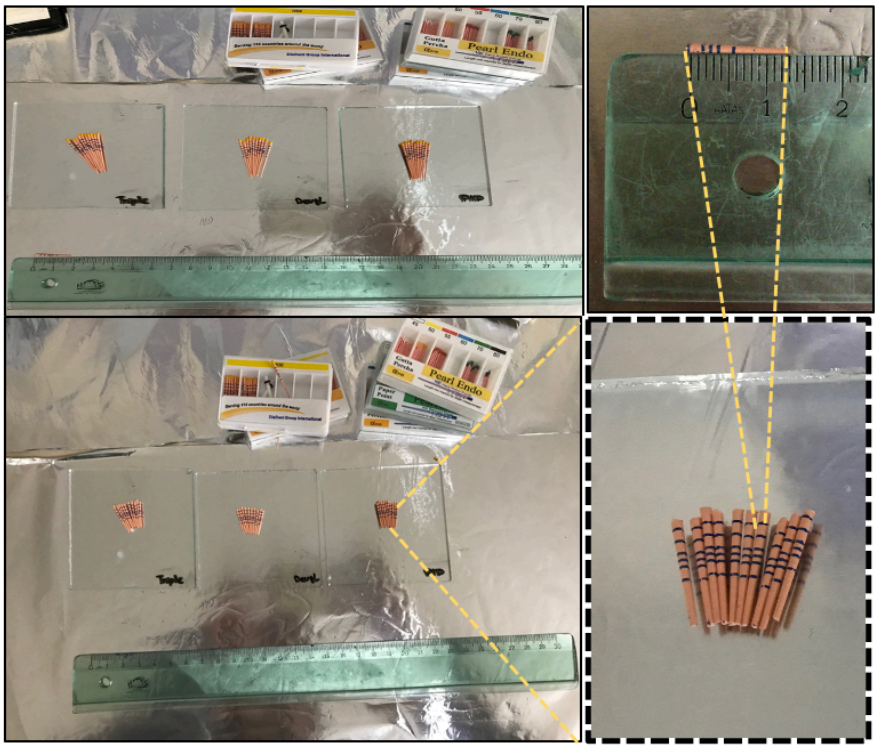


**Figure 3.9.** Preparing and cutting gutta-percha cones before placing them inside plasma device

Applied samples were placed inside the device tube **Figure 3.10** then the device was closed clearly, and device was started for 15 minutes until the irradiation would happen.

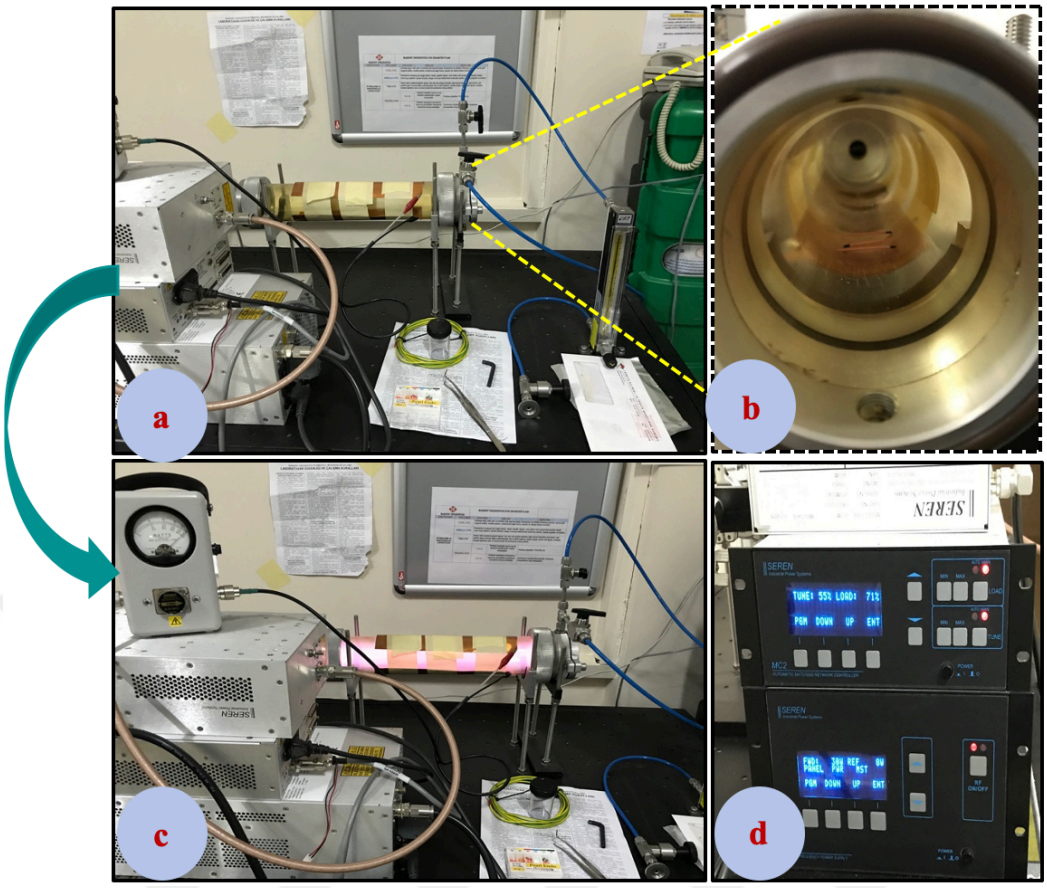


**Figure 3.10**. Gutta-percha surface modification was applied via plasma air irradiation

## 3.7. Characterization of Gutta-Percha

The characterization of the achieved gutta-percha cones after air irradiation process via plasma device and coating them with nanofibrous mats via electrospinning process was obtained by contact angel measurement test and X- Ray Photoelectron Spectroscopy (XPS) Analysis.

### 3.7.1 X-ray photoelectron spectroscopy (XPS) analysis

The elemental surface composition of gutta-percha surface before and after the air irradiation were identified by X-ray Photo electron spectroscopy **Figure 3.11a** (XPS, Thermo Scientific), equipped with a monochromatic Al/Ka as the X-ray source and the data was analyzed with Advantage software.

a). 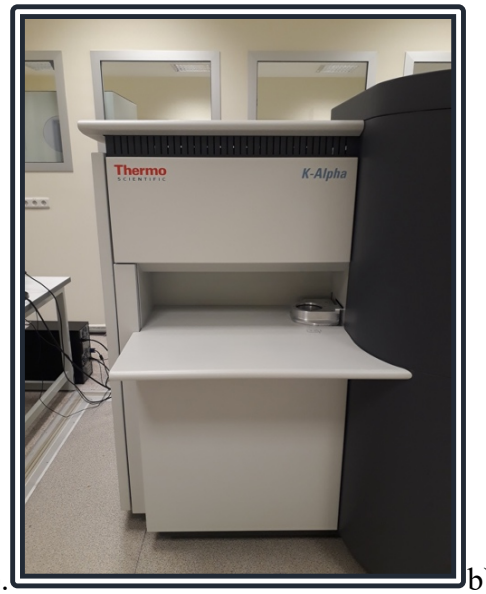

b). 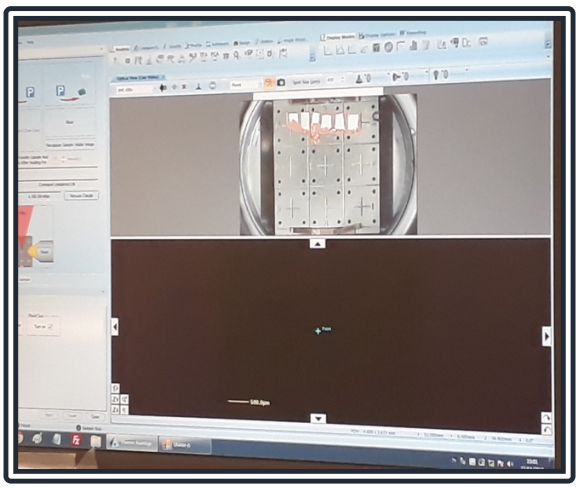

**Figure 3.11**. a). Vacuum device, b). Samples analyzing on XPS

### 3.8. Coating Gutta-Percha with Nanofiber mats via Electrospinning Strategy

After 15 minutes of air irradiation in the plasma device of the gutta-percha cones, samples were collected from the device tube and placed in the electrospinning device on the grounded collector **Figure 3.12** in order to achieve the spinning experiment upon the gutta-percha after the irradiation with air plasma. Electrospinning process was obtained by using the parameters 0.9 $ml.h^{-1}$ of flow rate, for 15 second, (0-40 kV) of flow rate and 15-cm distance among the nozzle and grounded collector at electrospinning device.

**Figure 3.12.** Coating process of Gutta-Percha with Nanofiber mats via Electrospinning device

After the electrospinning study, samples were analyzed morphologically by light microscope **Figure 3.13** (OLYMPUS, CX31, Başkent University, Ankara, Turkey) with 10x lens.

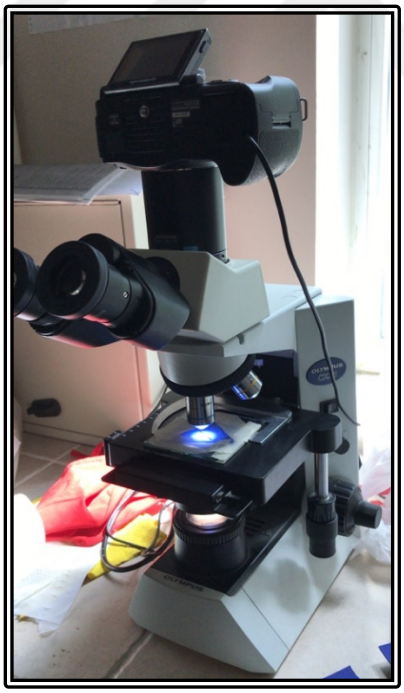

**Figure 3.13.** Light microscope device used to analysis the morphology of the gutta-perchas after coating with nanofibrous mats

### 3.9. Chemical Characterization of Dentin Surface

For this study 21 mature, single-root upper incisors teeth have extracted for causes not related to our experiments (periodontal, prosthetic reasons) were selected for this study. The analyzing in this study in order to measure the prepared samples effects on the mineral dentin content.

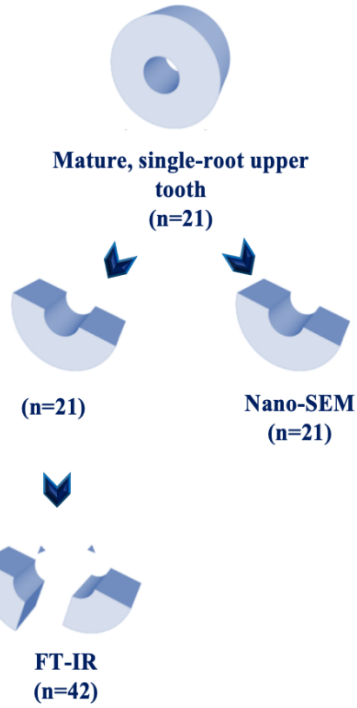


**Figure 3.14.** The shape and number of used teeth specimens at the different steps of this study

All 21 teeth were longitudinally divided into two parts **Figure 3.14,** 21 halves of the teeth were selected and were divided again for FT-IR analysis to determine the dentine mineral changing. One half of tooth was used as the experimental group and the other half as the control group. 42 specimens achieved from roots were assigned to 6 therapy groups (TAP, TA-NFs, DAP, DA-NFs, $Ca(OH)_2$ Paste, $Ca(OH)_{2}$-NFs) and 1 control group (deionized water). 6 root dentin segments of 4 mm will be used in each group. TAP was prepared as a control group by mixing antibiotic powders approved in a 1:1:1 ratio of MET, CIP, and MINO with deionized water (3:1). TA-NFs samples were prepared as an experiment group by applied the antibiotics loaded NFs upon the dentin specimens via electrospinning process **Figure 3.15** by direct spinning on the samples.

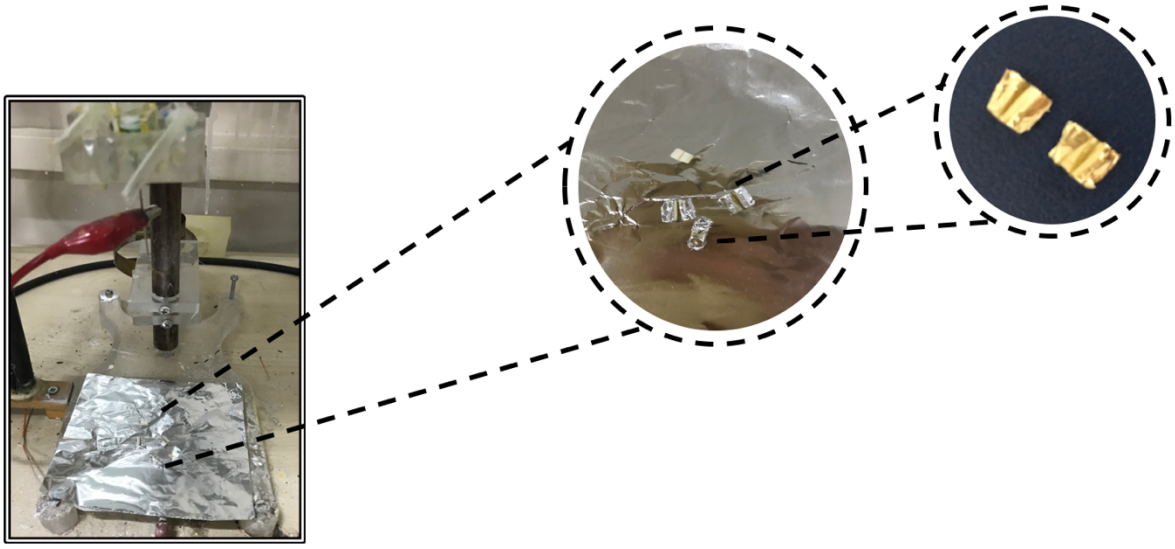

**Figure 3.15.** Electrospinning process upon human dentin specimens for injecting the medicament-NF samples in the root canals

DAP was prepared as a control group by mixing antibiotic powders approved in a ratio1:1 of MET and CIP with deionized water (2.5:1). DA-NFs samples were prepared as an experiment group by applied the antibiotics loaded NFs upon the dentin specimens via electrospinning process by direct spinning on the samples. $Ca(OH)_2$ paste was provided via mixing the powder of $Ca(OH)_2$ with DI water (2:1). $Ca(OH)_2$-NFs samples were prepared by applied the antibiotics loaded NFs upon the dentin specimens via electrospinning process by direct spinning on the samples. Each specimen was placed in a small 2-mL conical sample cup with saving them from air connection. The amount of pastes and nanofibers selected was just enough to cover the pulpal surface of each specimen. The containers were stored at 37$^{o}$C for 1 and 4 weeks. For the 1-week and 4-week groups, each specimen was washed by DI water every week. After each time, 21 samples from teeth were got, washed with DI water to obtain no visible paste w and completely air-dried. Sample size: Effect size = 0.48 power = 0.83 $\alpha$ = 0.05 was calculated as 42 (n = 6) in total (G Power 3.1.9.7).

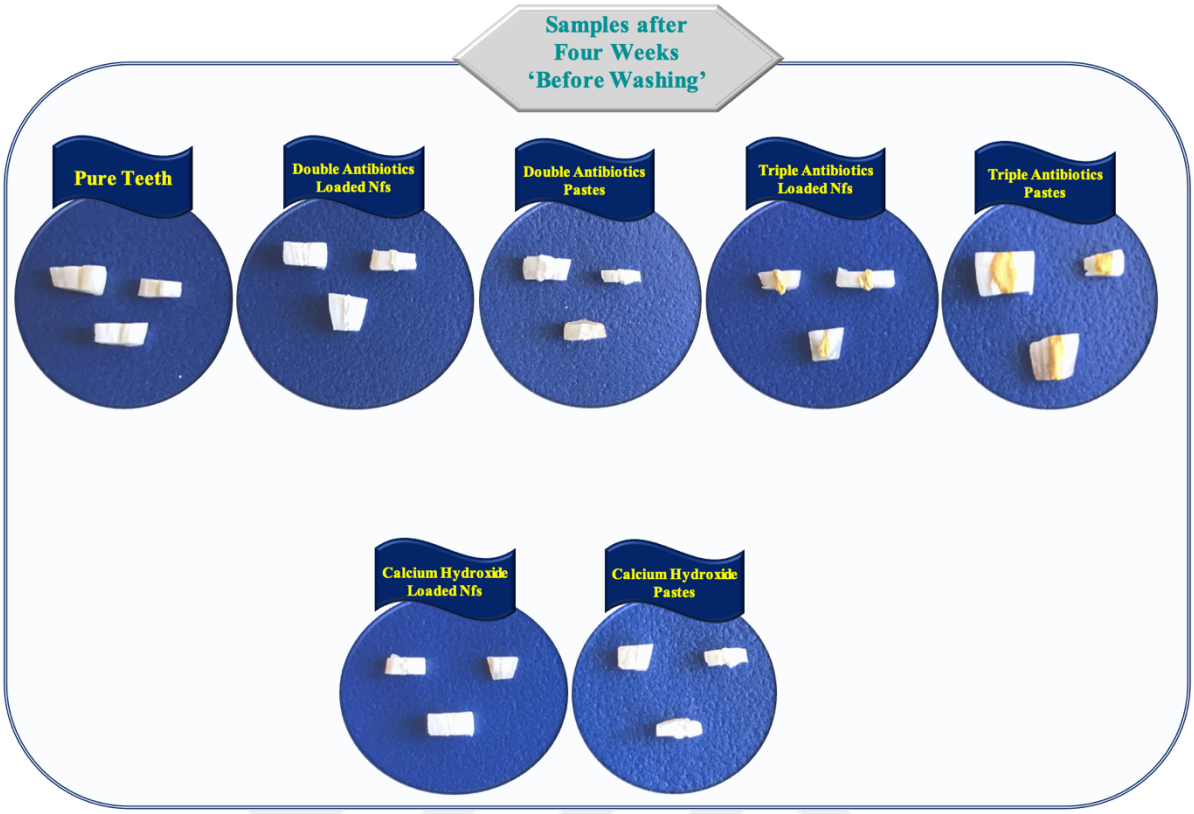


**Figure 3.16.** Teeth samples injected with different medicaments for four weeks before washing process for mineral content analysis

**Figure 3.17.** Teeth samples injected with different antibiotics for four weeks after washing process for mineral content analysis

Bruker Vertex 70 FT-IR Spectrometer was utilized for investigating the chemical structure of the root canal systems after 1 week and 4 weeks **Figure 3.16** and **Figure 3.17**of treating with different medicament groups with paste groups and loaded nanofibers groups at room temperature. FTIR spectrometer with a diamond ATR accessory **Figure 3.18** was used to obtain infrared spectra for analysis of dentin specimens. FTIR spectra were then collected between 800 and 2,000 $cm^{-1}$. The ATR-FTIR peak area were determined of phosphate v3 and amide I peak by the OPUS 6.5 software.

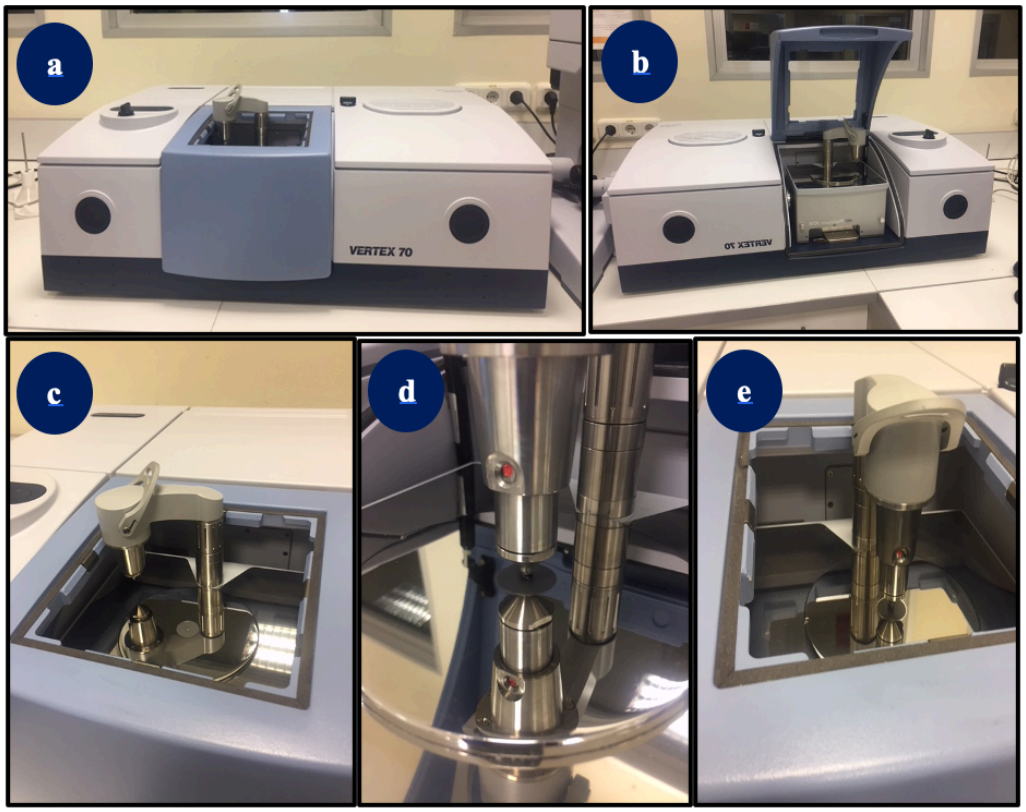


**Figure 3.18.** a), b), and c) Fourier-transform infrared spectroscopy (FT-IR) device, d). and e). placing teeth samples in the FT-IR device

### 3.10. Physical Characterization of Dentin Surface

12 halves of the teeth were selected and were divided to six groups for Nano-SEM analysis to determine the crusts/agglomerates over the dentin surface which exhibited after treating with different antibiotic groups. One half from each tooth was analyzed in Nano-SEM device and the other half in light microscope. 12 specimens obtained from roots were randomly assigned to 5 treatment groups (PVP-NFs, TAP, TA-NFs, DAP, DA-NFs) and 1

control group (non-treated). After 28 days of treatment via gutta-percha cones coated with (nanofibers or pastes), the first halves group were cleaned with distillate water to evaluate the dentin surface different antibiotics-loaded nanofibers, the other halves were kept untouched to analyze via microscope (pastes or scaffolds). For Nano-SEM samples, the specimens were sputter-coated with Au-Pd before imaging (FEI-NOVA, 430, NanoSEM). Images were taken with different focus points 100x, 2000x and 5000x for each sample.

# 4. Results

## 4.1. Pre-experiments Characterizations

Elimination of the microbial infections is a main goal of endodontic treatment, essentially infections consisting of anaerobic and aerobic bacteria. MET is the first choice of antibiotics, because most of bacteria within the root canal system are anaerobic. Where, CIP is a DNA inhibitor and it has an effect against gram-negative pathogens. $Ca(OH)_2$ is another type of medicaments used in regenerative endodontic. It is suggested to offer direct antibacterial effect and to its ability to provide an elevated and extended levels of disinfection have been needed in regenerative endodontic therapy. In order to obtain highly antimicrobial drug release systems, MET, CIP, and $Ca(OH)_2$ loaded-polymeric fibrous mats were synthesized and characterized for analyzing their morphologies and structures with unique release mechanism from PVP fibers to develop and improve their properties as effective drug release systems. Medicament loaded-fibrous mats (single, double or triple) may provide clinical benefit, so as pre-experiments we developed MIP, CIP, and $Ca(OH)_2$ loaded electrospun fibers to control their structures with different concentrations (20%(w/w) and 25%(w/w)), separately. In the electrospinning strategy, beside of polymer solution properties such as polymer concentration, viscosity, and the surface tension of the solvent, the system conditions such as nozzle-collector distance, applied voltage, and flow rate parameters effect on the morphological structures of the fibers. For that, in our study many different concentrations of medicaments and solvents were carried out with stable concentration of the polymer and with constant system conditions 0.9 $ml.h^{-1}$, 0-40 kV, and 15-cm for each flow rate, applied electric field, and distance between the nozzle and grounded collector at the electrospinning device for 15 second for all samples.

SEM images were taken from electrospun MET-PVP fibers for each sample, which obtained from two polymer solutions and constant electrospinning conditions to get detailed information of the morphologies of the fiber's structures. Besides, SEM images were also taken at high magnification to analyze the fiber diameters and their distributions.

Electrospun with two different doses of MET based 8%(w/w) of PVP nanofiber's SEM images were showed in **Figure 4.1**. In order to obtain best antibacterial effect of the drug release system would achieved 20%(w/w) of MET was developed, which is dissolved in ET-OH, was showed fiber structures with almost huge bead structures **Figure 4.1.a1 and a2** related to incorporate the drug inside the fiber structures in micron range of fiber diameters [10.245±3.48 µm ($4_{MIN}$-$21.3_{MAX}$ µm)] **Figure 4.1.a3** and non-uniformity. For this reason, the MET concentration has been raised to 25%(w/w) without change the polymer concentration and the system conditions. In the second sample which had 25%(w/w) of MET fiber structures were seen but with micron-level fiber structures [7.797 ±2.67 µm ($3.6_{MIN}$-$21.7_{MAX}$ µm)], also there was droplets and non-uniformity **Figure 4.1b1 and b2**.

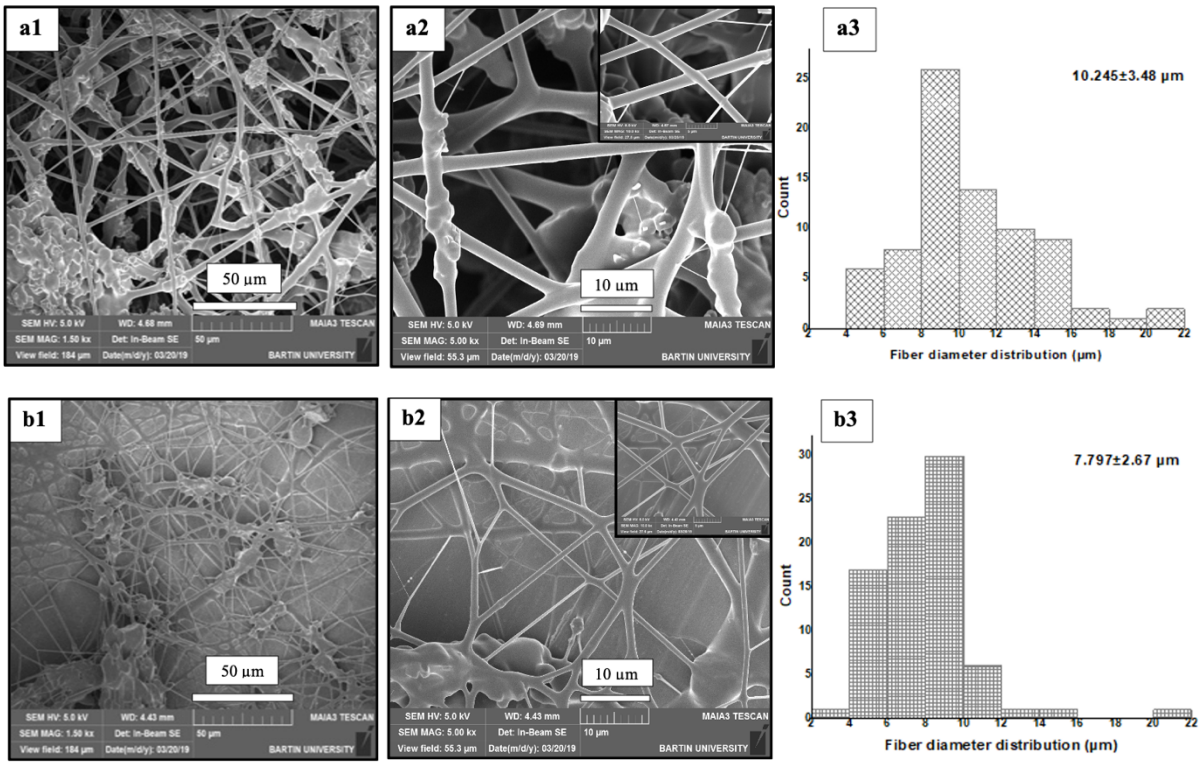


**Figure 4.1.** SEM images of electrospun one fibers in different concentrations of MET with PVP and different focus points of each concentration; a1). 20% MET-PVP (x1500), a2). 20% MET-PVP (x5000), a3). Fiber diameter distribution of 20% MET-PVP; b1). 25% MET-PVP (x1500), b2). 25% MET-PVP (x5000), b3). Fiber diameter distribution of 25% MET-PVP

SEM images of CIP-PVP with two different concentrations 20%(w/w) and 25%(w/w) of CIP were given in **Figure 4.2.a1 and a2** with focus point 50 µm, respectively. In these samples of CIP, it is clearly seen at all images that fiber structures were not seen in 20%(w/w), but they are slightly seen in the 25%(w/w) sample with dramatically increasing the diameters **Figure 4.1.b1 and b2.**

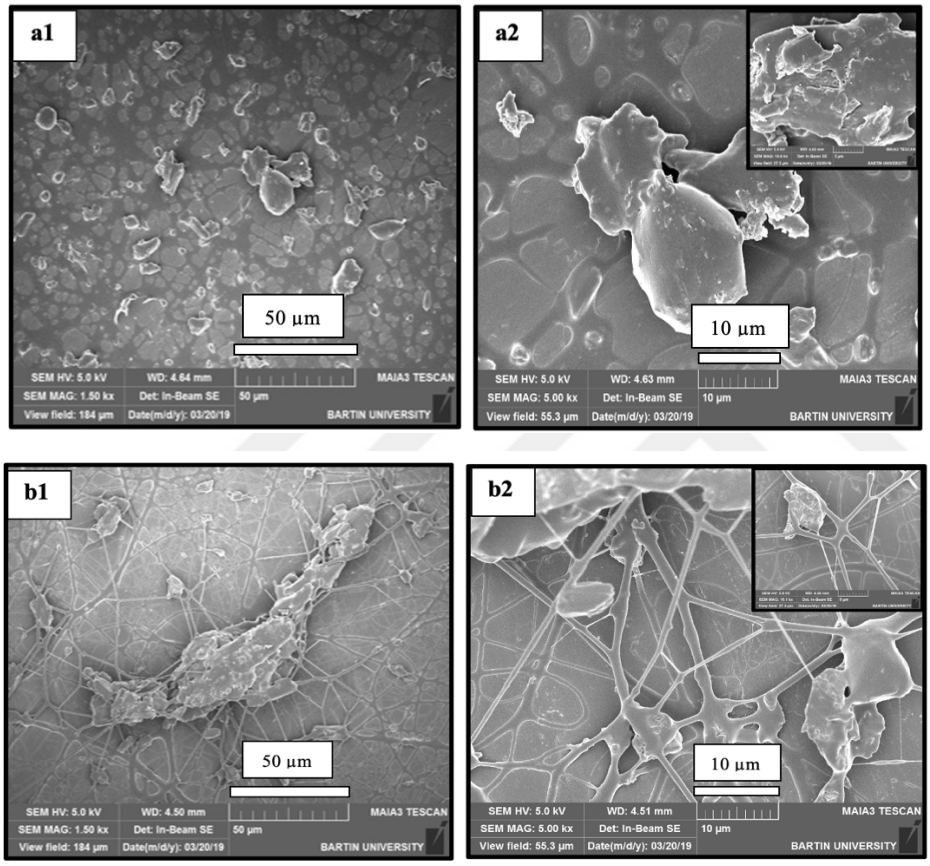


**Figure 4.2.** SEM images of electrospun nanofibers in different concentrations of CIP with PVP and different focus points of each concentration; a1). 20% CIP-PVP (x1500), a2). 20% CIP-PVP (x5000), b1). 25% CIP-PVP (x1500), b2). 25% CIP-PVP (x5000)

The chemical characterization of MET-PVP and CIP-PVP samples was obtained by analyzing the %20(w/w) concentration of each one. The several characteristic picks at MET-PVP showed presenting of oxygen, carbon and nitrogen with 67, 30.4, and 23 atomic percentages respectively **Figure 4.3a** with another element with low concentrations not related to the sample such aluminum element which presents from the aluminum foil was collected above. In the CIP-PVP sample beside of oxygen, carbon, and nitrogen, the floe pick was presented with 0.1 atomic percentage **Figure 4.3b.**

a.) 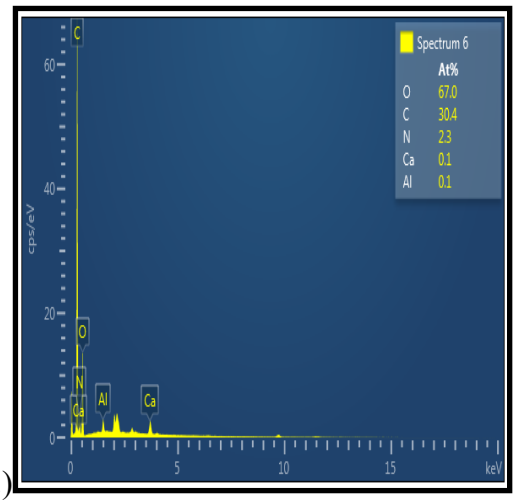

b) 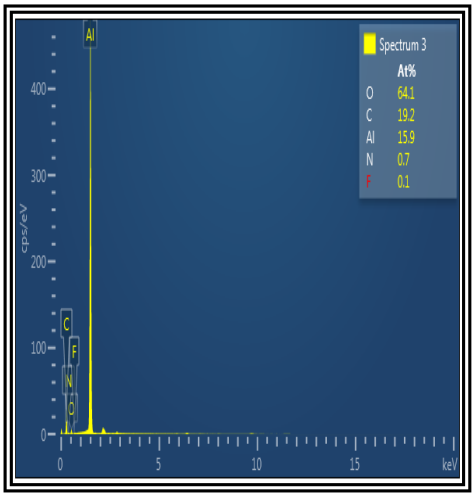


**Figure 4.3.** Chemical compositions of a) % 20 of MET-PVP and b) % 20 of CIP-PVP

## 4.2. Fabrication and Characterization of Poly(vinylpyrrolidone) Nanofiber Samples

In this study many different experiments have been carried out with Ethyl Alcohol solvent and PVP polymer during the production of optimum PVP fibers. Electrospinning was first performed with 8% (w/w) weight percent of PVP solutions which was dissolved in Ethyl Alcohol as a control group **Figure 4.4.**

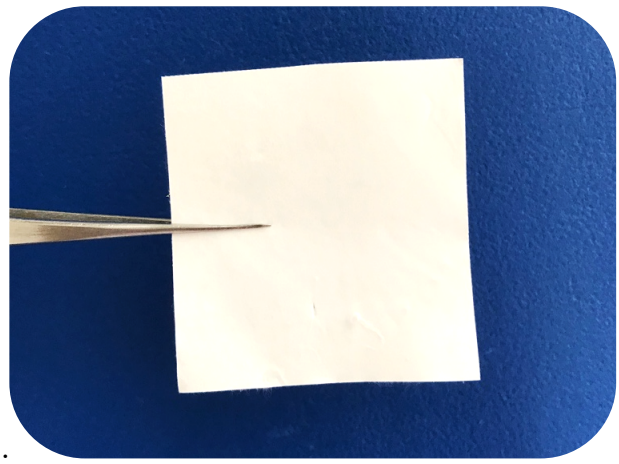

**Figure 4.5.** The optical photos of the 8%(w/w) of PVP nanofiber mat produced via electrospinning strategy

### 4.2.1 Scanning electron microscope (SEM) morphological analysis, fiber diameter and distribution determination

SEM images were taken from electrospun PVP fibers, which were obtained from the polymer solution and electrospinning conditions mentioned above to get detailed information of the morphologies of the fiber structures. Poly(vinylpyrrolidone) electrospun fiber's SEM images were given in **Figure 4.5a** is shown the 1500x focus point of PVP sample, this figure showed uniform and regular structure of the fibers. Also, the same situation was showed in the x10000 focus point for the same sample which shown in **Figure 4.5b.** A micron-fibrous network with interconnected micron-sized pores was seen for this sample, due to the polymer solution hydrophobic which makes it has more viscous structure during electrospinning. Under the applied conditions, fiber structure was seen with micro-level and uniformity fibers structures. A submicron fiber diameter was observed for antibiotic-free fiber sample [1087±285.24 ($598_{MİN}$-$1737_{MAX}$) nm] with a gaussian distribution (heterogenous) fiber distribution was noticed. The inset graph shows the fiber diameter distribution for this sample **Figure 4.5c.**

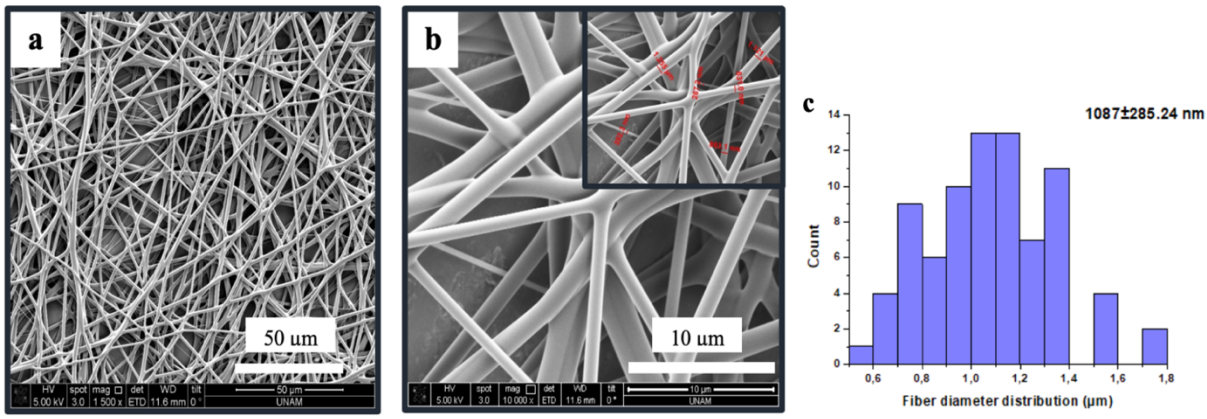


**Figure 4.6.** SEM images of %8 (w/w) Electrospun PVP fibers with a). x1500 and b). x10000 focused points c). fiber diameter distribution analysis of PVP electrospun fibers

### 4.2.2 Energy dispersive x-ray spectroscopy (EDX)

EDX of the pure electrospun PVP fibers with 8%(w/w) prepared by dissolving powder of PVP in ET-OH solvent showed in **Figure 4.6.** As a result, we can say that the PVP dissolved effectively in the solvent and lead to give these percentages in the structures of nanofibers. The chemical analysis of this sample showed chemical elements with difference percentages that carbon, nitrogen, and oxygen were showed 63.57, 13.64, and 22.78 values,

respectively. According to the chemical structure of PVP the detected elements analytically confirm it.

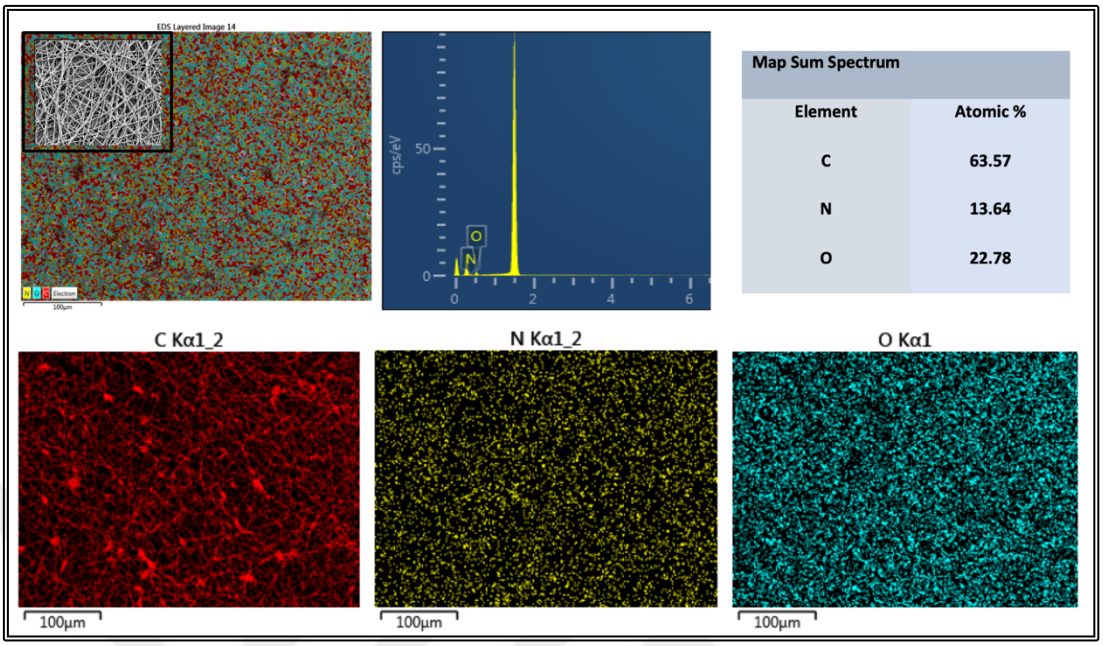


**Figure 4.7**. SEM-Energy Dispersive X-Ray Spectroscopy of pure PVP nanofiber mats

## 4.3. Fabrication and Characterization of Metronidazole-Poly(vinylpyrrolidone) Containing Nanofiber Samples

Since irregular fiber structures were obtained from the 20% and 25%(w/w) concentrations of MET in the pre-experiments, many different experiments have been carried out with different lower concentrations of MET antibiotic with 8% of PVP polymer during the production of optimum MET-PVP fibers. It was done by changing only the antibiotic concentrations with take the other conditions constant. Electrospinning was first performed with 2.5% (w/w) weight percent of metronidazole solution then with 5%, 7.5% and 10% respectively which were dissolved in Ethyl Alcohol. The digital Images of the all obtained metronidazole-poly(vinylpyrrolidone) fiber samples presented in **Figure 4.7**.

| Figure | Content (%) | Figure | Content (%) |
|---|---|---|---|
| 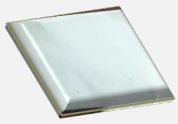 | MN-PVP 2.5% (w/w) | 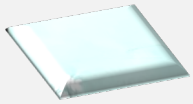 | MN-PVP 5% (w/w) |
| 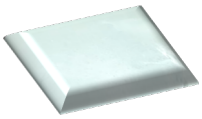 | MN-PVP 7.5% (w/w) | 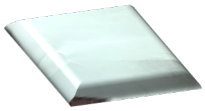 | MN-PVP 10% (w/w) |

**Figure 4.8.** The optical photos of the MET-loaded nanofibers mats with different concentrations produced via electrospinning strategy

#### 4.3.1.1 Scanning electron microscope (SEM) morphological analysis, fiber diameter and distribution determination

SEM images were taken from electrospun MET-PVP fibers, which were obtained from the polymer solution and electrospinning conditions mentioned above to get detailed information of the morphologies of the fiber structures. Besides, SEM images were also taken at high magnification to analyze the diameter and distribution of the fibers.

**Figure 4.8 a1 and a2** were showed two different focus points of the fibers that formed of 2.5% MET-PVP dissolved in Et-OH. These electrospun nanofibers were showed a uniform and regular structure as the previous sample as showed despite of adding 2.5% of the MET antibiotic. So due to the no change in the applied voltage and flow rate and adding the antibiotics there was no change in the nanofiber uniform structure. The 2.5% MET-PVP were dissolved as quick as of the bure PVP solution, where the solution properties were not changed after adding the 2.5% of metronidazole. In other side, as can be seen in **Figure 4.8 a3** fiber diameters were decreased according to adding the antibiotic with 8% (w/w) PVP. The fibers diameters showed 593±105 nm whereas the fiber diameters of bure PVP were 1087±285 nm. A nano-fibrous network with interconnected nano-sized pores was seen for this sample. Under the applied conditions, fiber structure was seen with nano-level and uniformity fibers structures. A fiber diameter was observed for 2.5% MET-PVP sample [593±105 ($358_{MİN}$-$857_{MAX}$) nm] with a gaussian distribution (heterogenous) fiber distribution was noticed for all MP-PVP samples. The inset graph shows the fiber diameter distribution for this sample **Figure 4.8 a3.** The second antibiotic concentration that added to the PVP solution was 5% (w/w) of MET. This concentration caused to form irregulated fiber

structure according to the previous sample (2.5% (w/w) MET-PVP). As shown in the **Figure 4.8**b1which shows the x1500 focus point of sample, there was tinny fiber structures but related with concentrated objects. According to use the same electrospinning fabricated conditions, **Figure 4.8b2** figure which is showed the x10000 focus point of the SEM image, these objects caused to increase the fiber diameters to [718±148 ($335_{MİN}$-$947_{MAX}$) nm]. As summarize, due to these objects the fiber diameters increased due to increase the antibiotic concentration. A micron-fibrous network with interconnected micron-sized pores was seen for this sample.

In order to increase the antibiotic concentration to 7,5% (w/w), the fiber structure was showed a really uniform and organized structure, but the diameters of this structure were showed slightly decreased [636±121 ($379_{MİN}$-$891_{MAX}$) nm]. Whereas, the interconnected network showed nano-sized pores **Figure 4.8 c1, c2, and c3.**

The last sample of MET-PVP had 10% (w/w), this concentration caused to fabricate slightly organized structure of nanofibers, but this structure had again tinny beads related to the nanofibers. Besides, these beads in this structure had not cause to highly increase of the fiber diameters but inspired to similar size of the 7,5% (w/w), was [772±192 ($370_{MİN}$-$1199_{MAX}$) nm] **Figure 4.8 d1, d2, and d3.**

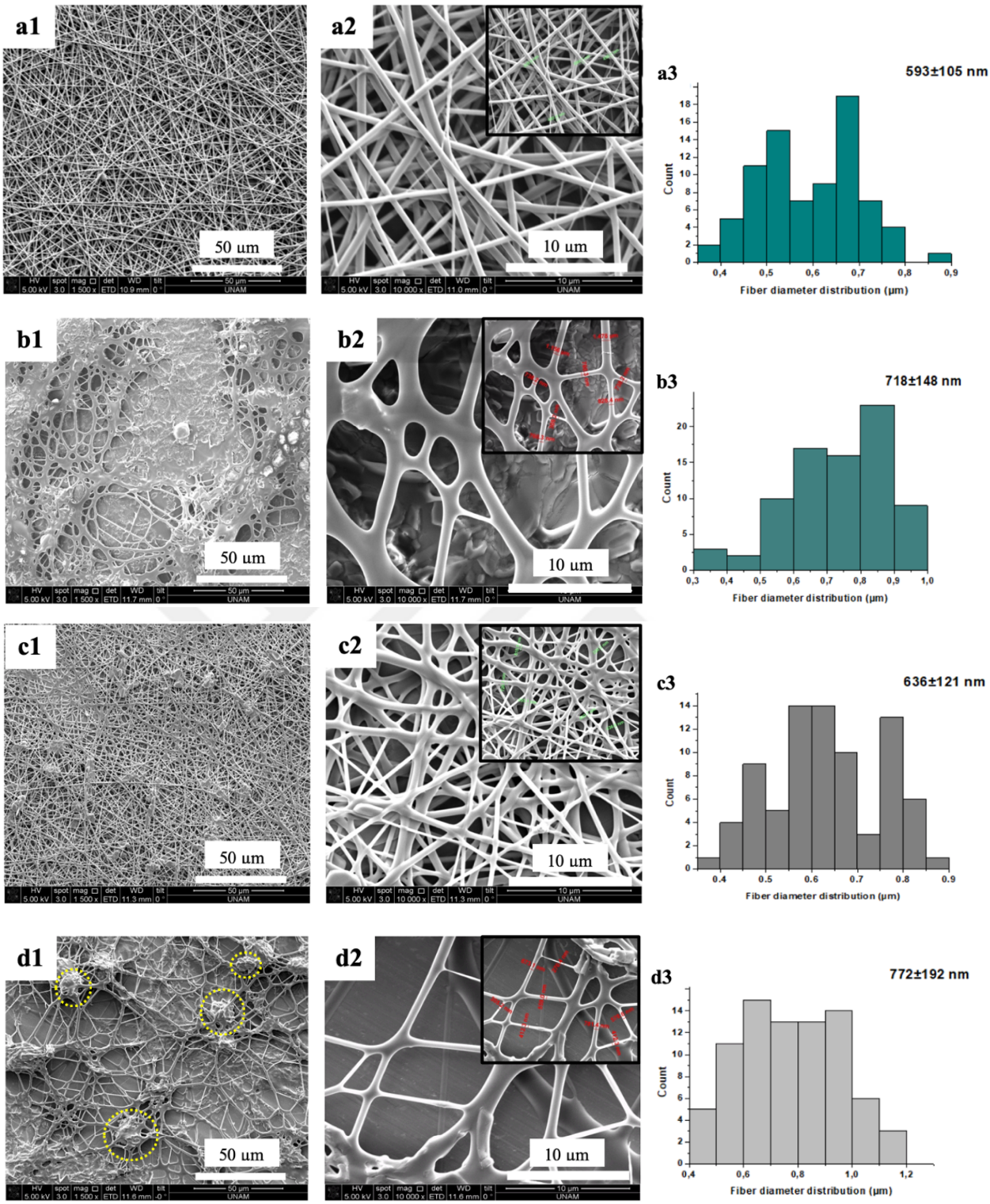


**Figure 4.9.** SEM images of electrospun nanofibers in different concentrations of MET with PVP and different focus points of each concentration; a1). 2.5% MET-PVP (x1500), a2). 2.5% MET-PVP (x10000), a3). Fiber diameter distribution of 2.5% MET-PVP; b1). 5% MET-PVP (x1500), b2). 5% MET-PVP (x10000), b3). Fiber diameter distribution of 5% MET-PVP; c1). 7.5% MET-PVP (x1500), c2). 7.5% MET-PVP (x10000), c3). Fiber diameter distribution of 7.5% MET-PVP; d1). 10% MET-PVP (x1500), d2). 10% MET-PVP (x10000), d3). Fiber diameter distribution of 10% MET-PVP

#### 4.3.1.2 Energy dispersive x-ray spectroscopy (EDX)

MET-PVP electrospun nanofiber samples were synthesized with different concentrations according to the nanofiber structures which had been deformed in some samples. So, as mentioned in the SEM results and according to controlling the antibiotics concentrations the chosen concentrations were as showed in **Figure 4.9** 2.5, 5, 7.5, 10%(w/w). Depending on that the MET-PVP solution have the same chemical elements in their chemical structures each one separately, we are waited to increase the percentages of the elements in the MET-PVP nanofiber mats. As represented the **Figure 4.9a** that is showed the chemical analysis of 2.5% (w/w) MET-PVP sample. Where, results showed the presence of carbon, nitrogen, and oxygen with atomic% of 57.57, 19.14, and 23.29 respectively. According to the chemical structures of the MET and PVP that confirm with it as a presence of the chemical elements.

By increasing the concentration of the MET inside the polymer solution to 5%(w/w) **Figure 4.9b** the chemical elements as showed the peaks increased with 73.41, 8.04, and 18.56 to carbon, nitrogen, and oxygen respectively. According to the previous sample the chemical elements in 7.5%(w/w) MET-PVP electrospun nanofiber mat **Figure 4.9c** sample showed slightly decreased in the carbon value, which was 70.10, and increasing to the nitrogen and oxygen elements 9.28 and 20.62 for each of nitrogen and oxygen respectively. 10%(w/w) MET-PVP electrospun nanofibers **Figure 4.9d** showed very similar results to the 7.5% one with 69.01, 9.76, and 21.22 for carbon, nitrogen, and 21.22 respectively.

a).2.5% (w/w) MET-PVP

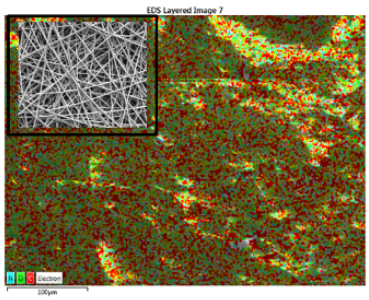


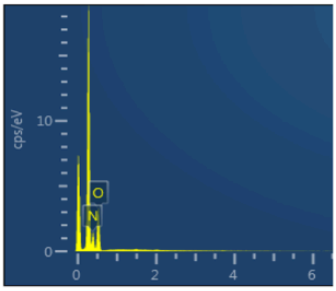


| Map Sum Spectrum | |
|---|---|
| Element | Atomic % |
| C | 57.57 |
| N | 19.14 |
| O | 23.29 |

C Kα1_2

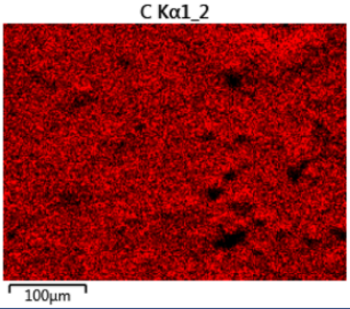


N Kα1_2

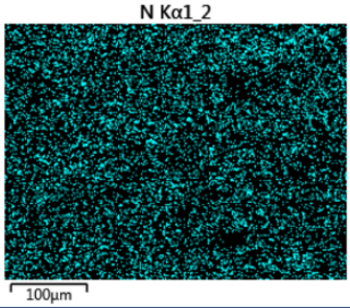


O Kα1

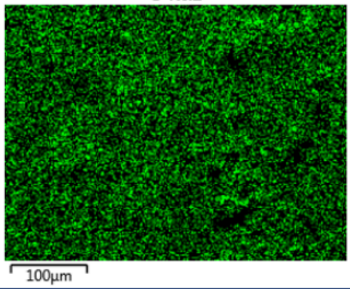


b).5% (w/w) MET -PVP

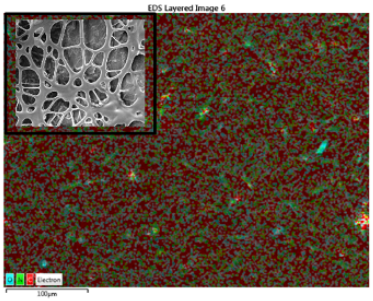


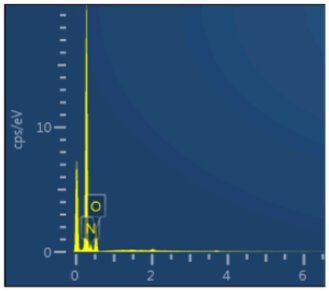


| Map Sum Spectrum | |
|---|---|
| Element | Atomic % |
| C | 73.41 |
| N | 8.04 |
| O | 18.56 |

C Kα1_2

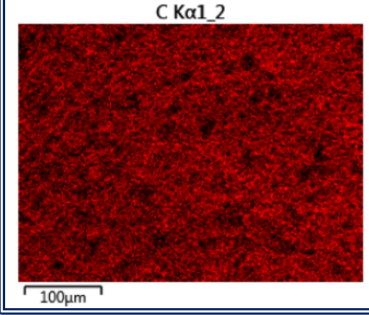


N Kα1_2

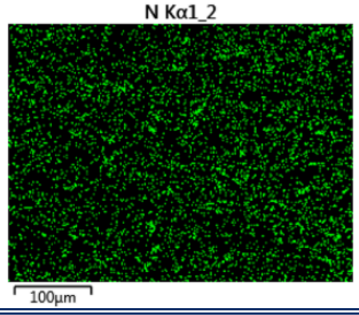


O Kα1

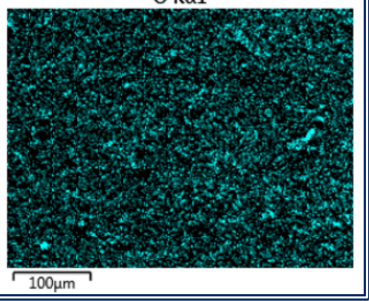

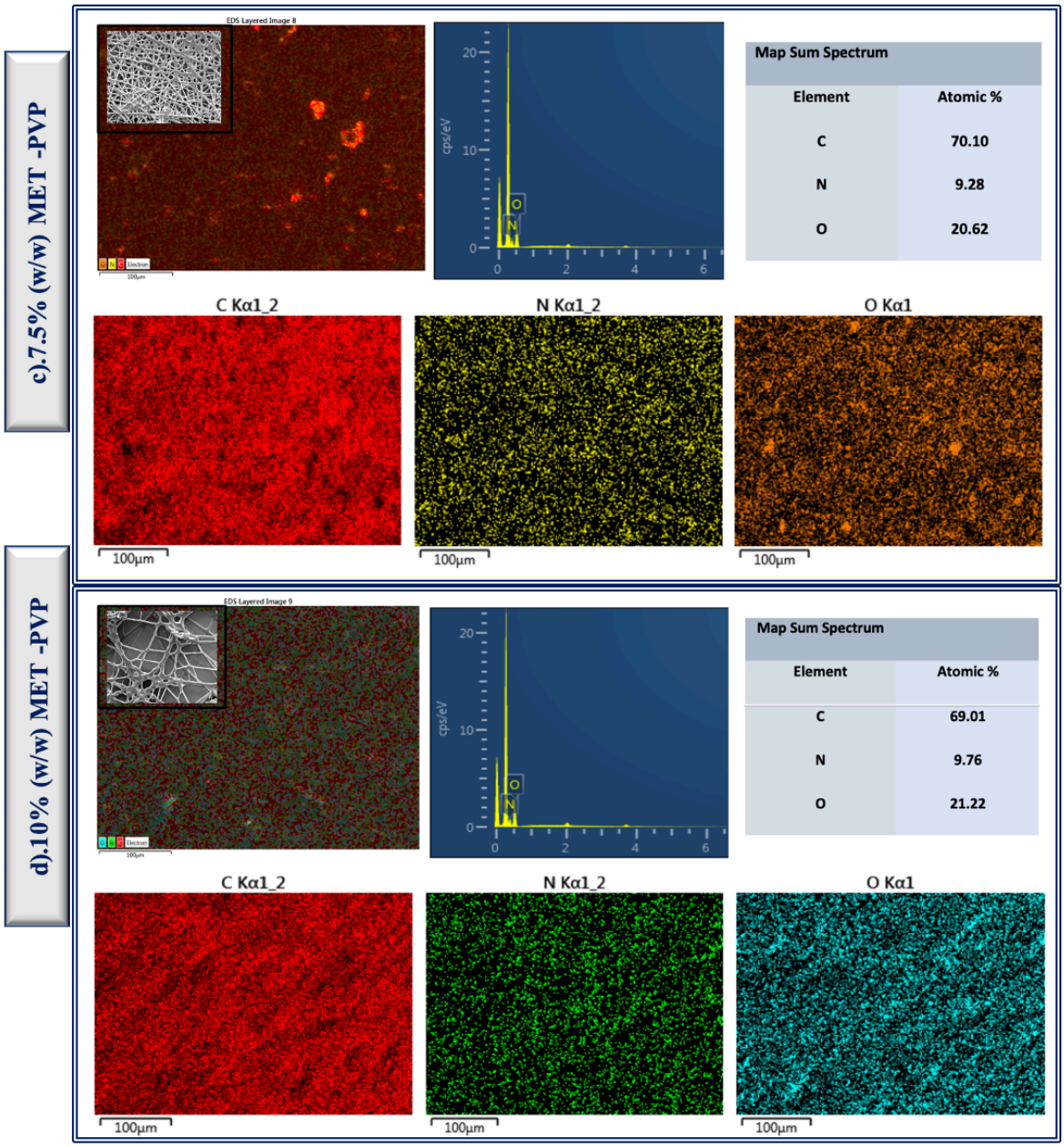


**Figure 4.10.** SEM-Energy Dispersive X-Ray Spectroscopy of a)2.5, b).5, c).7.5, and d).10% (w/w) MET-PVP electrospun nanofiber mats

### 4.3.2 Fabrication and characterization of ciprofloxacin-poly(vinylpyrrolidone) containing nanofiber samples

According to the non-fiber structures were obtained from the 20% and 25%(w/w) concentrations of CIP in the pre-experiments with 20%(w/w) and 25%(w/w) concentrations, in this experiment many different experiments have been carried out with lower concentrations of CIP antibiotic with 8% of PVP in order to produce optimum CIP-PVP

fibers. Electrospinning was first performed with 1% (w/w) weight percent of metronidazole solution then with 2.5%, 5% and 7.5% respectively which were dissolved in Ethyl Alcohol. The digital Images of the all obtained MET-PVP fiber samples presented in **Figure 4.10.**

| Figure | Content (%) | Figure | Content (%) |
|---|---|---|---|
| 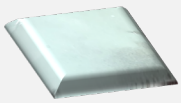 | Cipro-PVP 1% (w/w) | 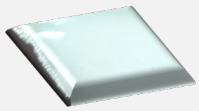 | Cipro-PVP 2.5% (w/w) |
| 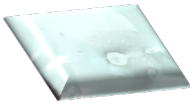 | Cipro-PVP 5% (w/w) | 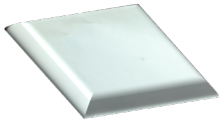 | Cipro-PVP 7.5% (w/w) |

**Figure 4.11.** The optical photos of the CIP-loaded nanofibers mats with different concentrations produced via electrospinning strategy

#### 4.3.2.1 Scanning electron microscope (SEM) morphological analysis, fiber diameter and distribution determination

The optical photos of the MET-loaded nanofibers mats taken with SEM method with different concentrations produced via electrospinning strategy CIP-PVP fibers, which were obtained from the polymer solution and electrospinning conditions mentioned above to get detailed information of the morphologies of the fiber structures. Besides, SEM images were also taken at high magnification to analyze the diameter and distribution of the fibers

The **Figure 4.11 a1 and a2** figures were showed two different focus points of the fibers that formed of 1% CIP-PVP dissolved in Et-OH. These electrospun nanofibers were showed a uniform and regular structure as the previous sample as showed despite of adding 1% of the CIP antibiotic. The 1% CIP-PVP were dissolved as quick as of the bure PVP solution, where the solution properties were not changed after adding the 1% of ciprofloxacin. In other side, as can be seen in **Figure 4.11a3**, fiber diameters were decreased according to adding the antibiotic with 8% (w/w) PVP. The fibers diameters showed [406±116 ($223_{MIN}$-$773_{MAX}$) nm]. A nano-fibrous network with interconnected nano-sized pores was seen for 1%, 2.5%, and 7.5% samples. Under the applied conditions, fiber structure was seen with nano-level and uniformity fibers structures. A fiber diameter was

observed for 1% CIP-PVP sample with a gaussian distribution (heterogenous) fiber distribution was noticed for all CIP-PVP samples. The inset graph shows the fiber diameter distribution for this sample.

The second antibiotic concentration that added to the PVP solution was 2.5% (w/w) of CIP This concentration caused to form regulated fiber structure according to the previous sample (1% (w/w) CIP-PVP). As shown in the **Figure 4.11b1** figure which shows the x1500 focus point of sample, there was tinny fiber structures but related with concentrated objects. According to use the same electrospinning fabricated conditions, the **Figure 4.11b2** figure which is showed the x10000 focus point of the SEM image, these objects caused to decrease the fiber diameters to [369±170 ($100_{MIN}$-$731_{MAX}$) nm] and improve the fiber diameter distributions **Figure 4.11b3**. As summarize, due to these objects the fiber diameters decreased due to increase the antibiotic concentration. A nano-fibrous network with interconnected nano-sized pores was seen for this sample. In order to increase the antibiotic concentration to 5% (w/w), the fiber structure was showed a really uniform and organized structure **Figure 4.11c1 and c2** with [337±169 ($167_{MIN}$-$805_{MAX}$) nm] diameter **Figure 4.11c3**, the interconnected network showed micro-sized pores due to perform structures in the middle parts of the sample. The last sample of CIP-PVP had 7.5% (w/w), this concentration caused to fabricate slightly organized structure of nanofibers [257±103 ($67_{MIN}$-$487_{MAX}$) nm] **Figure 4.11d3**.

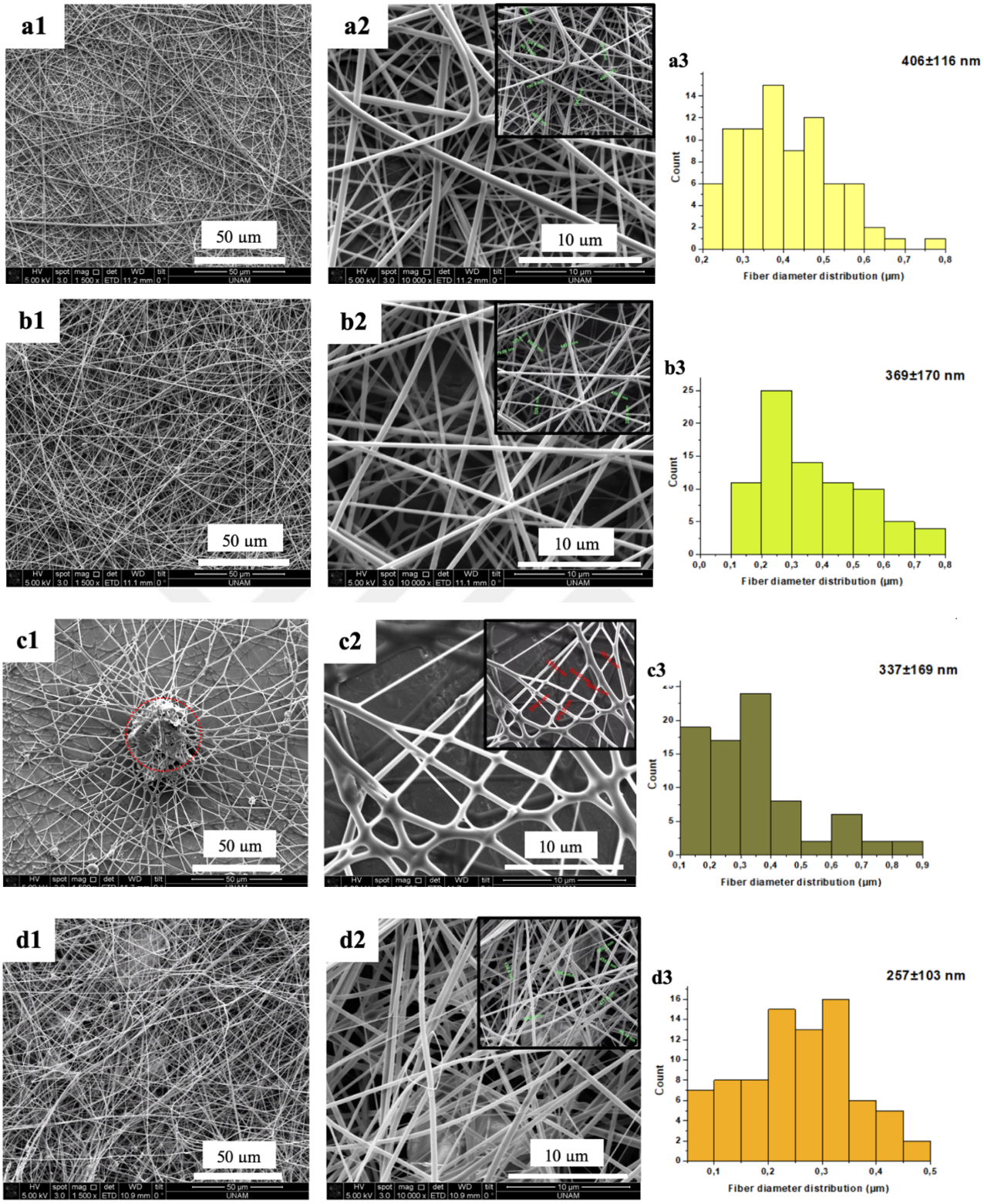


**Figure 4.12.** SEM images of electrospun nanofibers in different concentrations of MN with PVP and different focus points of each concentration; a1). 1% CIP-PVP (x1500), a2). 1% CIP-PVP (x10000), a3). Fiber diameter distribution of 1% CIP-PVP; b1). 2.5% CIP-PVP (x1500), b2). 2.5% CIP-PVP (x10000), b3). Fiber diameter distribution of 2.5% CIP-PVP; c1). 5% CIP-PVP (x1500), c2). 5% CIP-PVP (x10000), c3). Fiber diameter distribution of 5% CIP-PVP; d1). 7.5% CIP-PVP (x1500), d2). 7.5% CIP-PVP (x10000), d3). Fiber diameter distribution of 7.5% CIP-PVP

#### 4.3.2.2 Energy dispersive x-ray spectroscopy (EDX)

CIP-PVP electrospun nanofiber samples were synthesized with different concentrations according to the nanofiber structures which had been deformed in some samples. So, as mentioned in the SEM results and according to controlling the antibiotics concentrations, the chosen concentrations were as showed in **Figure 4.12a, b, c, and d respectively to** 1, 2.5, 5, 7.5 %(w/w). Depending on that the CIP-PVP solution has the same chemical elements in their chemical structures each one separately, we are waited to increase the percentages of the elements in the CIP-PVP nanofiber mats. As represented the **Figure 4.12a** that is showed the chemical analysis of 1% (w/w) CIP-PVP sample. Where, results showed the presence of carbon, nitrogen, and oxygen with atomic% of 55.49, 15.19, and 27.01 respectively. According to the chemical structures of the CIP and the increasing, the concentrations of it regarding the presence of the chemical elements flow it with parallel values. According to the presence of the flor in the structure of CIP increasing the concentrations lead to a decrease in the amount of flor in the nanofiber depended on the 1%(w/w) sample.

a).1% (w/w) CIP-PVP

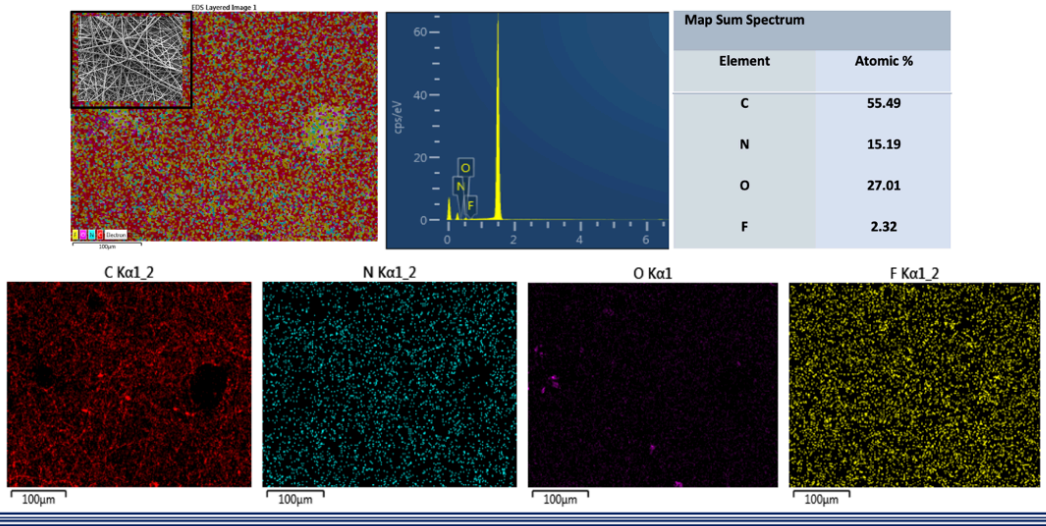


| Map Sum Spectrum | |
|---|---|
| Element | Atomic % |
| C | 55.49 |
| N | 15.19 |
| O | 27.01 |
| F | 2.32 |

b).2.5% (w/w) CIP-PVP

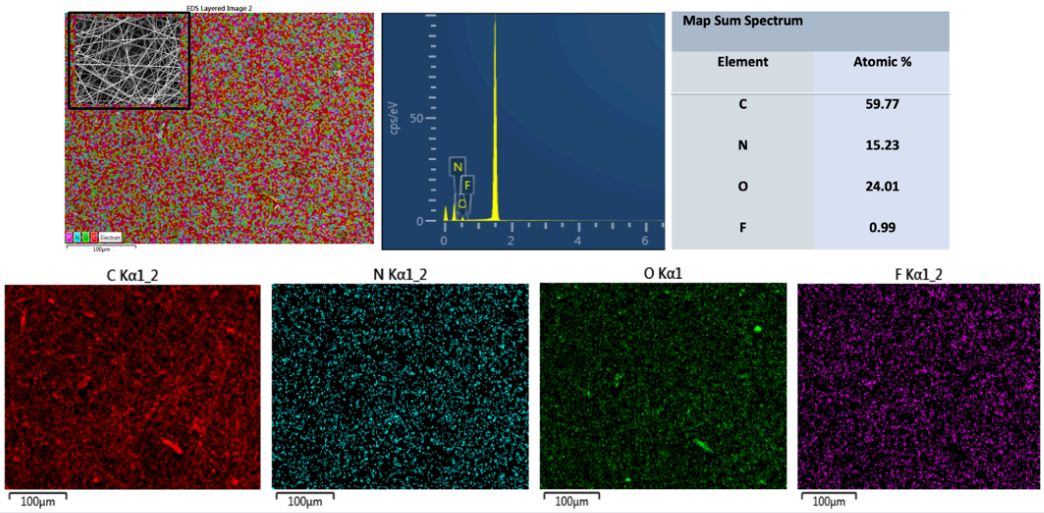


| Map Sum Spectrum | |
|---|---|
| Element | Atomic % |
| C | 59.77 |
| N | 15.23 |
| O | 24.01 |
| F | 0.99 |

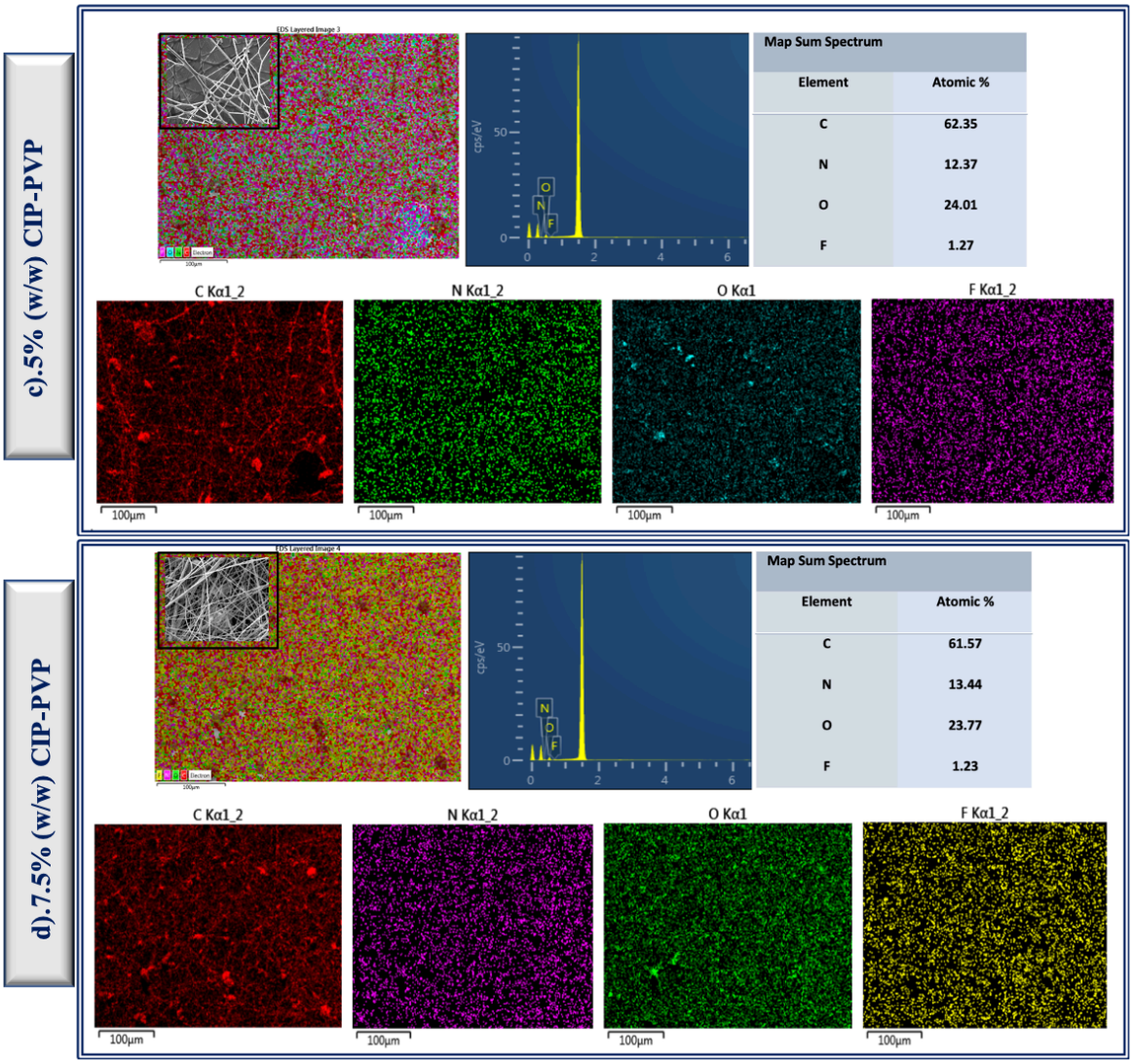


**Figure 4.13.** SEM-Energy Dispersive X-Ray Spectroscopy of a)1, b).2.5, c).5, and d).7.5% (w/w) CIP-PVP electrospun nanofiber mats

## 4.4. Fabrication and Characterization of Double Antibiotics Loaded-Poly(vinylpyrrolidone) Nanofibers Samples

The effective solution of endodontic injuries has requested a mixture of multi-antibiotics. MET and CIP have an effective antibacterial impact against obligate anaerobes and gram-negative bacteria. According to the pre-experiment's results which applied with high concentrations of medicaments and according to many limitations in regenerative endodontics procedures such as cell toxicity and non-completely removable of the medicaments from the root canal system associated with the use of high levels of

medicaments, we decided synthesis the double antibiotics loaded-PVP fiber group from low concentrations to high concentrations such as, 5%, 7%, 9% and 10%(w/w) respectively in order to exhibit more uniform fiber distributions and nanoscale diameters compared to the single antibiotic loaded-PVP fiber mates. The digital images of all obtained metronidazole-poly(vinylpyrrolidone) fiber samples are presented in **Figure 4.13.**

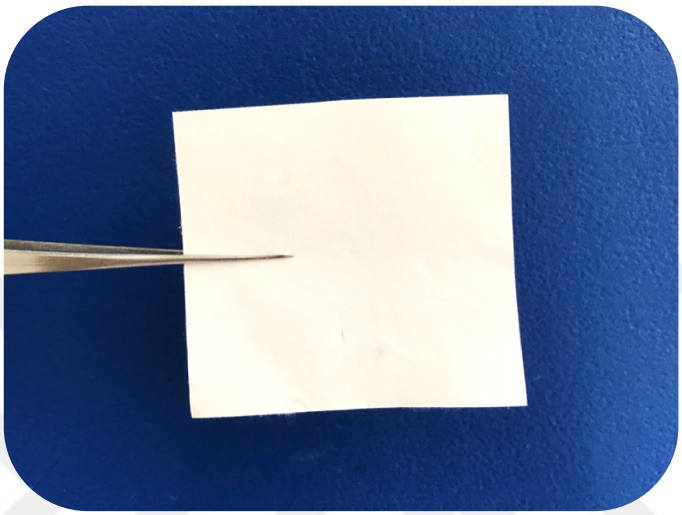

**Figure 4.14.** The optical photos of the 9%(w/w) of double antibiotics loaded nanofibers mat produced via electrospinning strategy

### 4.4.1 Scanning electron microscope (SEM) morphological analysis, fiber diameter and distribution determination

SEM images were taken from electrospun MET-CIP-PVP fibers, which were obtained from the polymer solution and electrospinning conditions mentioned above to get detailed information of the morphologies of the fiber structures. Besides, SEM images were also taken at high magnification to analyze the diameter and distribution of the fibers. **Figure 4.14 a1 and a2** figures were showed two different focus points of the fibers that formed of 5% MET-CIP-PVP dissolved in Et-OH.

A nano-fibrous network with interconnected micro-sized pores was seen for this sample. Under the applied conditions, fiber structure was seen with nano-level and slightly uniformity fibers structures. A fiber diameter was observed for 5% MET-PVP sample [804±255 ($313_{MİN}$-$1611_{MAX}$) nm] with a gaussian distribution (homogenous) fiber distribution was noticed for all 5% and 7% MET-CIP-PVP samples. The inset graph shows

the fiber diameter distribution for this sample **Figure 4.14 a3.** The second antibiotic concentration that was added to the PVP solution was 7% (w/w) of CIP-MET. This concentration caused to form a regulated fiber structure according to the previous sample 5% (w/w) CIP-MET-PVP. As shown in **Figure 4.14 b1** which shows the x1500 focus point of the sample, there were tinny fiber structures but related to concentrated objects. According to the use of the same electrospinning fabricated conditions, **Figure 4.14 b2** which is showed the x10000 focus point of the SEM image, these objects caused to an increase in the fiber diameters to [744±272 ($315_{MİN}$-$1595_{MAX}$) nm] **Figure 4.14 b3.** As summarize, due to these objects the fiber diameters decreased due to increase the antibiotics concentrations. A nano-fibrous network with interconnected nano-sized pores was seen for this sample. In order to increase the antibiotic concentration to 9% (w/w) **Figure 4.14 c1 and c2** the fiber structure was showed a really uniform and organized structure, and the diameters of this structure were showed slightly decreased [642±185 ($359_{MİN}$-$1198_{MAX}$) nm] **Figure 4.14 c3** Whereas, the interconnected network showed nano-sized pores. The last sample of CIP-MET-PVP had 11% (w/w), this concentration caused to fabricate a non-organized structure of nanofibers, but this structure had again tinny beads related to the nanofibers. Besides, these beads in this structure had not to cause to highly increase of the fiber diameters **Figure 4.14 d1 and d2** but inspired to a similar size of the 11% (w/w), was [690±208 ($312_{MİN}$-$1126_{MAX}$) nm]. Therefore, the experiments were continued by increasing the antibiotic concentrations from 5%(w/w) to 11%(w/w), according to the obtained SEM images the diameter analysis, the distributions of the fibers and to the antibiotic concentration in order to have effective antibacterial role of the sample will be used in the other studies, the 9%(w/w) of MET-CIP-PVP group was selected of double antibiotics-loaded PVP-fibers to apply it in the dentin studies.

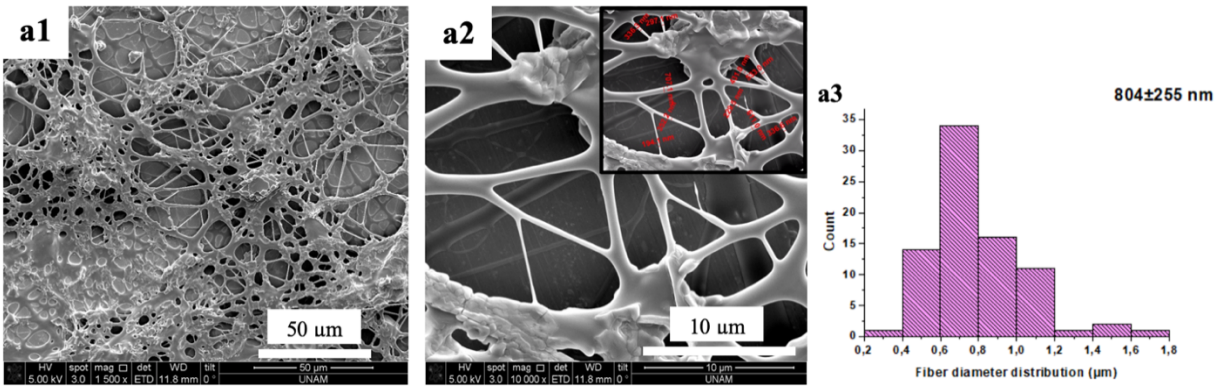

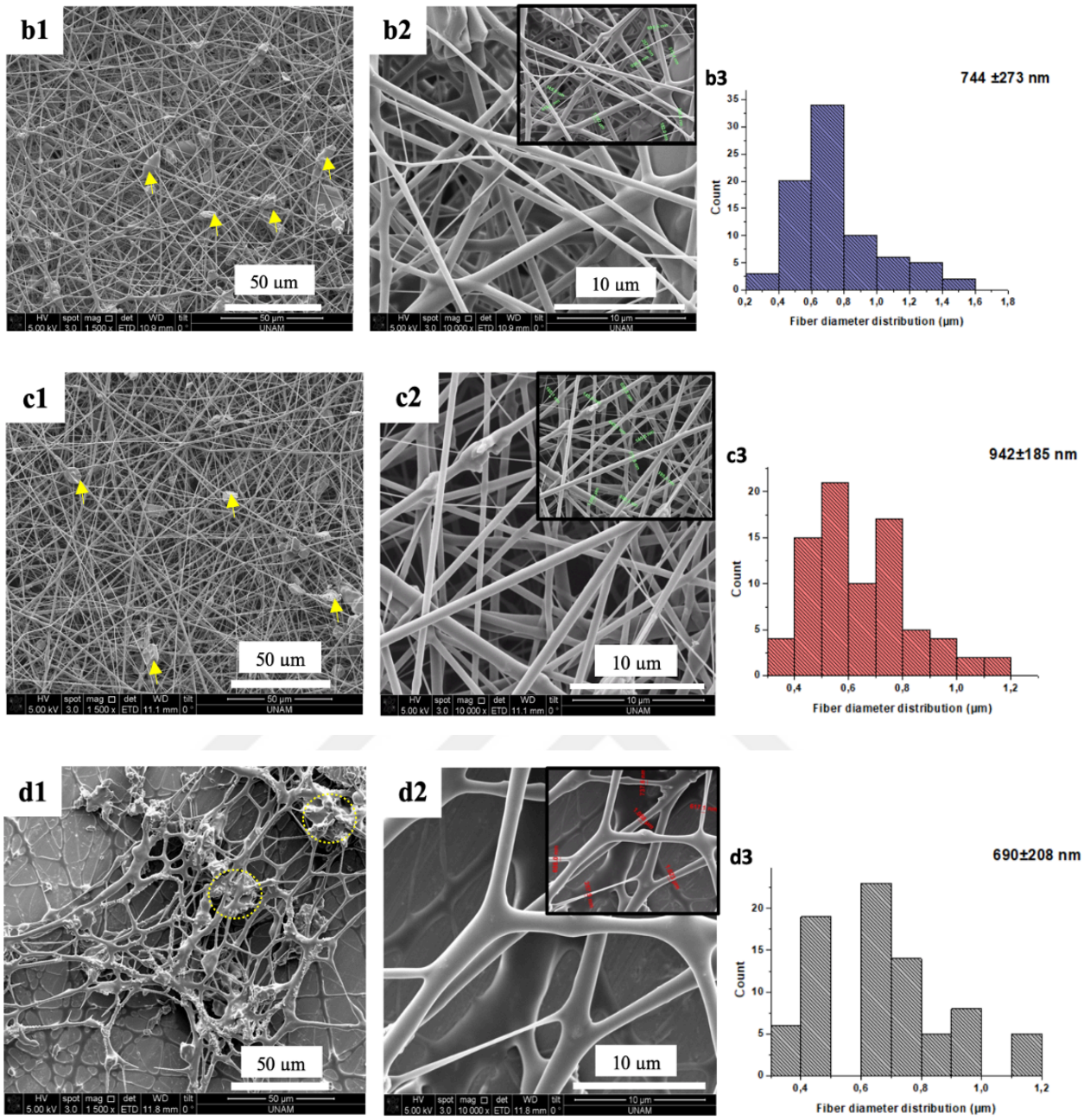


**Figure 4.15.** SEM images of electrospun nanofibers in different concentrations of CIP-MET. with PVP and different focus points of each concentration; a1). 5% CIP-MET-PVP (x1500), a2). 5% CIP-MET-PVP (x10000), a3). Fiber diameter distribution of 5% CIP-MET-PVP; b1). 7% CIP-MET-PVP (x1500), b2). 7% CIP-MET. -PVP (x10000), b3). Fiber diameter distribution of 7% CIP-MET-PVP; c1). 9% CIP-MET-PVP (x1500), c2). 9% CIP-MET-PVP (x10000), c3). Fiber diameter distribution of 9% CIP-MET-PVP; d1). 11% CIP-MET-PVP (x1500), d2). 11% CIP-MET-PVP (x10000), d3). Fiber diameter distribution of 11% CIP-MET-PVP

### 4.4.2 Energy dispersive x-ray spectroscopy (EDX)

CIP-MET-PVP electrospun nanofiber samples were synthesized with different concentrations according to the nanofiber structures which had been deformed in some samples. So, as mentioned in the SEM results and according to controlling the antibiotics concentrations, the chosen concentrations were as showed in **Figure 4.15** for 5, 7, 9, and 11%(w/w). Depending on that the double antibiotics have the same chemical elements with the Polymer in their chemical structures each one separately, we are waited to increase the percentages of the elements in the CIP-MET-PVP nanofiber mats. As represented the **Figure 4.15a** that is showed the chemical analysis of all samples results showed the presence of carbon, nitrogen, oxygen, and flor with slightly decreased atomic% values respectively.

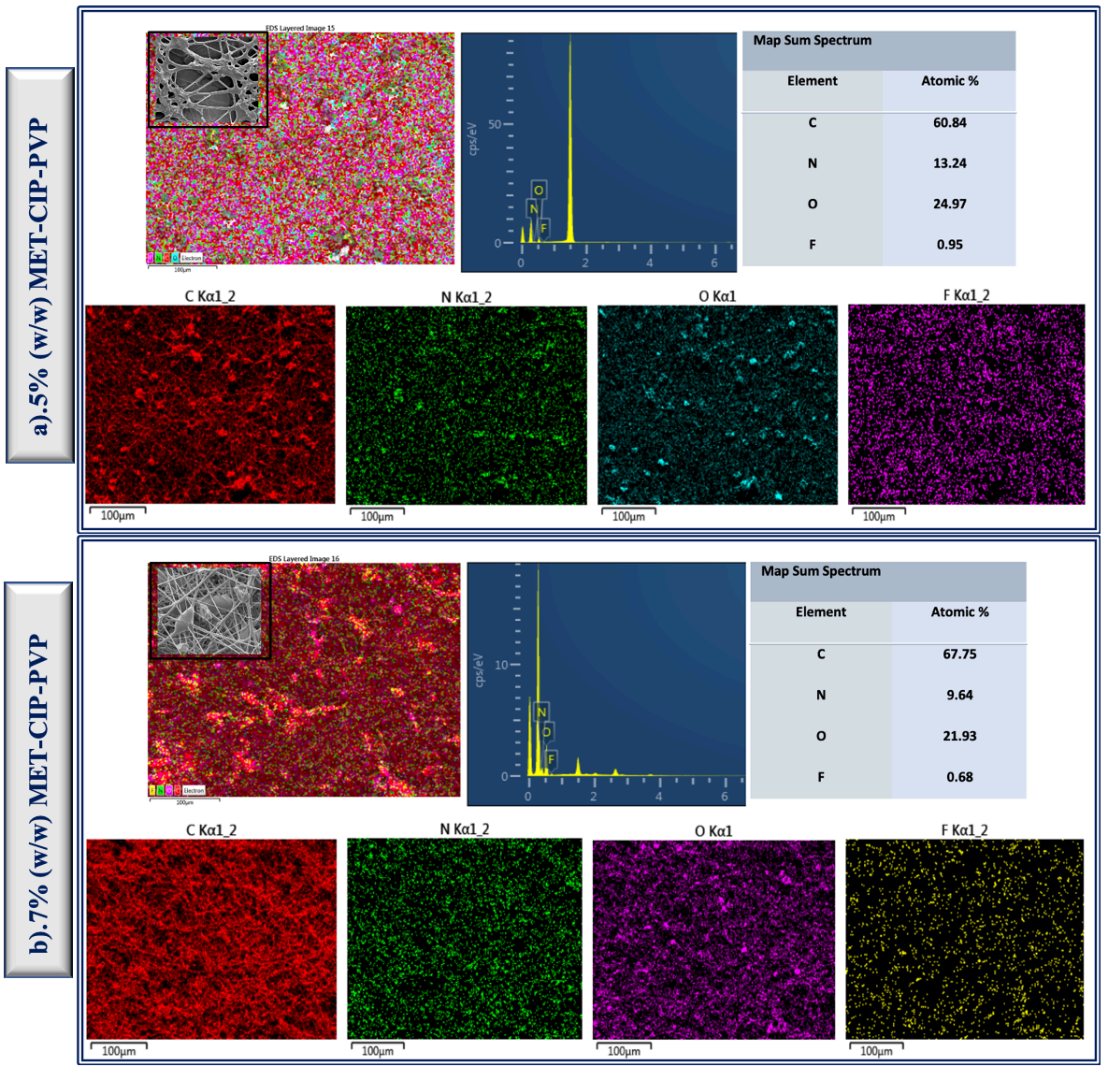

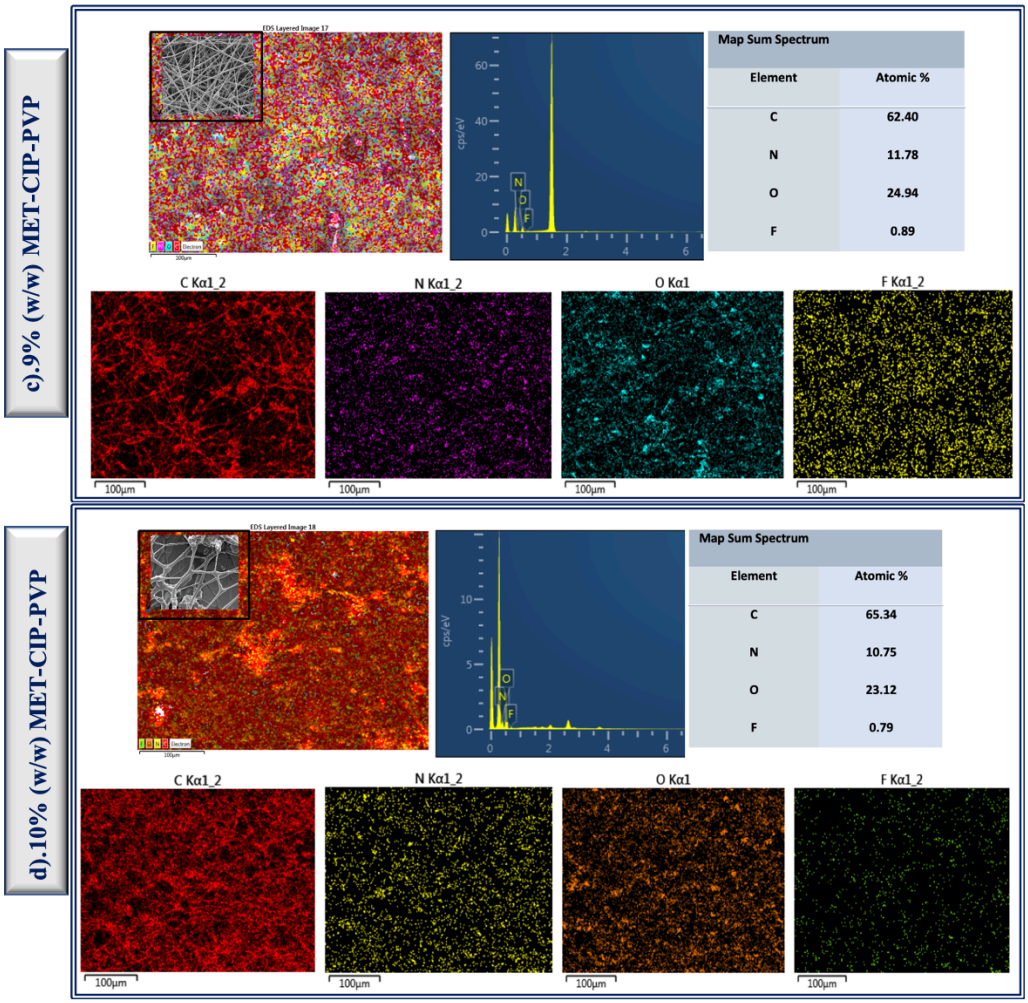


**Figure 4.16.** SEM-Energy Dispersive X-Ray Spectroscopy of a)5, b).7, c).9, and d).11% (w/w) CIP-MN-PVP electrospun nanofiber mats

## 4.5. Fabrication and Characterization of Triple Antibiotics Loaded-Poly(vinylptrrolidone) Nanofiber Samples

The triple antibiotic paste is an incorporation of three different antibiotics such as MET, CIP, and MINO. Triple antibiotic pastes were introduced by using three different antibiotics in the single antibiotic paste that can provide effective elimination of the microorganisms developed in the root canal system. Recent findings demonstrate not only the toxic effects of TAP on different types of dental cells but also significant dentin discoloration due to the presence of MINO with high concentration and difficulty with its complete removal from the canal systems.

In this experiment, many different experiments have been carried out with different concentrations of MET-CIP-MINO antibiotics with 8% of PVP polymer in order to develop optimum MET-CIP-MINO-PVP fibers with elimination the drawbacks mentioned above. Electrospinning was first performed with 5% (w/w) weight percent of metronidazole solution then with 7%, 9%, and 10% respectively which were dissolved in ET-OH. The digital images of all obtained metronidazole-poly(vinylpyrrolidone) fiber samples are presented in **Figure 4.16.**

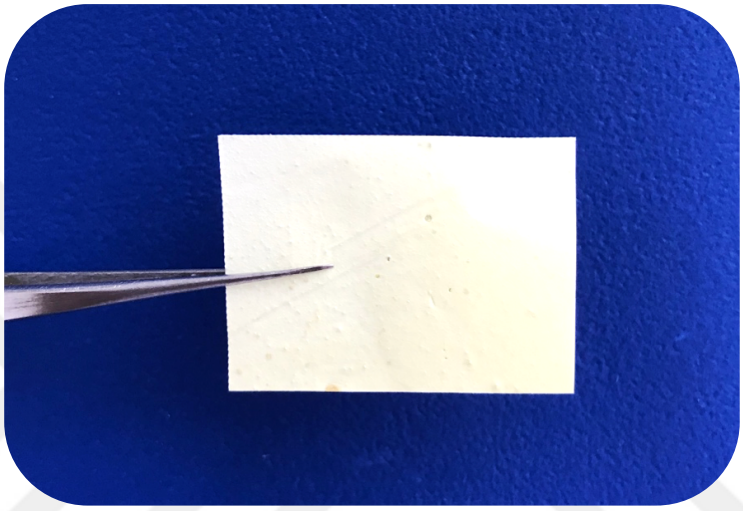

**Figure 4.17.** The optical photos of the 9%(w/w) of triple antibiotics loaded nanofibers mat produced via electrospinning strategy

### 4.5.1 Scanning electron microscope (SEM) morphological analysis, fiber diameter and distribution determination

SEM images were taken from electrospun MET-CIP-MINO-PVP fibers, which were obtained from the polymer solution and electrospinning conditions mentioned above to get detailed information of the morphologies of the fiber structures. Besides, SEM images were also taken at high magnification to analyze the diameter and distribution of the fibers. **Figure 4.17 a1 and a2** figures were showed two different focus points of the fibers that formed of 5% MET-CIP-MINO-PVP dissolved in Et-OH. A nano-fibrous network with interconnected micro-sized pores was seen for this sample. Under the applied conditions, fiber structure was seen with micro-level and slightly uniformity fibers structures. Fiber diameter was observed for a 5% MET-PVP sample [1657±987.6($120_{MİN}$-$3923_{MAX}$)nm] with a gaussian distribution (heterogenous) fiber distribution was noticed for all 5% and 7% MET-CIP-MINO-PVP

samples. The inset graph shows the fiber diameter distribution for this sample **Figure 4.17 a3.**

The second antibiotic concentration that was added to the PVP solution was 7% (w/w) of CIP-MET-MINO. This concentration caused to form a regulated fiber structure according to the previous sample 5% (w/w) CIP-MET-MINO-PVP. According to the use of the same electrospinning fabricated conditions, **Figure 4.17 b2** which is showed the x10000 focus point of the SEM image, these objects caused to an increase the fiber diameters to [1873±985 ($139_{MİN}$-$4903_{MAX}$)nm]. As summarize, due to these objects the fiber diameters decreased due to increase the antibiotics concentrations. A nano-fibrous network with interconnected nano-sized pores was seen for this sample. In order to increase in the antibiotic concentration to 9% (w/w), the fiber structure **Figure 4.17c1 and c2** was showed a really uniform and organized structure, and the diameters of this structure were showed slightly decreased [942±682 ($120_{MİN}$-$2944_{MAX}$)nm]. Whereas, the interconnected network showed nano-sized pores. The last sample of CIP-MET-MINO-PVP had 11% (w/w), this concentration caused to fabricate a non-organized structure of nanofibers **Figure 4.17d1 and d2**, but this structure had again tinny beads related to the nanofibers. Besides, these beads in this structure had not to cause to highly increase of the fiber diameters but inspired to a similar size of the 11% (w/w) was [591±465.2 ($159_{MİN}$-$2945_{MAX}$)nm]. Therefore, the experiments were continued by increasing the antibiotic concentrations from 5%(w/w) to 11%(w/w) too, according to the obtained SEM images, the diameter analysis, the distributions of the fibers and to the antibiotic concentration in order to have effective antibacterial role of the sample will be used in the other studies, the 9%(w/w) of MET-CIP-MINO-PVP group was selected of double antibiotics-loaded PVP-fibers to apply it in the dentin studies.

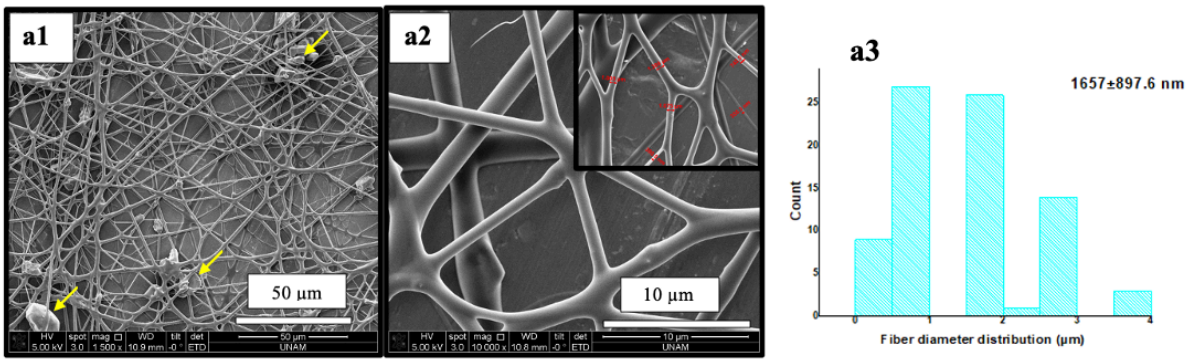

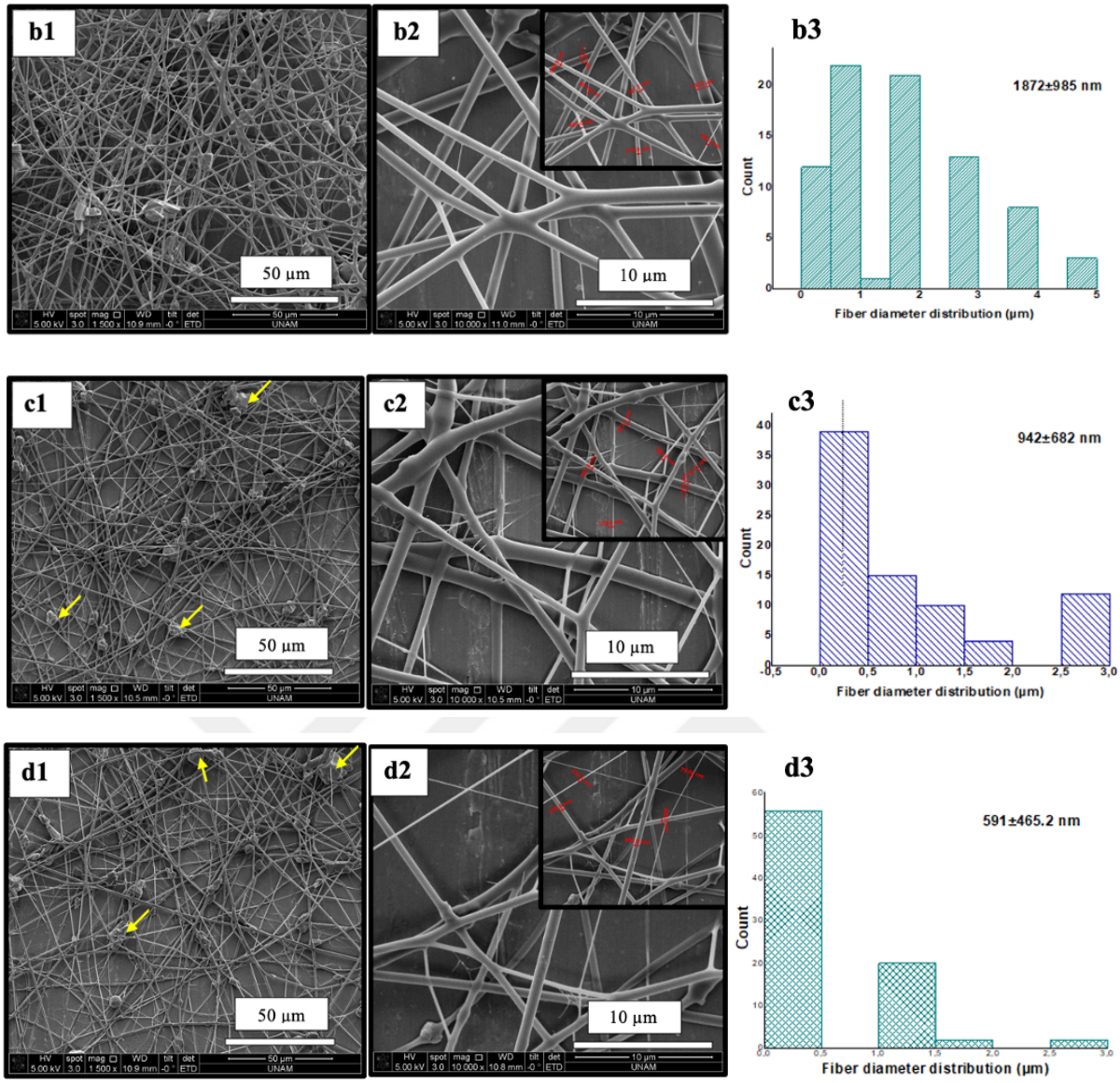


**Figure 4.18.** SEM images of electrospun nanofibers in different concentrations of CIP-MET-MINO. with PVP and different focus points of each concentration; a1). 5% CIP-MET-MINO-PVP (x1500), a2). 5% CIP-MET-MINO-PVP (x10000), a3). Fiber diameter distribution of 5% CIP-MET-MINO-PVP; b1). 7% CIP-MET-MINO-PVP (x1500), b2). 7% CIP-MET-MINO-PVP (x10000), b3). Fiber diameter distribution of 7% CIP-MET-MINO-PVP; c1). 9% CIP-MET-MINO -PVP (x1500), c2). 9% CIP-MET-MINO-PVP (x10000), c3). Fiber diameter distribution of 9% CIP-MET-MINO-PVP; d1). 11% CIP-MET-MINO-PVP (x1500), d2). 11% CIP-MET-MINO-PVP (x10000), d3). Fiber diameter distribution of 11% CIP-MET-MINO-PVP

### 4.5.2 Energy dispersive x-ray spectroscopy (EDX)

CIP-MET-MINO-PVP electrospun nanofiber samples were synthesized with different concentrations according to the nanofiber structures which had been deformed in some samples. So, as mentioned in the SEM results and according to controlling the antibiotics

concentrations the chosen concentrations, were as showed in **Figure 4.18** for 5, 7, 9, 11%(w/w). The polymer in their chemical structures each one separately, we are waited to increase the percentages of the elements in the CIP-MET-MINOPVP nanofiber mats. As represented the **Figure 4.17a** that is showed the chemical analysis of all samples results showed the presence of carbon, nitrogen, oxygen, and flor with slightly decreased atomic% values in some samples and increasing it in others.

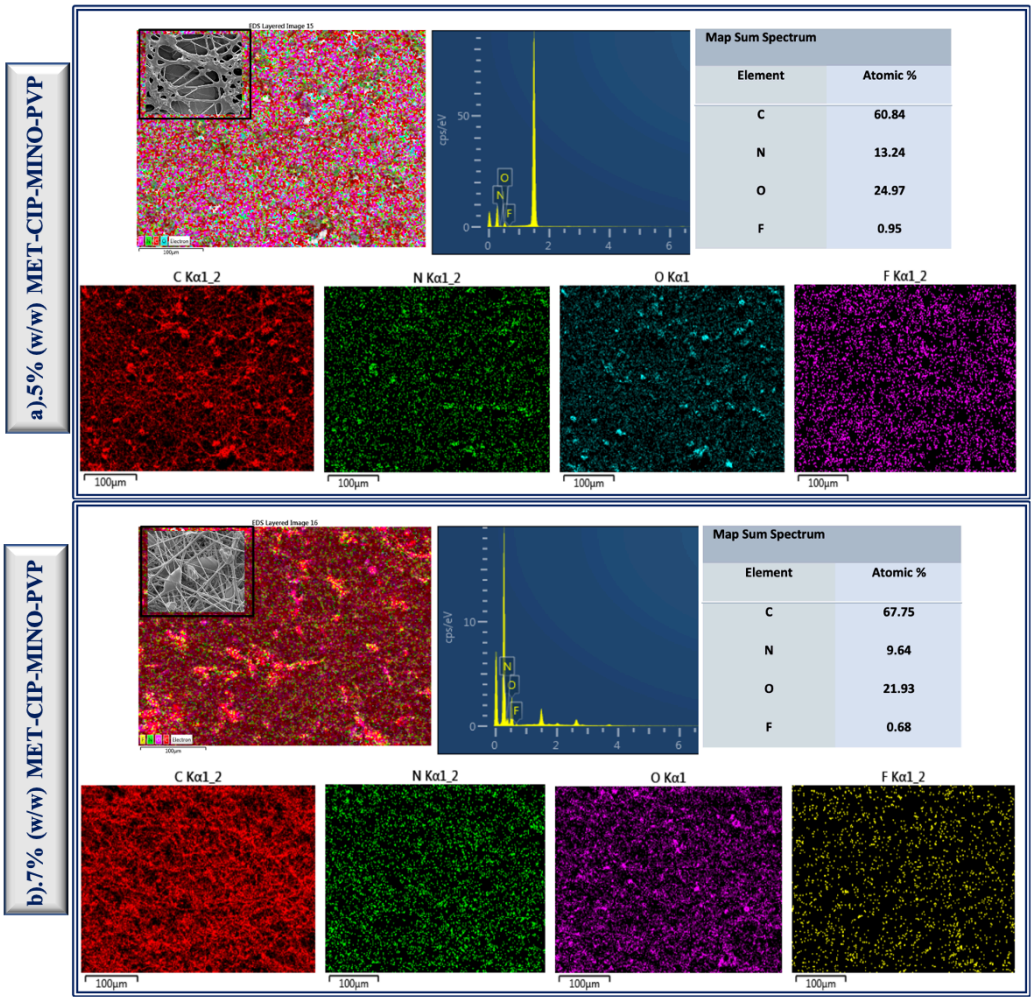

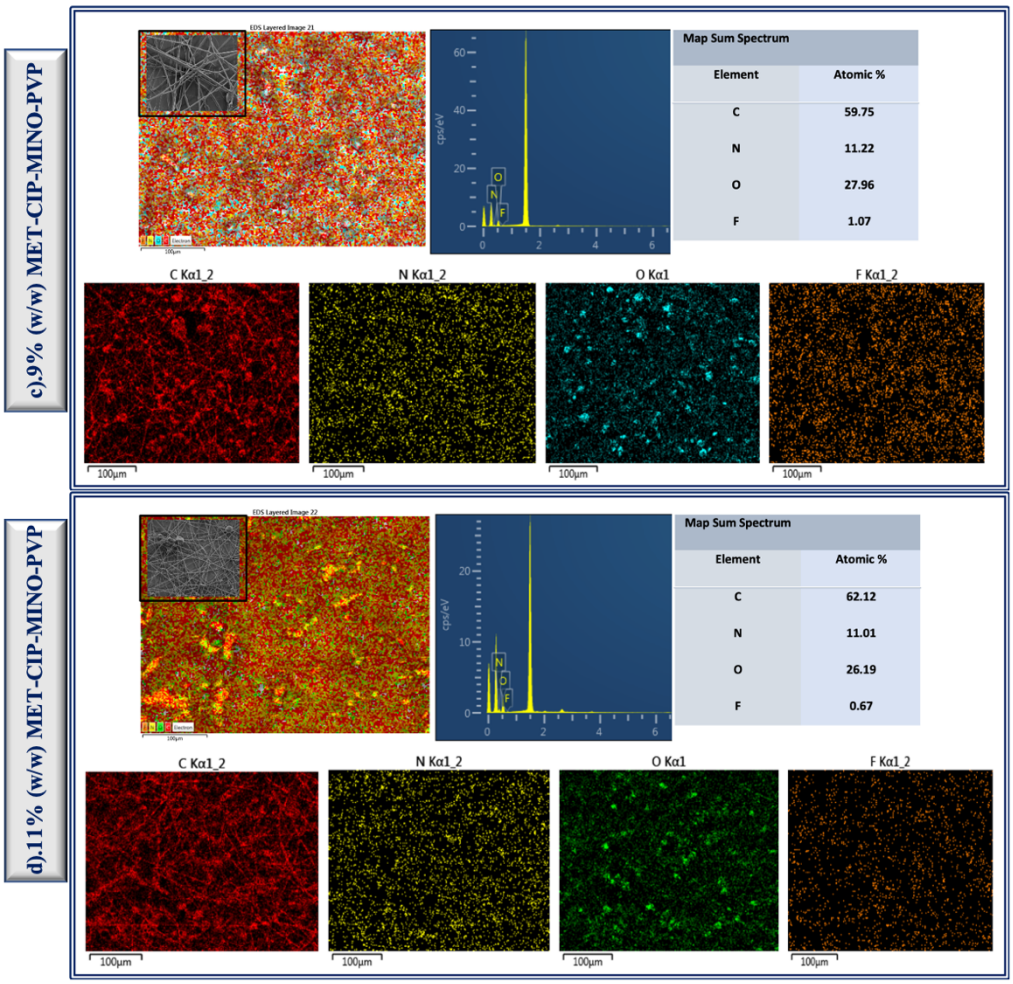


**Figure 4.19.** SEM-Energy Dispersive X-Ray Spectroscopy of a)5, b).7, c).9, and d).11% (w/w) CIP-MN-MINO-PVP electrospun nanofiber mats

## 4.6. Fabrication and Characterization of Calcium Hydroxide-Poly(vinylpyrrolidone) Containing Nanofiber Samples

In this experiment, four different concentrations of $Ca(OH)_2$ were mixed with 8%(w/w) of PVP powder in order to obtain uniform fiber structures. According to the pre-experiments of developing Ca(OH)2-PVP fibers, electrospinning was first performed from low concentration 2%(w/w) and 3%(w/w) **Figure 4.19** to high concentration 5%(w/w) too.

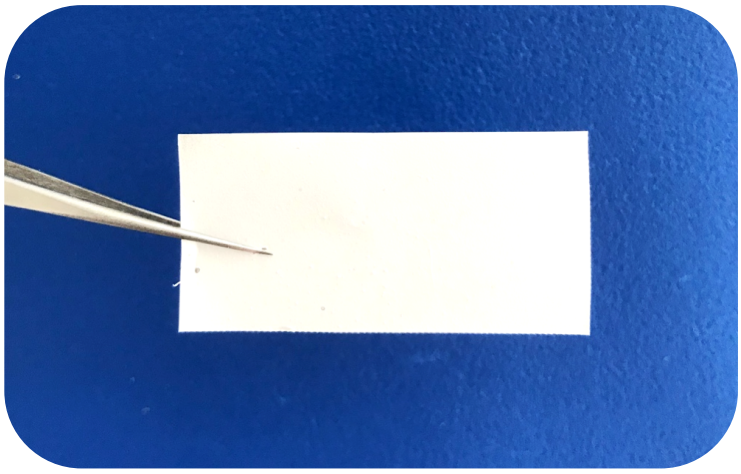

**Figure 4.20**. The optical photos of the 3%(w/w) of calcium hydroxide loaded nanofibers mat produced via electrospinning strategy

### 4.6.1 Scanning electron microscope (SEM) morphological analysis, fiber diameter and distribution determination

SEM images were taken from electrospun $Ca(OH)_2$-PVP fibers, which were obtained from the polymer solution and electrospinning conditions mentioned above to get detailed information of the morphologies of the fiber structures. Besides, SEM images were also taken at high magnification to analyze the diameter and distribution of the fibers. **Figure 4.20 a1 and a2** were showed two different focus points of the fibers that formed of a 2% $Ca(OH)_2$-PVP dissolved in Et-OH. A nano-fibrous network with interconnected micro-sized pores was seen for this sample. Under the applied conditions, fiber structure was seen with nano-level and slightly uniformity fibers structures. A fiber diameter was observed for 2% MET-PVP sample [545±177 ($224_{MİN}$-$949_{MAX}$)nm] with a gaussian distribution (heterogenous) fiber distribution was noticed for 2% Ca(OH)2-PVP samples. The inset graph shows the fiber diameter distribution for this sample **Figure 4.19 a3**. About the second sample which was prepared by dissolving 3% $Ca(OH)_2$-PVP in ET-OH and taken the SEM figures with two different focus points too. The fibers surfaces showed tinny beads presented homogenously upon the surfaces of the fibers, but these beads didn't affect on the fiber diameters volume and this sample showed fibers with a nano-level [642±192 ($302_{MİN}$-$1174_{MAX}$)nm] with slightly homogeneous of the fibers distributions. The third sample 4% which showed nano level with fiber diameters [683±244 ($299_{MİN}$-$1343_{MAX}$)nm]. Of fibers too and most heterogeneous of the distributions have also tinny beads on the surfaces of the fibers. The fourth sample is 5%(w/w) $Ca(OH)_2$-PVP, this sample didn't show any fiber forms

in its own structure. The 3%(w/w) of $Ca(OH)_2$-PVP group was selected to apply it in the dentin studies.

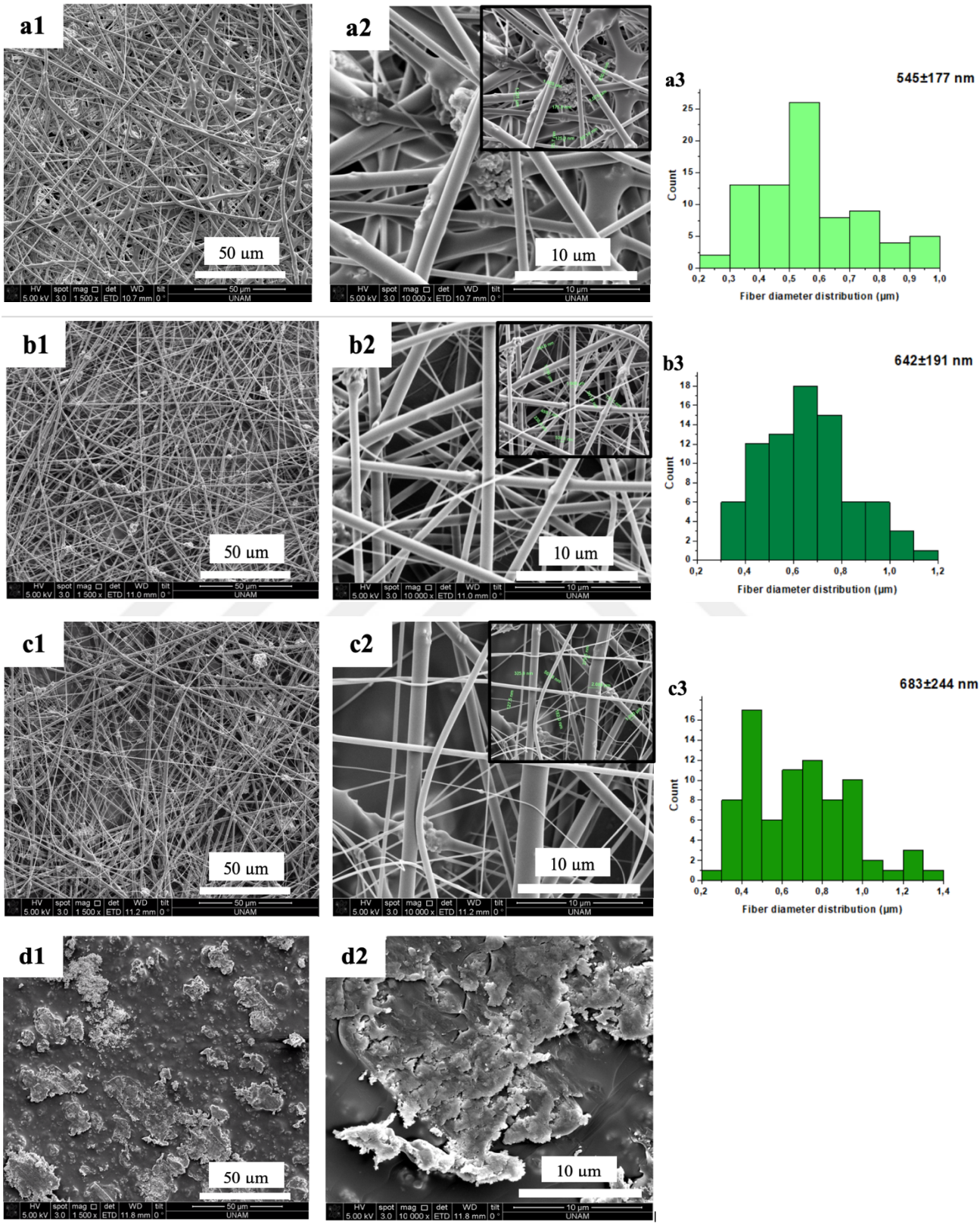

**Figure 4.21.** SEM images of electrospun nanofibers in different concentrations of MN with PVP and different focus points of each concentration; a1). 2% $Ca(OH)_2$-PVP (x1500), a2). 2% $Ca(OH)_2$-PVP (x10000), a3). Fiber diameter distribution of 2% $Ca(OH)_2$-PVP; b1). 3% $Ca(OH)_2$-PVP (x1500), b2). 3% $Ca(OH)_2$-PVP (x10000), b3). Fiber diameter distribution of 3% $Ca(OH)_2$-PVP; c1). 4% $Ca(OH)_2$-PVP (x1500), c2). 4% $Ca(OH)_2$-PVP (x10000), c3). Fiber diameter distribution of 4% $Ca(OH)_2$-PVP; d1). 5% $Ca(OH)_2$-PVP (x1500), d2). 5% $Ca(OH)_2$-PVP(x10000)

### 4.6.2 Energy dispersive x-ray spectroscopy (EDX)

For $Ca(OH)_2$ samples showed in **Figure 4.21** we can comment that the concentrations of carbon are among 58.78 and 68.09, 10.58-16.05 for nitrogen, 18.19, and 23.07 for oxygen. Related to increasing the $Ca(OH)_2$ values the chemical elements atomic% and EDX maps were showed increasing in 4%(w/w) sample and decreasing in the 3 and 5%(w/w) samples depended on the first sample 2(w/w).

a).2% (w/w) $Ca(OH)_2$-PVP

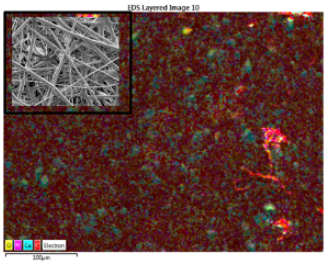

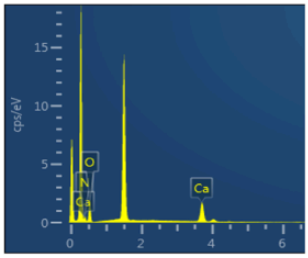


Map Sum Spectrum

| Element | Atomic % |
|---|---|
| C | 68.09 |
| N | 11.16 |
| O | 18.19 |
| Ca | 2.56 |

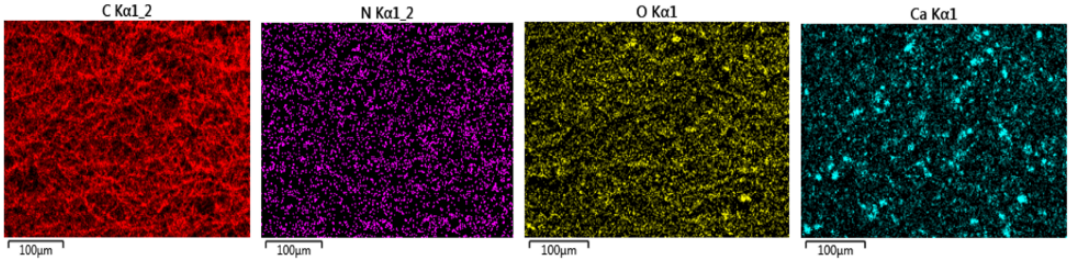


b).3% (w/w) $Ca(OH)_2$-PVP

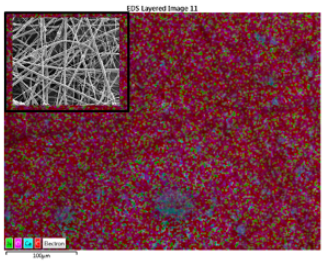

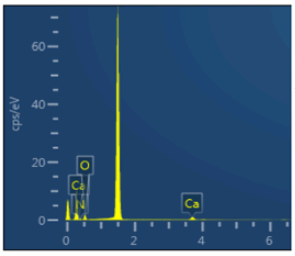


Map Sum Spectrum

| Element | Atomic % |
|---|---|
| C | 58.78 |
| N | 16.05 |
| O | 23.07 |
| Ca | 2.09 |

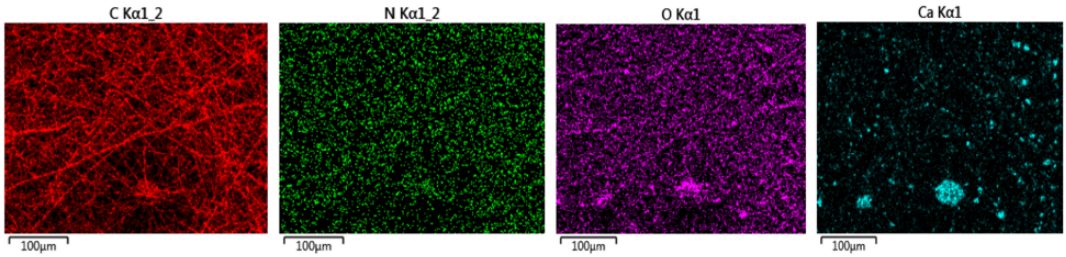

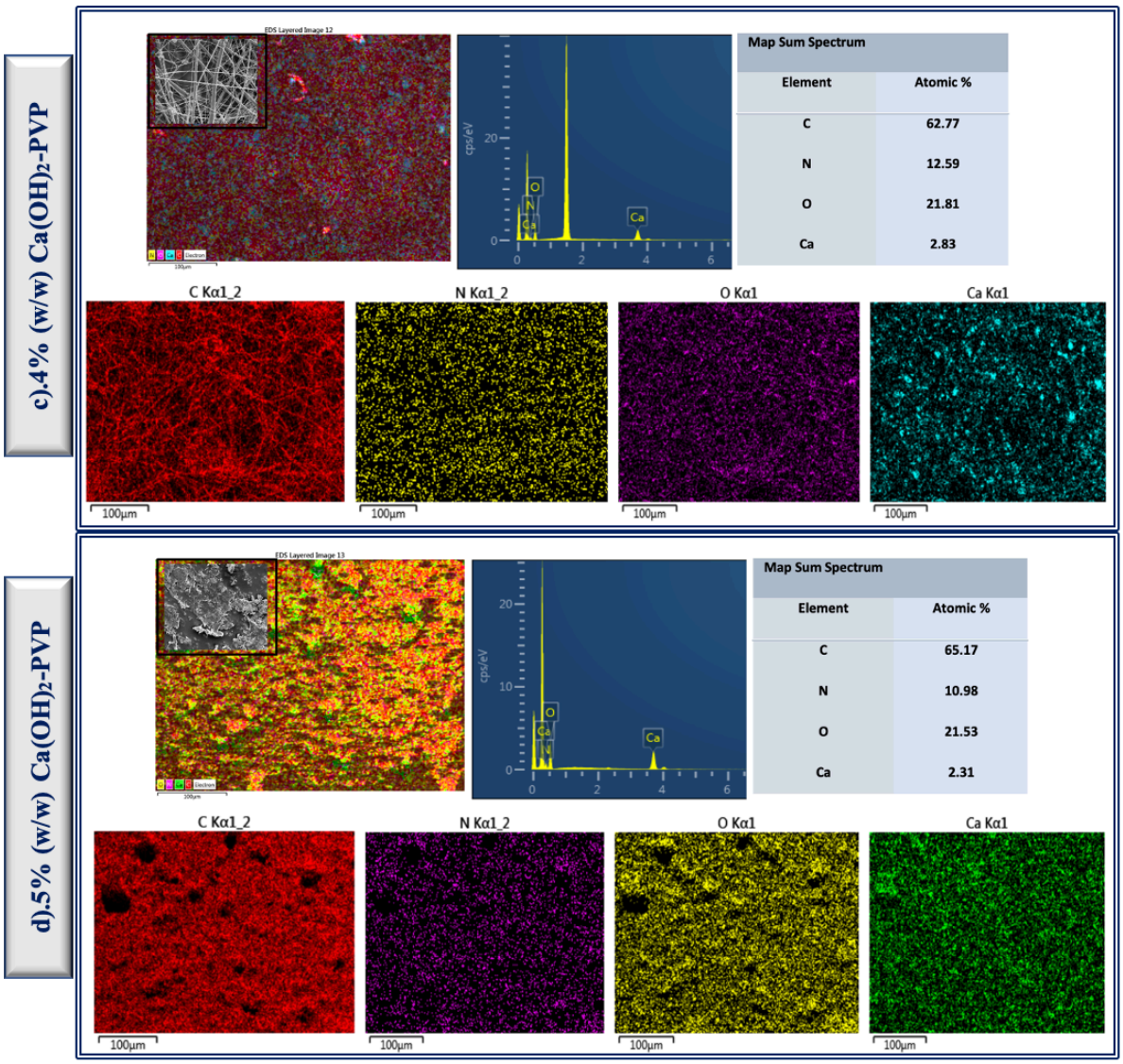


**Figure 4.22.** SEM-Energy Dispersive X-Ray Spectroscopy of a)2, b).3, c).4, and d).5% (w/w) $Ca(OH)_2$-PVP electrospun nanofiber mats

## 4.7. Characterization of Bare Modified Gutta-Percha

### 4.7.1 X-ray photoelectron spectroscopy (XPS) analysis

XPS measurements were performed in order to evaluate the surface' chemistry and functional groups present on the gutta-percha before and after the air irradiation process via plasma. **Figure 4.22a** shows the C1s, N1s, and O1s regions of the XP spectra corresponding to gutta-percha without any irradiation, respectively. As can be seen, this sample shows carbon **Figure 4.22b** and oxygen peaks **Figure 4.22c**. The positions of the carbon peaks of

the gutta-percha$_{control}$ group were 284.6 eV (C=C sp$^2$, and C-C sp$^3$) and 288.4 eV (C=O) (Figure b). XPS results presented that content of oxygen group on gutta-percha$_{control}$ group was 532 eV (C=O).

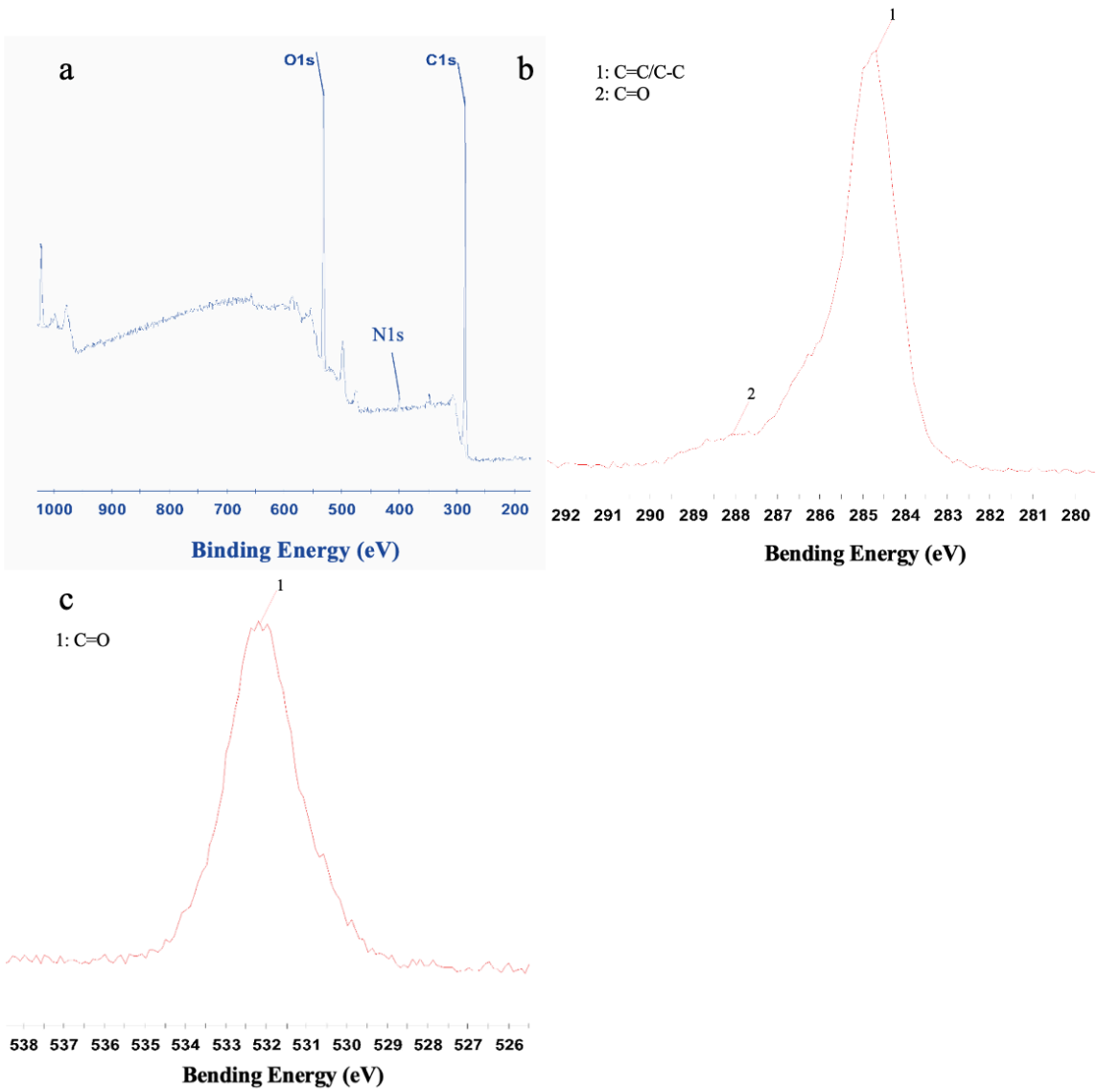


**Figure 4.23.** XPS analyzing data for a) Gutta-percha$_{control}$ surface, b). C1s, c) O1s

Compared to the gutta-percha$_{modified}$ group **Figure 4.23a,** the carbon peaks were 285 eV (C=C sp$^2$, and C-C sp$^3$) and 288.5 eV (C=O) **Figure 4.23b**. The oxygen peaks were 531.5 eV (C=O) **Figure 4.23c**. The relative area of oxygen peaks in the gutta-percha modified group was larger than the control group of corresponding to a more heterogeneous chemical environment. The intensity of oxygen is almost increased in the modified group

samples, and this indicates that the surface of the gutta-percha had successful air irradiation and had an active hydrophilic structure in order to coat gutta-percha cones with nanofiber mats **Table 4.1.** However, the carbon intensity decreased where the nitrogen intensity was slightly reduced.

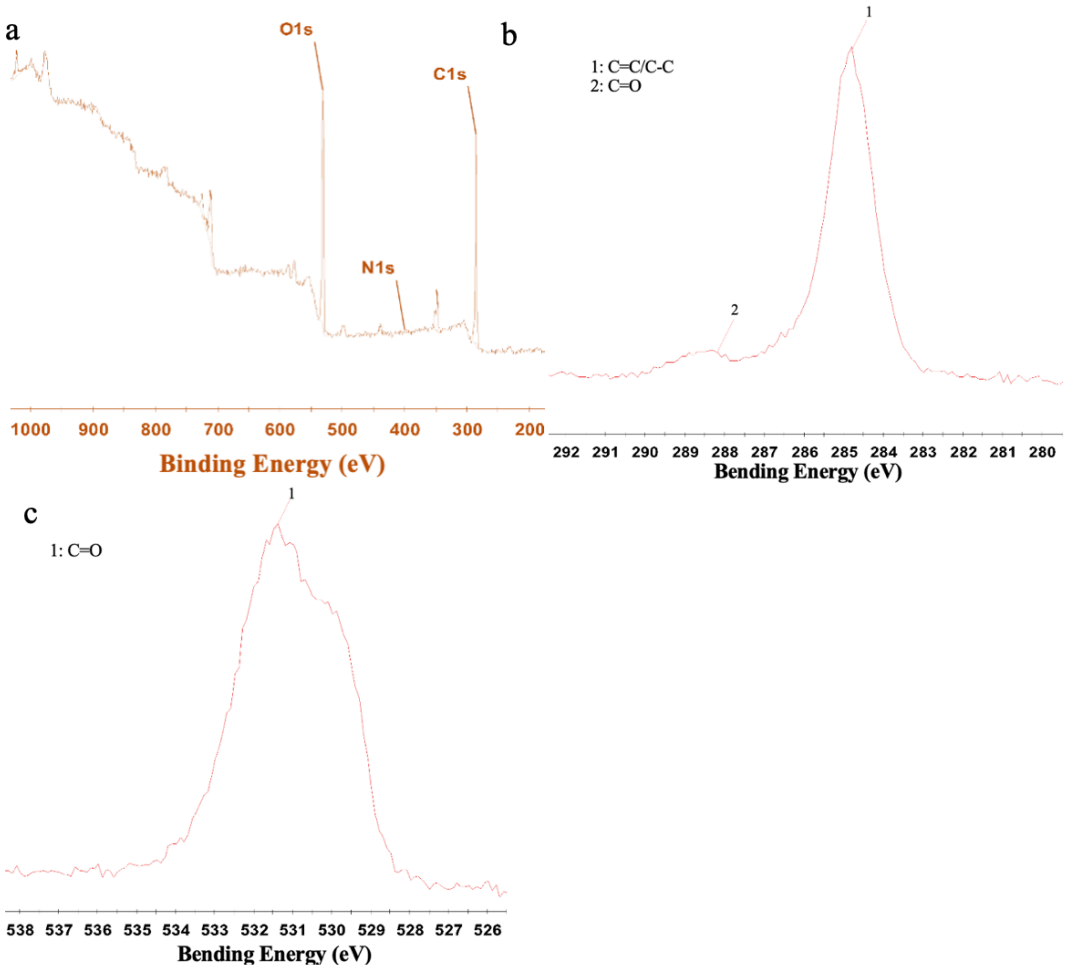


**Figure 4.24.** XPS analyzing data for a) Gutta-percha$_{modified}$ surface, b). C1s, c) O1s

**Table 4.1.** Percent atoms by XPS analysis

| Sample | %Atoms (XPS) | | | |
|---|---|---|---|---|
| | C | O | N | Ca |
| Gutta-Percha$_{control}$ | 67.31 | 23.16 | 3.17 | 0.39 |
| Gutta-Percha$_{modified}$ | 54.39 | 33.91 | 0.86 | 2.59 |

## 4.8. Characterization of Gutta-Percha Coated with Nanofiber Mats

After 15 minutes of air irradiation in the plasma device of the gutta-percha cones, samples were divided into 4 experiment groups and one control group. the sample groups

were chosen for this study were 9%, 9%, and 3%(w/w) of double antibiotics-loaded nanofiber mats, triple antibiotics-loaded nanofiber mats, and $Ca(OH)_2$-loaded nanofiber mats, respectively. The experiment groups were divided as (PVP-NFs, DA-NFs, TA-NFs, Ca(OH)2-NFs), and one pure gutta-percha. After the electrospinning process, all samples were collected from the device and were analyzed with a light microscope as shown in **Table 4.2** for each group.

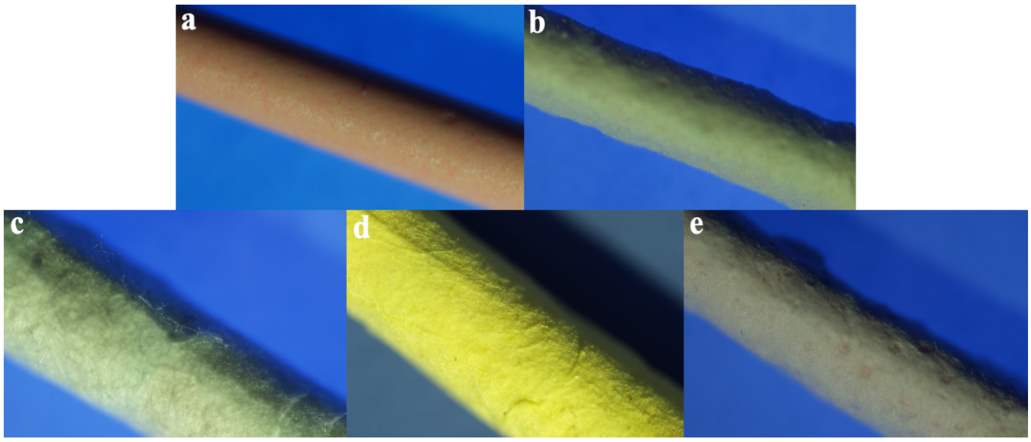


**Table 4.2.** Light microscope images of gutta-percha cones with different forms a) Bare gutta-percha b) coated with PVP-nanofiber mats c) double-antibiotics loaded PVP-nanofiber mats d) triple-antibiotics loaded PVP-nanofiber mats e) $Ca(OH)_2$ loaded PVP-nanofiber mats

## 4.9. Chemical Characterization of Dentin Surface

The FTIR spectra of all experiment groups and control group are shown in **Table 4.3** The broad bands in the 1013 $cm^{-1}$region can be attributed to the $PO_4^{3-}v_3$. The relatively weaker band at 1246 $cm^{-1}$can be assigned to the Amide III structure. It is interesting to note that the peak at 1411-1451 $cm^{-1}$ to the $CO_3^{2-}v_3$. Another adsorption band at 1645 $cm^{-1}$can be ascribed to the Amide I, while 1246, and 1551 $cm^{-1}$are attributed to the Amide III and Amide II, respectively.

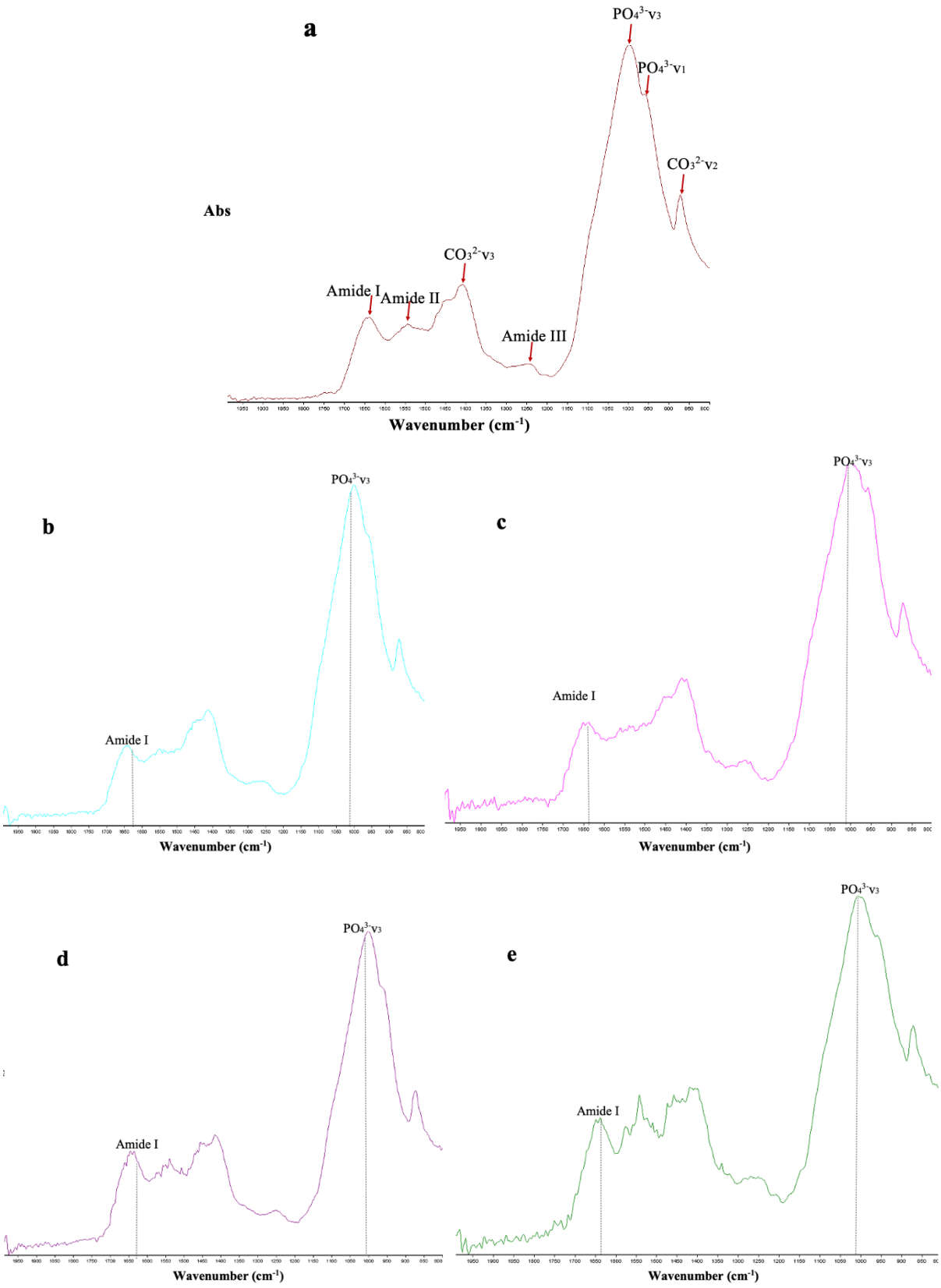
a
Abs
PO4 3- v3
PO4 3- v1
CO3 2- v2
CO3 2- v3
Amide I
Amide II
Amide III
Wavenumber (cm-1)
b
PO4 3- v3
Amide I
Wavenumber (cm-1)
c
PO4 3- v3
Amide I
Wavenumber (cm-1)
d
PO4 3- v3
Amide I
Wavenumber (cm-1)
e
PO4 3- v3
Amide I
Wavenumber (cm-1)

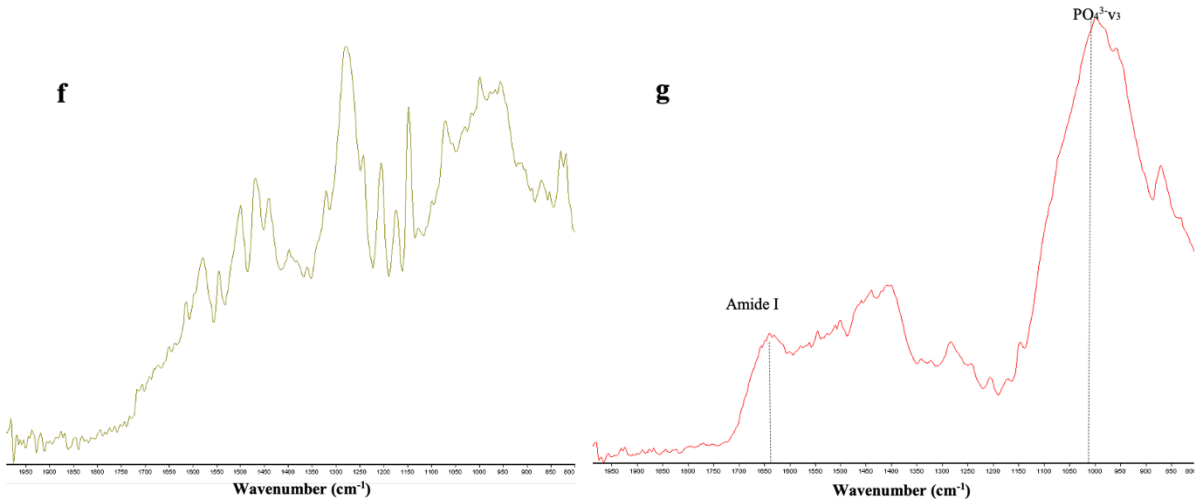


**Table 4.3.** Representative attenuated total reflectance (ATR) spectra of dentin from control group (untreated) a). Representative attenuated total reflectance (ATR) spectra of dentin after treated with DAP b), DA-NFs c), TAP d), TA-NFs e), $Ca(OH)_2$-paste f), and $Ca(OH)_2$-NFs g)

## 4.10. Physical Characterization of Dentin Surface

**Table 4.4** presents the SEM images of the dentin cleaned surfaces after 28 days of treatment with different focus points and the micrographs images of gutta-percha cones coated with different antibiotics loaded nanofibers in order to treat the dentin tubules. The control group (untreated specimens) and the group treated with DA-NFs$_{\%9}$ showed totally open dentinal tubules without any obliteration. Besides, specimens injected with bare PVP-nanofibers showed partial obliteration of the tubules. Whereas, specimens were treated with DAP and TAP presented thick crusts attached on the surface of dentin. Specimens treated with TA-NFs$_{\%9}$ showed non-obliteration of the tubules but with thin crusts attached on the edges of the dentin surface. In spite of that these agglomerates presented on the dentin surface of some groups treated with could be as an antibiotic's reservoir, but they can lead to changing the structure of the dentin tubules, tooth coloring, and effect negatively on the regeneration process of the stem cells.

**Tablo 4.4.** SEM micrographs showed the morphology of the dentin, light microscope figures showed the gutta-percha coated with nanofiber mats, and dentin discoloration results

| Groups | Cleaned Surface | | | Material's Surface | Dentin Surface |
|---|---|---|---|---|---|
| | SEM-100x | SEM-2000x | SEM-5000x | Light Microscope | |
| Control | 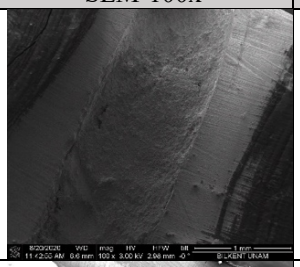 | 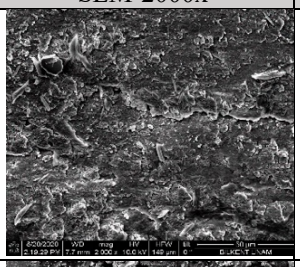 | 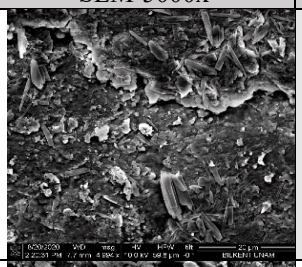 | | |
| Bare PVP-nanofiber | | 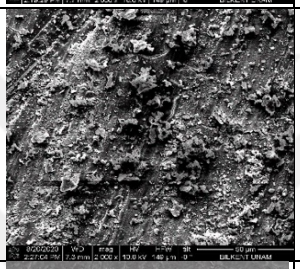 | 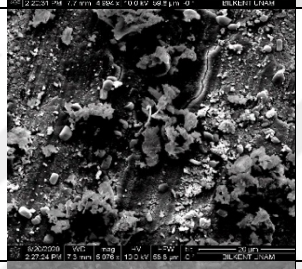 | 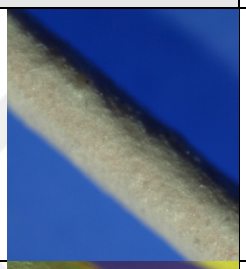 | |
| DA-NFs%9 | | | 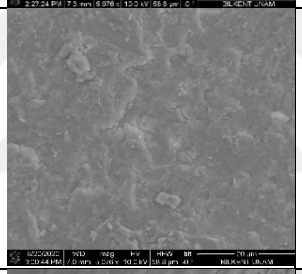 | 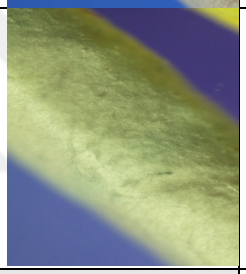 | |
| DAP | 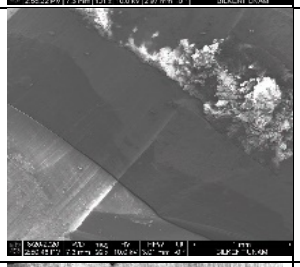 | 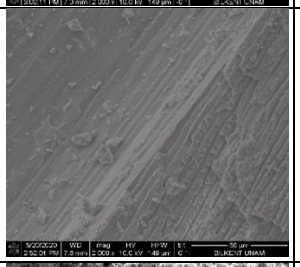 | 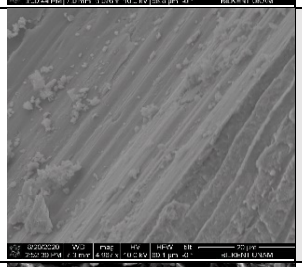 | | 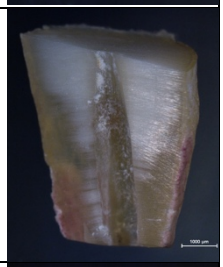 |
| TA-NFs%9 | 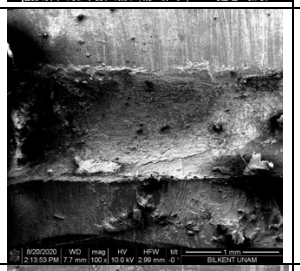 | 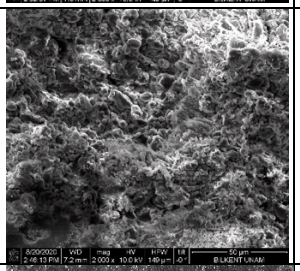 | 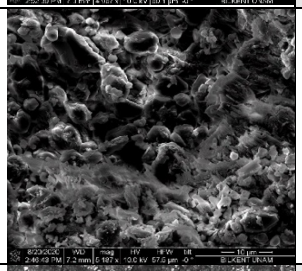 | 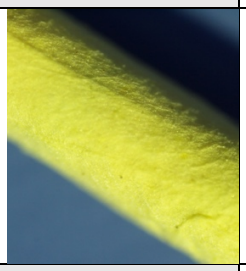 | |
| TAP | 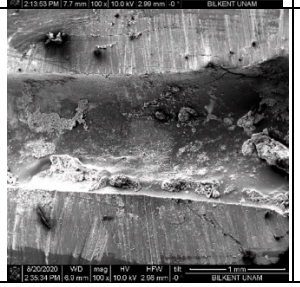 | 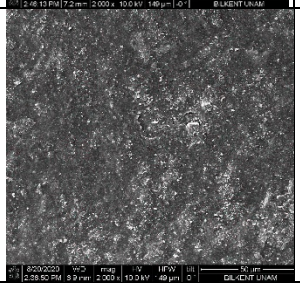 | 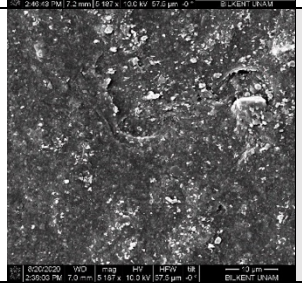 | | |

# 5. Discussion

In this thesis, different medicaments (MET, CIP, MINO, and $Ca(OH)_2$) loaded nanofiber mats were synthesized by electrospinning method in order to develop drug release systems for regenerative endodontic treatment. During these processes, fibers optimized, and the obtained final fiber structures were characterized by SEM and EDX for the evaluation of their morphologies and the chemical structures. After the electrospinning process and the characterization methods, the surfaces gutta-percha cones were irradiated via air plasma in order to achieve a better coating process of the fiber's mats upon the gutta-percha. XPS analysis was obtained in order to characterize the surface of gutta-percha cones after the plasma process then the obtained cones were transferred to the electrospinning device. Different gutta-percha cones were coated with various groups of medicaments injected within fiber mats for the first time. After characterized the samples, they applied inside mature teeth in order to analyze the chemical and physical structures of the dentin surface after treating them with those coated cones for 28 days by FT-IR and Nano-ESM devices, respectively.

Dental pulp shows a staminal role in the development of the teeth as appropriated cells that are responsible for dentin synthesis. Any bacterial infection of the dental pulp could lead to inflammation. Recently, regenerative endodontics has changed the teeth therapeutics with dental infections for forming new dentin. Many clinical approaches have been recommended applying root canal disinfection; chemical techniques besides mechanical approaches, covering but not limited to endodontic area, intracanal medicaments have been used with many available options. Among the available options, SAP, DAP, and TAP have been suggested in regenerative-based procedures. Despite significant their advancements such as effective disinfection, stem cells non-toxicity, and low probability of allergic reactions, as mentioned above recently there are findings have warned of the potentially toxic effects of the high concentrations of these antibiotic pastes on dental pulp stem cells and teeth discoloration caused by MINO in TAP samples. Electrospinning is a basic nanotechnology-based method able to synthesize antibiotics-eluting polymer nanofibers as systems for drug delivery. The development of nanomaterials to achieve advanced applications in endodontics to handle the mentioned challenges is far from elementary. It needs special knowledge to drive unparalleled adaptations of nanotechnologies, also updating the clinicians on how

nanotechnologies may be applied in practices. We categorized the drug delivery systems applied by nanofibers loaded with different antibiotics for different aims according to the count of the antibiotics were injected within NFs as SA-NFs, DA-NFs, and TA-NFs, respectively. Using these forms of systems can provide encapsulate low concentrations of antibiotics into biomimetic, self-assemble, and injectable NF systems. We established the concept of antibiotic-loaded NFs as drug releasing systems with PVP polymer as the carrier structure applied in constant concentration.

Briefly, in this thesis, different antibiotic concentrations injected within PVP for the first time in order to achieve more cell-friendly disinfection drug release systems by nanofiber mats coated gutta-percha via modifying its surface by plasma irradiation compared to the currently used paste forms. Besides that, it was measured their effect on the dentin chemical and physical structures.

# 6. Conclusion

Our results demonstrated that the obtained fibrous fibers with specific concentrations mentioned before can serve as effective drug release systems for avoiding the drawbacks achieved with their paste forms. Moreover, current works are continued to evaluate the antimicrobial efficacy of our three main experiment groups (triple antibiotics loaded nanofibers (TA-NFs), double antibiotics loaded nanofibers (DA-NFs), and calcium hydroxide loaded nanofibers ($Ca(OH)_2$-NFs)) against different types of bacteria, measurement the cytocompatibility of the nanofiber mats, and to measurement the ability of dental pulp stem cells (DPSCs) to adhere and proliferation.

# REFERENCES


[1] "Cohen's Pathways of the Pulp Expert Consult 12th Edition." https://www.nobelkitabevi.com.tr/dis-hekimligi/7959-cohen-s-pathways-of-the-pulp-expert-consult-12th-edition.html (accessed Aug. 22, 2020).

[2] J. F. Siqueira, I. N. Rôças, and M. G. Silva, "Prevalence and Clonal Analysis of Porphyromonas gingivalis in Primary Endodontic Infections," *J. Endod.*, vol. 34, no. 11, pp. 1332–1336, Nov. 2008, doi: 10.1016/j.joen.2008.08.021.

[3] A. R. Diogenes, N. B. Ruparel, F. B. Teixeira, and K. M. Hargreaves, "Translational science in disinfection for regenerative endodontics," *J. Endod.*, vol. 40, no. 4 SUPPL., 2014, doi: 10.1016/j.joen.2014.01.015.

[4] S. I. Iwaya, M. Ikawa, and M. Kubota, "Revascularization of an immature permanent tooth with apical periodontitis and sinus tract," *Dent. Traumatol.*, vol. 17, no. 4, pp. 185–187, Aug. 2001, doi: 10.1034/j.1600-9657.2001.017004185.x.

[5] N. B. Ruparel, F. B. Teixeira, C. C. R. Ferraz, and A. Diogenes, "Direct effect of intracanal medicaments on survival of stem cells of the apical papilla," *J. Endod.*, vol. 38, no. 10, pp. 1372–1375, Oct. 2012, doi: 10.1016/j.joen.2012.06.018.

[6] K. M. Galler, "Clinical procedures for revitalization: current knowledge and considerations," *Int. Endod. J.*, vol. 49, no. 10, pp. 926–936, Oct. 2016, doi: 10.1111/iej.12606.

[7] S. Ramakrishna, K. Fujihara, W.-E. Teo, T.-C. Lim, and Z. Ma, "Electrospinning Process," in *An Introduction to Electrospinning and Nanofibers*, WORLD SCIENTIFIC, 2005, pp. 90–154.

[8] R. I. Althumairy, F. B. Teixeira, and A. Diogenes, "Effect of dentin conditioning with intracanal medicaments on survival of stem cells of apical papilla," *J. Endod.*, vol. 40, no. 4, pp. 521–525, 2014, doi: 10.1016/j.joen.2013.11.008.

[9] J. Wang and M. Windbergs, “Controlled dual drug release by coaxial electrospun fibers – Impact of the core fluid on drug encapsulation and release,” *Int. J. Pharm.*, vol. 556, pp. 363–371, Feb. 2019, doi: 10.1016/j.ijpharm.2018.12.026.

[10] M. T. P. Albuquerque, M. C. Valera, M. Nakashima, J. E. Nör, and M. C. Bottino, “Tissue-engineering-based strategies for regenerative endodontics,” *Journal of Dental Research*, vol. 93, no. 12. SAGE Publications Inc., pp. 1222–1231, Dec. 25, 2014, doi: 10.1177/0022034514549809.

[11] M. C. Bottino *et al.*, “Bioactive nanofibrous scaffolds for regenerative endodontics,” *J. Dent. Res.*, vol. 92, no. 11, pp. 963–969, Nov. 2013, doi: 10.1177/0022034513505770.

[12] M. L. A. Porter, E. A. Münchow, M. T. P. Albuquerque, K. J. Spolnik, A. T. Hara, and M. C. Bottino, “Effects of Novel 3-dimensional Antibiotic-containing Electrospun Scaffolds on Dentin Discoloration,” *J. Endod.*, vol. 42, no. 1, pp. 106–112, Jan. 2016, doi: 10.1016/j.joen.2015.09.013.

[13] M. T. P. Albuquerque *et al.*, “Antimicrobial Effects of Novel Triple Antibiotic Paste-Mimic Scaffolds on Actinomyces naeslundii Biofilm,” *J. Endod.*, vol. 41, no. 8, pp. 1337–1343, Aug. 2015, doi: 10.1016/j.joen.2015.03.005.

[14] M. T. P. Albuquerque, M. C. Valera, C. S. Moreira, E. Bresciani, R. M. De Melo, and M. C. Bottino, “Effects of Ciprofloxacin-containing Scaffolds on Enterococcus faecalis Biofilms,” *J. Endod.*, vol. 41, no. 5, pp. 710–714, May 2015, doi: 10.1016/j.joen.2014.12.025.

[15] M. C. Bottino *et al.*, “A novel three-dimensional scaffold for regenerative endodontics: Materials and biological characterizations,” *J. Tissue Eng. Regen. Med.*, vol. 9, no. 11, pp. E116–E123, Nov. 2015, doi: 10.1002/term.1712.

[16] M. G. C. Sousa, M. R. Maximiano, R. A. Costa, T. M. B. Rezende, and O. L. Franco, “Nanofibers as drug-delivery systems for infection control in dentistry,”

*Expert Opinion on Drug Delivery*, vol. 17, no. 7. Taylor and Francis Ltd, pp. 919–930, Jul. 02, 2020, doi: 10.1080/17425247.2020.1762564.

[17] S. Ghabraei, B. Bolhari, M. M. Sabbagh, and M. S. Afshar, "Comparison of Antimicrobial Effects of Triple Antibiotic Paste and Calcium Hydroxide Mixed with 2% Chlorhexidine as Intracanal Medicaments Against Enterococcus faecalis Biofilm.," *J. Dent. (Tehran).*, vol. 15, no. 3, pp. 151–160, May 2018, Accessed: Aug. 22, 2020. [Online]. Available:http://www.ncbi.nlm.nih.gov/pubmed/30090115.

[18] D. Pankajakshan, M. T. P. Albuquerque, J. D. Evans, M. M. Kamocka, R. L. Gregory, and M. C. Bottino, "Triple Antibiotic Polymer Nanofibers for Intracanal Drug Delivery: Effects on Dual Species Biofilm and Cell Function," *J. Endod.*, vol. 42, no. 10, pp. 1490–1495, Oct. 2016, doi: 10.1016/j.joen.2016.07.019.

[19] K. Kamocki, J. E. Nör, and M. C. Bottino, "Effects of ciprofloxacin-containing antimicrobial scaffolds on dental pulp stem cell viability - In vitro studies," *Arch. Oral Biol.*, vol. 60, no. 8, pp. 1131–1137, May 2015, doi:10.1016/j.archoralbio.2015.05.002.

[20] M. T. P. Albuquerque, J. D. Evans, R. L. Gregory, M. C. Valera, and M. C. Bottino, "Antibacterial TAP-mimic electrospun polymer scaffold: effects on P. gingivalis-infected dentin biofilm," *Clin. Oral Investig.*, vol. 20, no. 2, pp. 387–393, Mar. 2016, doi: 10.1007/s00784-015-1577-2.

[21] J. A. Petrino, K. K. Boda, S. Shambarger, W. R. Bowles, and S. B. McClanahan, "Challenges in Regenerative Endodontics: A Case Series," *J. Endod.*, vol. 36, no. 3, pp. 536–541, Mar. 2010, doi: 10.1016/j.joen.2009.10.006.

[22] W. P. Cruse and R. Bellizzi, "A historic review of endodontics, 1689-1963, part 1," *J. Endod.*, vol. 6, no. 3, pp. 495–499, 1980, doi: 10.1016/S0099-2399(80)80008-2.

[23] J. F. Siqueira, "Endodontic infections: Concepts, paradigms, and perspectives," *Oral Surg. Oral Med. Oral Pathol. Oral Radiol. Endod.*, vol. 94, no. 3, pp. 281–293, Sep. 2002, doi: 10.1067/moe.2002.126163.

[24] “4: Biological and clinical rationale for root-canal treatment and management of its failure | Pocket Dentistry.” https://pocketdentistry.com/4-biological-and-clinical-rationale-for-root-canal-treatment-and-management-of-its-failure/ (accessed Aug. 20, 2020).

[25] “The eight dental specialties: their origin and rise - PubMed.” https://pubmed.ncbi.nlm.nih.gov/2931970/ (accessed Aug. 20, 2020).

[26] “Cohen’s Pathways of the Pulp Expert Consult - 10th Edition.” https://www.elsevier.com/books/cohens-pathways-of-the-pulp-expert-consult/hargreaves/978-0-323-06489-7 (accessed Aug. 20, 2020).

[27] S. Seltzer, I. B. Bender, H. Nazimov, and I. Sinai, “Pulpitis-Induced Interradicular Periodontal Changes in Experimental Animals,” *J. Periodontol.*, vol. 38, no. 2, pp. 124–129, Mar. 1967, doi: 10.1902/jop.1967.38.2.124.

[28] M. Hülsmann, C. Rümmelin, and F. Schäfers, “Root canal cleanliness after preparation with different endodontic handpieces and hand instruments: A comparative SEM investigation,” *J. Endod.*, vol. 23, no. 5, pp. 301–306, 1997, doi: 10.1016/S0099-2399(97)80410-4.

[29] “the tooth anatomy: Yandex.Görsel’de 11 bin görsel bulundu.” https://yandex.com.tr/gorsel/search?pos=2&from=tabbar&img_url=https%3A%2F%2Fupload.wikimedia.org%2Fwikipedia%2Fcommons%2Fthumb%2F9%2F99%2FBlausen_0863_ToothAnatomy_02.png%2F500px-Blausen_0863_ToothAnatomy_02.png&text=the tooth anatomy&rpt=simage (accessed Aug. 20, 2020).

[30] “Clinical Endodontics: A Textbook - Kindle edition by Tronstad, Leif. Professional & Technical Kindle eBooks @ Amazon.com.” https://www.amazon.com/Clinical-Endodontics-Textbook-Leif-Tronstad-ebook/dp/B005WJJLR2 (accessed Aug. 20, 2020).

[31] "Textbook of Dental Anatomy, Physiology and Occlusion: 9789350259405: Medicine & Health Science Books @ Amazon.com." https://www.amazon.com/Textbook-Dental-Anatomy-Physiology-Occlusion/dp/9350259400 (accessed Aug. 20, 2020).

[32] F. J. Vertucci, "Root canal morphology and its relationship to endodontic procedures," *Endod. Top.*, vol. 10, no. 1, pp. 3–29, Mar. 2005, doi: 10.1111/j.1601-1546.2005.00129.x.

[33] P. Carrotte, "Endodontics: Part 4. Morphology of the root canal system," *Br. Dent. J.*, vol. 197, no. 7, pp. 379–383, Oct. 2004, doi: 10.1038/sj.bdj.4811711.

[34] K. Kerekes and L. Tronstad, "Long-term results of endodontic treatment performed with a standardized technique," *J. Endod.*, vol. 5, no. 3, pp. 83–90, 1979, doi: 10.1016/S0099-2399(79)80154-5.

[35] M. D. Benner, D. D. Peters, M. Grower, and W. E. Bernier, "Evaluation of a new thermoplastic gutta-percha obturation technique using 45CA," *J. Endod.*, vol. 7, no. 11, pp. 500–508, Jan. 1981, doi: 10.1016/S0099-2399(81)80112-4.

[36] L. Spångberg, "Biologic effects of root canal filling materials. The effect on bone tissue of two formaldehyde-containing root canal filling pastes: N2 and Riebler's paste," *Oral Surgery, Oral Med. Oral Pathol.*, vol. 38, no. 6, pp. 934–944, Dec. 1974, doi: 10.1016/0030-4220(74)90347-8.

[37] S. I. Iwaya, M. Ikawa, and M. Kubota, "Revascularization of an immature permanent tooth with apical periodontitis and sinus tract," *Dent. Traumatol.*, vol. 17, no. 4, pp. 185–187, Aug. 2001, doi: 10.1034/j.1600-9657.2001.017004185.x.

[38] F. Banchs and M. Trope, "Revascularization of immature permanent teeth with apical periodontitis: New treatment protocol?," *J. Endod.*, vol. 30, no. 4, pp. 196–200, 2004, doi: 10.1097/00004770-200404000-00003.

[39] A. Angelova Volponi, L. K. Zaugg, V. Neves, Y. Liu, and P. T. Sharpe, "Tooth

Repair and Regeneration," *Curr. Oral Heal. Reports*, vol. 5, no. 4, pp. 295–303, Dec. 2018, doi: 10.1007/s40496-018-0196-9.

[40] G. T. J. Huang *et al.*, "Stem/Progenitor cell-mediated de novo regeneration of dental pulp with newly deposited continuous layer of dentin in an in vivo model," in *Tissue Engineering - Part A*, Feb. 2010, vol. 16, no. 2, pp. 605–615, doi: 10.1089/ten.tea.2009.0518.

[41] M. S. R. Kumar, K. M. Varma, R. K. Satish, R. M. K. Nanduri, S. M. K. Raju, and M. Rao, "Stem cells in endodontic therapy," *Int. J. Med. Res. Heal. Sci.*, vol. 3, no. 4, p. 977, 2014, doi: 10.5958/2319-5886.2014.00035.6.

[42] C. Morsczeck *et al.*, "Isolation of precursor cells (PCs) from human dental follicle of wisdom teeth," *Matrix Biol.*, vol. 24, no. 2, pp. 155–165, Apr. 2005, doi: 10.1016/j.matbio.2004.12.004.

[43] M. M. Cordeiro *et al.*, "Dental Pulp Tissue Engineering with Stem Cells from Exfoliated Deciduous Teeth," *J. Endod.*, vol. 34, no. 8, pp. 962–969, Aug. 2008, doi: 10.1016/j.joen.2008.04.009.

[44] S. Shabeenataj and L. Priya, "Stem cell Therapy for Thalassemia: A review," *Int. J. PharmTech Res.*, vol. 6, no. 4, pp. 1306–1308, 2014.

[45] J. Zhou, Q. Chen, Y. Zou, H. Chen, L. Qi, and Y. Chen, "Stem cells and cellular origins of breast cancer: Updates in the rationale, controversies, and therapeutic implications," *Frontiers in Oncology*, vol. 9, no. AUG. Frontiers Media S.A., p. 820, 2019, doi: 10.3389/fonc.2019.00820.

[46] K. Jhajharia, "Microbiology of endodontic diseases: A review article," *~ 227 ~ Int. J. Appl. Dent. Sci.*, vol. 5, no. 1, pp. 227–230, 2019, Accessed: Aug. 20, 2020. [Online]. Available: www.oraljournal.com.

[47] U. SJÖGREN, D. FIGDOR, S. PERSSON, and G. SUNDQVIST, "Influence of infection at the time of root filling on the outcome of endodontic treatment of teeth

with apical periodontitis," *Int. Endod. J.*, vol. 30, no. 5, pp. 297–306, Oct. 2003, doi: 10.1046/j.1365-2591.1997.00092.x.

[48] F. J. Vertucci, "Root canal anatomy of the human permanent teeth," *Oral Surgery, Oral Med. Oral Pathol.*, vol. 58, no. 5, pp. 589–599, 1984, doi: 10.1016/0030-4220(84)90085-9.

[49] L. C. de Paz, "Redefining the Persistent Infection in Root Canals: Possible Role of Biofilm Communities," *J. Endod.*, vol. 33, no. 6, pp. 652–662, 2007, doi: 10.1016/j.joen.2006.11.004.

[50] R. Huang, M. Li, and R. L. Gregory, "Bacterial interactions in dental biofilm," *Virulence*, vol. 2, no. 5. Taylor and Francis Inc., pp. 435–444, 2011, doi: 10.4161/viru.2.5.16140.

[51] H. Hotokezaka *et al.*, "Molecular analysis of RANKL-independent cell fusion of osteoclast-like cells induced by TNF-α, lipopolysaccharide, or peptidoglycan," *J. Cell. Biochem.*, vol. 101, no. 1, pp. 122–134, May 2007, doi: 10.1002/jcb.21167.

[52] A. I. Bolstad, H. B. Jensen, and V. Bakken, "Taxonomy, biology, and periodontal aspects of Fusobacterium nucleatum," *Clinical Microbiology Reviews*, vol. 9, no. 1. American Society for Microbiology, pp. 55–71, 1996, doi: 10.1128/cmr.9.1.55-71.1996.

[53] J. F. Siqueira, I. N. Rôças, and M. G. Silva, "Prevalence and Clonal Analysis of Porphyromonas gingivalis in Primary Endodontic Infections," *J. Endod.*, vol. 34, no. 11, pp. 1332–1336, Nov. 2008, doi: 10.1016/j.joen.2008.08.021.

[54] S. JF and S. BH, "Fungi in endodontic infections," *Oral Surg. Oral Med. Oral Pathol. Oral Radiol. Endod.*, vol. 97, no. 5, 2004, doi: 10.1016/S1079210404000046.

[55] H. C. Slavkin and P. M. Bartold, "Challenges and potential in tissue engineering," *Periodontology 2000*, vol. 41, no. 1. Periodontol 2000, pp. 9–15, Jun. 2006, doi:

10.1111/j.1600-0757.2006.00172.x.

[56] P. M. Bartold, Y. Xiao, S. P. Lyngstaadas, M. L. Paine, and M. L. Snead, "Principles and applications of cell delivery systems for periodontal regeneration," *Periodontology 2000*, vol. 41, no. 1. Periodontol 2000, pp. 123–135, Jun. 2006, doi: 10.1111/j.1600-0757.2006.00156.x.

[57] B. J. Baum and S. D. Tran, "Synergy between genetic and tissue engineering: creating an artificial salivary gland," *Periodontol. 2000*, vol. 41, no. 1, pp. 218–223, Jun. 2006, doi: 10.1111/j.1600-0757.2006.00160.x.

[58] M. T. Duailibi, S. E. Duailibi, C. S. Young, J. D. Bartlett, J. P. Vacanti, and P. C. Yelick, "Bioengineered teeth from cultured rat tooth bud cells," *J. Dent. Res.*, vol. 83, no. 7, pp. 523–528, 2004, doi: 10.1177/154405910408300703.

[59] E. Lavik and R. Langer, "Tissue engineering: Current state and perspectives," *Applied Microbiology and Biotechnology*, vol. 65, no. 1. Springer Verlag, pp. 1–8, 2004, doi: 10.1007/s00253-004-1580-z.

[60] M. T. P. Albuquerque, M. C. Valera, M. Nakashima, J. E. Nör, and M. C. Bottino, "Tissue-engineering-based Strategies for Regenerative Endodontics," *J. Dent. Res.*, vol. 93, no. 12, pp. 1222–1231, Dec. 2014, doi: 10.1177/0022034514549809.

[61] "Reforming dental health professions education: a white paper - PubMed." https://pubmed.ncbi.nlm.nih.gov/15520233/ (accessed Aug. 20, 2020).

[62] S. M. Rao, G. M. Ugale, and S. B. Warad, "Bone morphogenetic proteins: Periodontal regeneration," *North American Journal of Medical Sciences*, vol. 5, no. 3. Wolters Kluwer -- Medknow Publications, pp. 161–168, Mar. 2013, doi: 10.4103/1947-2714.109175.

[63] H. C. Slavkin, "Applications of pharmacogenomics in general dental practice," *Pharmacogenomics*, vol. 4, no. 2. Pharmacogenomics, pp. 163–170, Mar. 2003, doi: 10.1517/phgs.4.2.163.22626.

[64] F. J. Hughes, W. Turner, G. Belibasakis, and G. Martuscelli, “Effects of growth factors and cytokines on osteoblast differentiation,” *Periodontology 2000*, vol. 41, no. 1. Periodontol 2000, pp. 48–72, Jun. 2006, doi: 10.1111/j.1600-0757.2006.00161.x.

[65] Y. Chai and H. C. Slavkin, “Prospects for tooth regeneration in the 21st century: A perspective,” *Microscopy Research and Technique*, vol. 60, no. 5. Microsc Res Tech, pp. 469–479, Apr. 01, 2003, doi: 10.1002/jemt.10287.

[66] J. E. Ellingsen, P. Thomsen, and S. P. Lyngstadaas, “Advances in dental implant materials and tissue regeneration,” *Periodontology 2000*, vol. 41, no. 1. Periodontol 2000, pp. 136–156, Jun. 2006, doi: 10.1111/j.1600-0757.2006.00175.x.

[67] S. Gronthos, S. O. Akintoye, C. Y. Wang, and S. Shi, “Bone marrow stromal stem cells for tissue engineering,” *Periodontology 2000*, vol. 41, no. 1. Periodontol 2000, pp. 188–195, Jun. 2006, doi: 10.1111/j.1600-0757.2006.00154.x.

[68] K. Iohara, M. Nakashima, M. Ito, M. Ishikawa, A. Nakasima, and A. Akamine, “Dentin regeneration by dental pulp stem cell therapy with recombinant human bone morphogenetic protein 2,” *J. Dent. Res.*, vol. 83, no. 8, pp. 590–595, 2004, doi: 10.1177/154405910408300802.

[69] J. Folkman, “Watson and DNA: Making a Scientific Revolution,” *Nat. Med.*, vol. 9, no. 4, pp. 387–387, Apr. 2003, doi: 10.1038/nm0403-387.

[70] M. Miura *et al.*, “SHED: Stem cells from human exfoliated deciduous teeth,” *Proc. Natl. Acad. Sci. U. S. A.*, vol. 100, no. 10, pp. 5807–5812, May 2003, doi: 10.1073/pnas.0937635100.

[71] D. S. Kaufman, E. T. Hanson, R. L. Lewis, R. Auerbach, and J. A. Thomson, “Hematopoietic colony-forming cells derived from human embryonic stem cells,” *Proc. Natl. Acad. Sci. U. S. A.*, vol. 98, no. 19, pp. 10716–10721, Sep. 2001, doi: 10.1073/pnas.191362598.

[72] "Endodontics: Principles and Practice 6th Edition - NOBEL Kitabevi." https://www.nobelkitabevi.com.tr/dis-hekimligi/17995-endodontics-principles-and-practice-6th-edition.html (accessed Aug. 20, 2020).

[73] S. Ayoub, A. Cheayto, S. Bassam, M. Najar, A. Berbéri, and M. Fayyad-Kazan, "The Effects of Intracanal Irrigants and Medicaments on Dental-Derived Stem Cells Fate in Regenerative Endodontics: An update," *Stem Cell Reviews and Reports*, vol. 16, no. 4. Springer, pp. 650–660, Aug. 01, 2020, doi: 10.1007/s12015-020-09982-9.

[74] M. Zehnder, D. Kosicki, H. Luder, B. Sener, and T. Waltimo, "Tissue-dissolving capacity and antibacterial effect of buffered and unbuffered hypochlorite solutions," *Oral Surg. Oral Med. Oral Pathol. Oral Radiol. Endod.*, vol. 94, no. 6, pp. 756–762, 2002, doi: 10.1067/moe.2002.128961.

[75] K. H. Foster, J. C. Kulild, and R. N. Weller, "Effect of smear layer removal on the diffusion of calcium hydroxide through radicular dentin," *J. Endod.*, vol. 19, no. 3, pp. 136–140, 1993, doi: 10.1016/S0099-2399(06)80508-X.

[76] E. Berutti and R. Marini, "A scanning electron microscopic evaluation of the debridement capability of sodium hypochlorite at different temperatures," *J. Endod.*, vol. 22, no. 9, pp. 467–470, 1996, doi: 10.1016/S0099-2399(96)80079-3.

[77] M. Marending, F. Paqué, J. Fischer, and M. Zehnder, "Impact of Irrigant Sequence on Mechanical Properties of Human Root Dentin," *J. Endod.*, vol. 33, no. 11, pp. 1325–1328, Nov. 2007, doi: 10.1016/j.joen.2007.08.005.

[78] J. Craig Baumgartner and C. L. Mader, "A scanning electron microscopic evaluation of four root canal irrigation regimens," *J. Endod.*, vol. 13, no. 4, pp. 147–157, Apr. 1987, doi: 10.1016/S0099-2399(87)80132-2.

[79] M. Haapasalo and D. Ørstavik, "In vitro Infection and Disinfection of Dentinal Tubules," *J. Dent. Res.*, vol. 66, no. 8, pp. 1375–1379, 1987, doi: 10.1177/00220345870660081801.

[80] D. Ørstavik and M. Haapasalo, “Disinfection by endodontic irrigants and dressings of experimentally infected dentinal tubules,” *Dent. Traumatol.*, vol. 6, no. 4, pp. 142–149, Aug. 1990, doi: 10.1111/j.1600-9657.1990.tb00409.x.

[81] S. Çalt and A. Serper, “Time-dependent effects of EDTA on dentin structures,” *J. Endod.*, vol. 28, no. 1, pp. 17–19, 2002, doi: 10.1097/00004770-200201000-00004.

[82] B. J. Crumpton, G. G. Goodell, and S. B. McClanahan, “Effects on smear layer and debris removal with varying volumes of 17% REDTA after rotary instrumentation,” *J. Endod.*, vol. 31, no. 7, pp. 536–538, 2005, doi: 10.1097/01.don.0000148871.72896.1d.

[83] J. F. SIQUEIRA, A. G. MACHADO, R. M. SILVEIRA, H. P. LOPES, and M. UZEDA, “Evaluation of the effectiveness of sodium hypochlorite used with three irrigation methods in the elimination of Enterococcus faecalis from the root canal,in vitro,” *Int. Endod. J.*, vol. 30, no. 4, pp. 279–282, Oct. 2003, doi: 10.1046/j.1365-2591.1997.00096.x.

[84] A. D. Russell, “Activity of biocides against mycobacteria,” *J. Appl. Bacteriol.*, vol. 81, pp. 87S-101S, Dec. 1996, doi: 10.1111/j.1365-2672.1996.tb04602.x.

[85] L. A. Shaker, B. N. Dancer, A. D. Russell, and J. R. Furr, “Emergence and development of chlorhexidine resistance during sporulation of *Bacillus subtilis* 168,” *FEMS Microbiol. Lett.*, vol. 51, no. 1, pp. 73–76, Jun. 1988, doi: 10.1111/j.1574-6968.1988.tb02971.x.

[86] A. D. Russell and M. J. Day, “Antibacterial activity of chlorhexidine,” *J. Hosp. Infect.*, vol. 25, no. 4, pp. 229–238, Dec. 1993, doi: 10.1016/0195-6701(93)90109-D.

[87] N. B. Ruparel, F. B. Teixeira, C. C. R. Ferraz, and A. Diogenes, “Direct effect of intracanal medicaments on survival of stem cells of the apical papilla,” *J. Endod.*, vol. 38, no. 10, pp. 1372–1375, Oct. 2012, doi: 10.1016/j.joen.2012.06.018.

[88] E. G. Kontakiotis, C. G. Filippatos, G. N. Tzanetakis, and A. Agrafioti, "Regenerative endodontic therapy: A data analysis of clinical protocols," *Journal of Endodontics*, vol. 41, no. 2. Elsevier Inc., pp. 146–154, Feb. 01, 2015, doi: 10.1016/j.joen.2014.08.003.

[89] K. M. Hargreaves, A. Diogenes, and F. B. Teixeira, "Paradigm lost: A perspective on the design and interpretation of regenerative endodontic research," *J. Endod.*, vol. 40, no. 4 SUPPL., pp. S65–S69, Apr. 2014, doi: 10.1016/j.joen.2014.01.023.

[90] P. Montero-Miralles, J. Martín-González, O. Alonso-Ezpeleta, M. C. Jiménez-Sánchez, E. Velasco-Ortega, and J. J. Segura-Egea, "Effectiveness and clinical implications of the use of topical antibiotics in regenerative endodontic procedures: a review," *International Endodontic Journal*, vol. 51, no. 9. Blackwell Publishing Ltd, pp. 981–988, Sep. 01, 2018, doi: 10.1111/iej.12913.

[91] D. Kim and E. Kim, " Antimicrobial effect of calcium hydroxide as an intracanal medicament in root canal treatment: a literature review - Part I. In vitro studies ," *Restor. Dent. Endod.*, vol. 39, no. 4, p. 241, 2014, doi: 10.5395/rde.2014.39.4.241.

[92] T. Turk, B. Ozisik, and B. Aydin, "Time-dependent effectiveness of the intracanal medicaments used for pulp revascularization on the dislocation resistance of MTA," *BMC Oral Health*, vol. 15, no. 1, Oct. 2015, doi: 10.1186/s12903-015-0117-4.

[93] M. Frough Reyhani *et al.*, "Evaluation of Antimicrobial Effects of Different Concentrations of Triple Antibiotic Paste on Mature Biofilm of Enterococcus faecalis," *J. Dent. Res. Dent. Clin. Dent. Prospects*, vol. 9, no. 3, pp. 138–143, Sep. 2015, doi: 10.15171/joddd.2015.027.

[94] D. Pankajakshan, M. T. P. Albuquerque, J. D. Evans, M. M. Kamocka, R. L. Gregory, and M. C. Bottino, "Triple Antibiotic Polymer Nanofibers for Intracanal Drug Delivery: Effects on Dual Species Biofilm and Cell Function," *J. Endod.*, vol. 42, no. 10, pp. 1490–1495, Oct. 2016, doi: 10.1016/j.joen.2016.07.019.

[95] Kenry and C. T. Lim, “Nanofiber technology: current status and emerging developments,” *Progress in Polymer Science*, vol. 70. Elsevier Ltd, pp. 1–17, Jul. 01, 2017, doi: 10.1016/j.progpolymsci.2017.03.002.

[96] M. H. Ahmadi, M. Alhuyi Nazari, R. Ghasempour, H. Madah, M. B. Shafii, and M. A. Ahmadi, “Thermal conductivity ratio prediction of Al2O3/water nanofluid by applying connectionist methods,” *Colloids Surfaces A Physicochem. Eng. Asp.*, vol. 541, pp. 154–164, Mar. 2018, doi: 10.1016/j.colsurfa.2018.01.030.

[97] M. Taslimifar, M. Mohammadi, H. Afshin, M. H. Saidi, and M. B. Shafii, “Overall thermal performance of ferrofluidic open loop pulsating heat pipes: An experimental approach,” *Int. J. Therm. Sci.*, vol. 65, pp. 234–241, Mar. 2013, doi: 10.1016/j.ijthermalsci.2012.10.016.

[98] S. Jiang *et al.*, “Comparison of compressive strength and electrical resistivity of cementitious composites with different nano- and micro-fillers,” *Arch. Civ. Mech. Eng.*, vol. 18, no. 1, pp. 60–68, Jan. 2018, doi: 10.1016/j.acme.2017.05.010.

[99] S. S. Mantri and S. Mantri, “The nano era in dentistry,” *Journal of Natural Science, Biology and Medicine*, vol. 4, no. 1. Wolters Kluwer -- Medknow Publications, pp. 39–44, Jan. 2013, doi: 10.4103/0976-9668.107258.

[100] M. S. Huda, L. T. Drzal, A. K. Mohanty, and M. Misra, “Effect of fiber surface-treatments on the properties of laminated biocomposites from poly(lactic acid) (PLA) and kenaf fibers,” *Compos. Sci. Technol.*, vol. 68, no. 2, pp. 424–432, Feb. 2008, doi: 10.1016/j.compscitech.2007.06.022.

[101] “(PDF) NANOMANUFACTURING TECHNOLOGIES: ADVANCES AND OPPORTUNITIES.” https://www.researchgate.net/publication/237134360_NANOMANUFACTURING_TECHNOLOGIES_ADVANCES_AND_OPPORTUNITIES (accessed Aug. 20, 2020).

[102] Y. Y. Fan, H. M. Cheng, Y. L. Wei, G. Su, and Z. H. Shen, “Influence of

preparation parameters on the mass production of vapor-grown carbon nanofibers," *Carbon N. Y.*, vol. 38, no. 6, pp. 789–795, Jan. 2000, doi: 10.1016/S0008-6223(99)00178-5.

[103] "Contemporary Polymer Chemistry - H. R. Allcock, Frederick Walter Lampe - Google Kitaplar." https://books.google.com.tr/books/about/Contemporary_polymer_chemistry.html?id=7eKFAAAAIAAJ&redir_esc=y (accessed Aug. 20, 2020).

[104] "New Fibers - 2nd Edition." https://www.elsevier.com/books/new-fibers/hongu/978-1-85573-334-3 (accessed Aug. 20, 2020).

[105] F. K. Ko and Y. Wan, *Introduction to nanofiber materials*, vol. 9780521879835. Cambridge University Press, 2014.

[106] K. Garg and G. L. Bowlin, "Electrospinning jets and nanofibrous structures," *Biomicrofluidics*, vol. 5, no. 1, 2011, doi: 10.1063/1.3567097.

[107] Y. Sun, S. Cheng, W. Lu, Y. Wang, P. Zhang, and Q. Yao, "Electrospun fibers and their application in drug controlled release, biological dressings, tissue repair, and enzyme immobilization," *RSC Advances*, vol. 9, no. 44. Royal Society of Chemistry, pp. 25712–25729, Aug. 13, 2019, doi: 10.1039/c9ra05012d.

[108] *Handbook of Nanofibers*. Springer International Publishing, 2019.

[109] I. M. Alibe *et al.*, "Effects of polyvinylpyrrolidone on structural and optical properties of willemite semiconductor nanoparticles by polymer thermal treatment method," *J. Therm. Anal. Calorim.*, vol. 136, no. 6, pp. 2249–2268, Jun. 2019, doi: 10.1007/s10973-018-7874-7.

[110] J. Shi, A. R. Votruba, O. C. Farokhzad, and R. Langer, "Nanotechnology in drug delivery and tissue engineering: From discovery to applications," *Nano Letters*, vol. 10, no. 9. NIH Public Access, pp. 3223–3230, Sep. 08, 2010, doi: 10.1021/nl102184c.

[111] "Nanocarriers for Drug Delivery - 1st Edition." https://www.elsevier.com/books/nanocarriers-for-drug-delivery/mohapatra/978-0-12-814033-8 (accessed Aug. 20, 2020).

[112] "Evaluation of metronidazole toxicity: a prospective study - PubMed." https://pubmed.ncbi.nlm.nih.gov/10761537/ (accessed Aug. 20, 2020).

[113] A. Rizzo, R. Paolillo, L. Guida, M. Annunziata, N. Bevilacqua, and M. A. Tufano, "Effect of metronidazole and modulation of cytokine production on human periodontal ligament cells," *Int. Immunopharmacol.*, vol. 10, no. 7, pp. 744–750, Jul. 2010, doi: 10.1016/j.intimp.2010.04.004.

[114] K. Kamocki, J. E. Nör, and M. C. Bottino, "Dental pulp stem cell responses to novel antibiotic-containing scaffolds for regenerative endodontics," *Int. Endod. J.*, vol. 48, no. 12, pp. 1147–1156, Dec. 2015, doi: 10.1111/iej.12414.

[115] J. Palasuk *et al.*, "Bimix antimicrobial scaffolds for regenerative endodontics," *J. Endod.*, vol. 40, no. 11, pp. 1879–1884, Nov. 2014, doi: 10.1016/j.joen.2014.07.017.

[116] E. Hoshino *et al.*, "In-vitro antibacterial susceptibility of bacteria taken from infected root dentine to a mixture of ciprofloxacin, metronidazole and minocycline," *Int. Endod. J.*, vol. 29, no. 2, pp. 125–130, 1996, doi: 10.1111/j.1365-2591.1996.tb01173.x.

[117] A. R. Diogenes, N. B. Ruparel, F. B. Teixeira, and K. M. Hargreaves, "Translational science in disinfection for regenerative endodontics," *J. Endod.*, vol. 40, no. 4 SUPPL., 2014, doi: 10.1016/j.joen.2014.01.015.

[118] P. S. Stewart and M. J. Franklin, "Physiological heterogeneity in biofilms," *Nature Reviews Microbiology*, vol. 6, no. 3. Nature Publishing Group, pp. 199–210, Mar. 2008, doi: 10.1038/nrmicro1838.

[119] J. A. Berkhoff, P. B. Chen, F. B. Teixeira, and A. Diogenes, "Evaluation of triple

antibiotic paste removal by different irrigation procedures," *J. Endod.*, vol. 40, no. 8, pp. 1172–1177, 2014, doi: 10.1016/j.joen.2013.12.027.

[120] J. H. Kim, Y. Kim, S. J. Shin, J. W. Park, and I. Y. Jung, "Tooth discoloration of immature permanent incisor associated with triple antibiotic therapy: A case report," *J. Endod.*, vol. 36, no. 6, pp. 1086–1091, 2010, doi: 10.1016/j.joen.2010.03.031.

[121] N. Zargar, M. Rayat Hosein Abadi, M. Sabeti, Z. Yadegari, A. Akbarzadeh Baghban, and O. Dianat, "Antimicrobial efficacy of clindamycin and triple antibiotic paste as root canal medicaments on tubular infection: An in vitro study," *Aust. Endod. J.*, vol. 45, no. 1, pp. 86–91, Apr. 2019, doi: 10.1111/aej.12288.

[122] S. E. Hadi, "ONE-POT SYNTHESIS OF HYBRID CORE-SHELL NANOPARTICLES FOR ANTIBACTERIAL PHOTODYNAMIC THERAPY," Bilkent University, Aug. 2019. Accessed: Aug. 21, 2020. [Online]. Available: http://repository.bilkent.edu.tr/handle/11693/52358.

[123] U. S. N. L. of M. PubChem, "Metronidazole (Compound)," *Experimental Properties. Physical Description.*, 2019. https://pubchem.ncbi.nlm.nih.gov/compound/Metronidazole (accessed Aug. 21, 2020).

[124] "Ciprofloxacin | C17H18FN3O3 - PubChem." https://pubchem.ncbi.nlm.nih.gov/compound/Ciprofloxacin (accessed Aug. 21, 2020).

[125] "Minocycline - Wikipedia." https://en.wikipedia.org/wiki/Minocycline (accessed Aug. 21, 2020).

[126] "calcium hydroxide chemical structure 3d: Yandex.Görsel'de 11 bin görsel bulundu." https://yandex.com.tr/gorsel/search?pos=2&img_url=https%3A%2F%2F2012books.lardbucket.org%2Fbooks%2Fprinciples-of-general-chemistry-v1.0%2Fsection_07%2Fb94ba0ad8a79c1b0772cc74d4870a26e.jpg&text=calcium

hydroxide chemical structure 3d&lr=11503&rpt=simage&source=wiz (accessed Aug. 21, 2020).